BLANK PAGES
IN THIS
DOCUMENT
WERE NOT
FILMED

SPECIAL REPORT

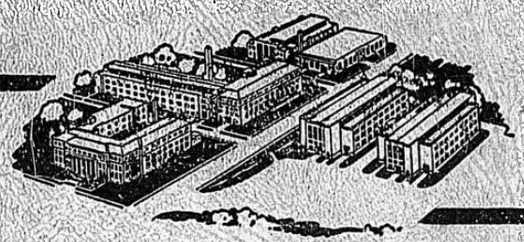

BATTELLE MEMORIAL INSTITUTE

SUMMARY REPORT

on

HIGH-TEMPERATURE PROPERTIES AND ALLOYING BEHAVIOR OF THE REFRACTORY PLATINUM-GROUP METALS

to

OFFICE OF NAVAL RESEARCH

August 31, 1961

by
R. W. Douglass, C. A. Krier, and R. I. Jaffee

BATTELLE MEMORIAL INSTITUTE
505 King Avenue
Columbus 1, Ohio

Battelle Memorial Institute

505 KING AVENUE COLUMBUS 1, OHIO

October 27, 1961

Dr. E. I. Salkovitz
Chief, Metallurgy Branch
Office of Naval Research
Department of the Navy
Washington 25, D.C.

Dear Dr. Salkovitz:

Enclosed are 10 copies of a summary report on the project, "High-Temperature Properties and Alloying Behavior of the Refractory Platinum-Group Metals", Contract No. Nonr-2547(00), NR 039-067, covering the period from April 1, 1958, to August 31, 1961, the entire contract period to date. We plan to issue several technical reports on specific topics in the near future, but thought it would be well to bring together the extensive data generated on the project for over-all review. This will facilitate planning of future studies under the continuation of the program.

We would be pleased to have your comments on the report.

Yours very truly,

Robert I. Jaffee
Technical Manager
Department of Metallurgy

RIJ:cjw

Enc. (10)
Air mail
cc: Mr. Charles G. Jacobsen (2)

DISTRIBUTION LIST

Chief of Naval Research (2)
Department of the Navy
Washington 25, D. C.
Attn: Code 423

Commanding Officer (1)
Office of Naval Research
Branch Office
86 E. Randolph Street
Chicago 1, Illinois

Assistant Naval Attaché for Research (5)
Office of Naval Research
Branch Office, London
Navy 100, Box 39
F. P. O., N. Y., N. Y.

Director
U. S. Naval Research Laboratory
Washington 25, D. C.
Attn: Technical Information
Officer, Code 2000 (6)
Code 2020 (1)
Code 6200 (1)
Code 6300 (2)

Chief, Bureau of Aeronautics
Department of the Navy
Washington 25, D. C.
Attn: Code AE 4 (1)
Code TD 41 (1)

Commanding Officer (1)
U. S. Naval Air Material Center
Philadelphia, Pennsylvania
Attn: Aeronautical Materials Laboratory

Chief, Bureau of Ordnance
Department of the Navy
Washington 25, D. C.
Attn: Code Res-1e (1)
Code Ad-3 (1)
Code Rec-1 (1)

Post Graduate School (1)
U. S. Naval Academy
Monterey, California
Attn: Dept. of Metallurgy

Office of Technical Services (1)
Department of Commerce
Washington 25, D. C.

Armed Services Technical
Information Agency (ASTIA) (5)
Documents Service Center
Knott Building
Dayton 2, Ohio

Commanding Officer
Watertown Arsenal
Watertown, Massachusetts
Attn: Ordnance Materials Research Office (1)
Laboratory Division (1)

Superintendent (1)
U. S. Naval Gun Factory
Washington 25, D. C.
Attn: Code 720

Commanding Officer (1)
U. S. Naval Ordnance Laboratory
White Oaks, Maryland

Commanding Officer (1)
U. S. Naval Ordnance Test Station
Inyokern, California

Commanding Officer (1)
U. S. Naval Proving Ground
Dahlgren, Virginia
Attn: Laboratory Division

Chief, Bureau of Ships
Department of the Navy
Washington 25, D. C.
Attn: Code 330 (1)
Code 337L (1)
Code 343 (1)

Commanding Officer (1)
U. S. Naval Engineering Experiment
Station
Annapolis, Maryland
Attn: Metals Laboratory

Materials Laboratory (1)
New York Naval Shipyard
Brooklyn 1, New York
Attn: Code 907

Chief, Bureau of Yards and Docks (1)
Department of the Navy
Washington 25, D. C.
Attn: Research and Standards Division

Commanding Officer (1)
David Taylor Model Basin
Washington 7, D. C.

National Bureau of Standards
Washington 25, D. C.
Attn: Metallurgy Division (1)
Mineral Products Division (1)

National Advisory Committee
for Aeronautics (1)
1512 H Street, N. W.
Washington 25, D. C.

National Advisory Committee for
Aeronautics (1)
Lewis Flight Propulsion Laboratory
Cleveland, Ohio
Attn: Materials and Thermodynamics
Division

U. S. Atomic Energy Commission (1)
1901 Constitution Avenue
Washington 25, D. C.
Attn: Technical Library

DISTRIBUTION LIST
(Continued)

Commanding Officer (1)
Frankford Arsenal
Frankford, Pennsylvania
Attn: Laboratory Division

Commanding Officer (1)
Office of Ordnance Research
Box CM, Duke Station
Duke University
Durham, North Carolina
Attn: Metallurgy Division

Commander
Wright Air Development Center
Wright-Patterson Air Force Base
Ohio
Attn: Aeronautical Research Lab. (WCRRH) (1)
Aeronautical Research Lab. (WCRRL) (1)
Materials Laboratory (WCRTL) (1)

U. S. Air Force ARDC (1)
Office of Scientific Research
Washington 25, D. C.
Attn: Solid State Division (SRQB) (1)

Los Alamos Scientific Laboratory (1)
P. O. Box 1663
Los Alamos, New Mexico
Attn: Report Librarian

Union Carbide Nuclear Co. (1)
K-25 Plant Records Department
P. O. Box P
Oak Ridge, Tennessee

Union Carbide Nuclear Co. (1)
Y-12 Plant Records Department
Central Files
P. O. Box Y
Oak Ridge, Tennessee

General Electric Company (1)
P. O. Box 100
Richland, Washington
Attn: Technical Information Division

Iowa State College (1)
P. O. Box 14A, Station A
Ames, Iowa
Attn: F. H. Spedding

U. S. Atomic Energy Commission
Washington 25, D. C.
Attn: Metals and Materials Branch, Division of Research (1)
Eng. Develop. Branch, Division of Reactor Develop. (1)

Argonne National Laboratory (1)
P. O. Box 299
Lemont, Illinois
Attn: H. D. Young, Librarian

Brookhaven National Laboratory (1)
Technical Information Division
Upton, Long Island
New York
Attn: Research Library

Union Carbide Nuclear Co.
Oak Ridge National Laboratory
P. O. Box P
Oak Ridge, Tennessee
Attn: Metallurgy Division (1)
Solid State Physics Division (1)
Laboratory Records Dept. (1)

U. S. Atomic Energy Commission
Technical Information Service Extension
P. O. Box 62
Oak Ridge, Tennessee
Attn: Reference Branch

University of California (1)
Radiation Laboratory
Information Division
Room 128, Building 50
Berkeley, California
Attn: R. K. Wakerling

Bettis Plant (1)
U. S. Atomic Energy Commission
Bettis Field
P. O. Box 1468
Pittsburgh 30, Pennsylvania
Attn: Mrs. Virginia Sternberg
Librarian

Officer in Charge (1)
U. S. Naval Civil Engineering Research and Evaluation Laboratory
Construction Battalion Center
Fort Hueneme, California

Knolls Atomic Power Laboratory (1)
P. O. Box 1072
Schenectady, New York
Attn: Document Librarian

Mound Laboratory (1)
Monsanto Chemical Co.
P. O. Box 32
Miamisburg, Ohio

U. S. Atomic Energy Commission (1)
New York Operations Office
70 Columbus Avenue
New York 23, New York
Attn: Document Custodian

Sandia Corporation (1)
Sandia Base
Albuquerque, New Mexico
Attn: Library

DISTRIBUTION LIST
(Continued)

Mr. P. A. Santoli (1)
Allegheny-Ludlum Steel Corporation
Watervliet, New York

Dr. W. Rostoker (1)
Metals Research Department
Armour Research Foundation
3350 South Federal Street
Chicago 16, Illinois

Dr. J. Port (1)
Chase Brass and Copper Company
Waterbury 20, Connecticut

Mr. M. Semchyshen (1)
Climax Molybdenum Corporation
14410 Woodrow Wilson Avenue
Detroit 38, Michigan

Prof. D. W. Bainbridge (1)
Department of Metallurgical Engineering
Colorado School of Mines
Golden, Colorado

Mr. L. A. Yerkovich (1)
Cornell Aeronautical Laboratory
4455 Genesee Street
Buffalo 21, New York

Dr. A. B. Michael (1)
Fansteel Metallurgical Corporation
North Chicago, Illinois

Chief, Bureau of Ordnance (1)
Special Projects Division
Washington 25, D. C.
Attn: W. Cohen

Defense Metals Information Center (1)
Battelle Memorial Institute
505 King Avenue
Columbus 1, Ohio
Attn: R. Runck

Climax Molybdenum Company (1)
Metallurgical Development Division
500 Fifth Avenue
New York 36, New York

Ferrous Metals and Ferroalloys Branch (1)
Minerals Division
U. S. Bureau of Mines
Department of Interior
Washington 25, D. C.
Attn: R. Holliday

Prof. P. Duwez (1)
Department of Mechanical Engineering
California Institute of Technology
Pasadena, California

Prof. E. R. Parker (1)
Division of Mineral Technology
University of California
Berkeley 4, California

Dr. R. A. Perkins (1)
Lockheed Missiles and Space Div.
Sunnyvale, California

Dr. L. D. Jaffe (1)
Jet Propulsion Laboratory
California Institute of Technology
4800 Oak Grove Drive
Pasadena 3, California

Dr. W. R. Hibbard (1)
Research Laboratories
General Electric Corporation
Schenectady, New York

Dr. L. P. Jahnke (1)
Aircraft Gas Turbine Development
Dept.
General Electric Company
Building 200
Cincinnati 15, Ohio

Dr. John Push (1)
Lamp Wire and Phosphorus Department
General Electric Company
1331 Chardon Road
Cleveland 17, Ohio

Mr. W. L. Badger (1)
Small Aircraft Engine Department
920 Western Avenue
West Lynn 3, Massachusetts

Mr. L. J. Cronin (1)
Techniques Department
Raytheon Manufacturing Company
Waltham 54, Massachusetts

Dr. A. J. Opinsky (1)
Sylvania Electric Products, Inc.
Bayside, Long Island
New York

Mr. P. C. Rossin (1)
Universal Cyclops Steel Corporation
Bridgeville, Pennsylvania

Prof. R. Maddin (1)
School of Metallurgical Engineering
University of Pennsylvania
Philadelphia, Pennsylvania

Mr. C. T. Sims (1)
Large Steam Turbine Division
General Electric Corporation
Schenectady, New York

DISTRIBUTION LIST
(Continued)

Prof. N. J. Grant (1)
Department of Metallurgical Engineering
Massachusetts Institute of Technology
Cambridge 39, Massachusetts

Prof. J. Wulff (1)
Department of Metallurgical Engineering
Massachusetts Institute of Technology
Cambridge 39, Massachusetts

Prof. J. W. Freeman (1)
Engineering Research Institute
University of Michigan
Ann Arbor, Michigan

Dr. R. Speiser (1)
Department of Metallurgy
The Ohio State University
Columbus, Ohio

Mr. J. H. Bechtold (1)
Westinghouse Electric Corporation
Research Laboratories
Beulah Road
Churchill Borough
Pittsburgh 35, Pennsylvania

Dr. W. C. Lilliendahl (1)
Westinghouse Electric Corporation
Bloomfield, New Jersey

Mr. Glen Fritzlen (1)
Haynes-Stellite Corporation
Kokomo, Indiana

Dr. H. P. Croft (1)
Kennecott Copper Corporation
161 E. 42nd Street
New York, New York

Mr. Walter Betteridge (1)
The Mond Nickel Company
Development and Research Department
Bashley Road
London, NW-10
England

Mr. Theron Reed (1)
Owens-Corning Fiberglas Company
Newark, Ohio

Mr. Ray Vines (1)
The International Nickel Company
67 Wall Street
New York 5, New York

Dr. H. J. Albert (2)
Baker Platinum Division
Engelhard Industries, Inc.
Newark, New Jersey

TABLE OF CONTENTS

TABLE OF CONTENTS (Continued)

LIST OF FIGURES

LIST OF FIGURES (Continued)

LIST OF FIGURES (Continued)

LIST OF FIGURES (Continued)

LIST OF FIGURES (Continued)

LIST OF FIGURES (Continued)

LIST OF TABLES

LIST OF TABLES (Continued)

SUMMARY REPORT

on

HIGH-TEMPERATURE PROPERTIES AND ALLOYING BEHAVIOR OF THE REFRACTORY PLATINUM-GROUP METALS

to

OFFICE OF NAVAL RESEARCH

from

BATTELLE MEMORIAL INSTITUTE

August 31, 1961

INTRODUCTION

This report summarizes the results of three years of study of the platinum-group metals. The object of the program was to evaluate the high-temperature mechanical properties and alloying behavior of the refractory platinum-group metals. The published literature was reviewed during the first year of the program to determine the specific metallurgical areas most lacking in information. These were many. Experimental programs were based largely on the results of this literature survey.

During the course of the program, many problem areas of scientific and technological interest were defined. Chief among these was the unusually low ductility of rhodium and iridium. Accordingly, the scope of the program was broadened to include the study of such significant problems.

Other problem areas encountered were related to the preparation and examination of experimental materials. These were studied to determine experimental techniques and to develop a state of the art of the consolidation, fabrication, and examination of the refractory platinum-group metals.

The results of this program have been reviewed periodically and published in appropriate technical journals or as Technical Reports. The results of the literature survey were published as a Technical Phase Report, entitled "High-Temperature Properties and Alloying Behavior of the Refractory Platinum-Group Metals", August 14, 1959, R. W. Douglass, F. C. Holden, and R. I. Jaffee.

Technical papers that have been published or are in preparation are listed below:

"Tensile Properties of the Platinum-Group Metals", F. C. Holden, R. W. Douglass, and R. I. Jaffee, ASTM Special Technical Publication No. 272 (1959).

"A Study of the Spectral Emissivities and Melting Temperatures of Osmium and Ruthenium", R. W. Douglass and E. F. Adkins, Trans. AIME, 221 (April, 1961), p 248.

"Rhenium and the Refractory Platinum-Group Metals", R. I. Jaffee, D. J. Maykuth, and R. W. Douglass, presented at AIME-IMD Refractory Metals Symposium, Detroit (May, 1960); to be published by AIME.

"High-Temperature Tensile and Creep Behavior of Iridium, Rhodium, and Ruthenium", R. W. Douglass and R. I. Jaffee, in preparation.

"High-Temperature Oxidation of the Platinum-Group Metals", C. A. Krier and R. I. Jaffee, in preparation.

"The Deformation and Fracture of Rhodium and Iridium", R. W. Douglass and R. I. Jaffee, in preparation.

The experimental program has been divided into five metallurgical subject areas for reporting convenience. These are fabrication, annealing, oxidation, mechanical properties, and alloying. Because of the scope of the program, the significance of the results are discussed as the results are reported.

EXPERIMENTAL MATERIALS AND PROCEDURES

Materials

The experimental materials were supplied by The International Nickel Company, through Englehard Industries, Inc., on a loan basis. Two lots of material were studied. The platinum, palladium, and iridium included in the first lot were not of the purity required, and, in some cases, contained serious fabrication defects. These were replaced by a second lot containing high-purity material.

The metals were supplied in three forms, powder (or sponge), 0.150-inch-diameter rod, and 0.1-inch-thick rolled strip. The latter two were supplied in the worked condition.

Analyses of the first lot of materials were not supplied by the producers. This lot was analyzed at Battelle and by the Coleman Laboratories of Philadelphia, Pennsylvania. Analysis of most of the replacement materials were supplied by the producer. Analyses of both lots are presented in Table 1.

TABLE 1. SPECTROGRAPHIC ANALYSIS OF PLATINUM-GROUP METALS

Material	Major Impurities, 0.X per cent by weight	Minor Impurities, 0.0X per cent by weight	Trace Impurities, 0.00X per cent by weight or less
Platinum rod (commercial purity)	Ni, Pd	Al, Cu, Fe, Re, Rh, Ir	Ca, Mg, Si, Ag, Sn, Ti, Bi, Be, Mn
Platinum rod (high purity)	None	None	Al, Ca, Cu, Fe, Mg, Ni, Si, Ag, Sn, Pb, Mn, Zn, Au, Ru, Pd, Rh
Palladium rod (commercial purity)	Cu, Fe	Ni, Si, Ag	Al, Ca, Pt, Mn
Palladium rod (high purity)	None	Pt	Al, Ca, Cu, Fe, Mg, Ni, Si, Ag, Pb, Zn, Au, Ru, Rh
Rhodium rod	None	Fe, Ir	Al, Ca, Cu, Ni, Si, Ag, Pt, Bi, Co, Te, Ru
Iridium rod (first lot)	None	Fe, Ni, Si, Zr	Al, Ca, Cu, Mg, Pt, Cr, Mn
Ruthenium powder (first lot)	Co, Ti	Ca, Cu, Fe, Cd, Mo, Ir	Al, Mg, Au, Pd, Pt, Rh, Si, Pb, Ni, Sn
Osmium powder (first lot)	None	Al, Si, W	Ca, Cu, Fe, Pb, Mg, Mn, Pt, Ru, Ir

The reliability of the analyses often was reduced by the apparent lack of high purity standards for each metal. This, in turn, severely handicapped the interpretation of experimental results, as will be described later.

The concentration of the gases (oxygen, hydrogen, and nitrogen) was determined for selected metals by vacuum fusion analysis. Representative gas analyses, for the metals in a variety of conditions, are reported in Table 2.

The vacuum-fusion data illustrate that oxygen, although dissolved or absorbed in the as-received metal, can be reduced to low concentrations by electron-beam melting or sintering, and is not redissolved to an appreciable extent by subsequent exposure in air at high temperatures.

Metallographic Techniques

Metallographic techniques for the preparation of specimens of the platinum-group metals were not well known, nor well developed, at the start of this research. The techniques developed for preparation of metallographic samples are as follows: Grinding, to remove cold work effects from sectioning, was done on standard SiC discs, through the 600-grit size. Platinum and palladium were final polished in three steps:

(1) Rough polishing

0-2 micron diamond paste on red felt wheel at medium (500 rpm) speed; kerosene lubricant..

TABLE 2. VACUUM-FUSION ANALYSES OF PLATINUM-GROUP METALS[a]

Metal	Condition	Vacuum-Fusion Analysis, ppm		
		Oxygen	Hydrogen	Nitrogen
Rhodium	High-purity commercial rod, 99.9 per cent rhodium	27	0.2	3
	Electron-beam melted	2	0.2	3
	Electron-beam melted, tensile treated in air at 1000 C	7	0.9	--
Iridium	First lot, as-received rod	760	52	--
	Electron-beam melted, tensile tested in air at 1000 C	4	0.5	--
	Second lot, high-purity rod, tensile tested in air at 1000 C	2	0.5	--
Osmium	Powder, 99.5 per cent osmium	947	22	--
	Hydrogen sintered	38	0.7	--
	Electron-beam melted	20	1.2	--
Ruthenium	Powder, 99 per cent ruthenium	3220	20	118
	Vacuum sintered	63	0.4	2
	Hydrogen sintered	268	4.6	--
	Electron-beam melted	7	0.2	3

(a) The sensitivity of the vacuum-fusion apparatus is equivalent to ±7 ppm oxygen and ±0.9 ppm hydrogen. Many of the values reported are close to or below the sensitivity limits and must be considered with reservations.

(2) Semifinal polishing

0-1/2 micron diamond paste on Buehler Miracloth wheel at 500 rpm; kerosene lubricant.

(3) Final polishing

slurry of 10-gram ferric oxide, 35 cc H_2O, 5 cc 20 per cent chromic acid on Buehler Miracloth wheel at slow (250 rpm) speed.

Ruthenium, rhodium, iridium, and osmium were final polished in two steps as follows:

(1) Semifinal polishing

slurry of 15 grams fine alumina, 35 cc H_2O, 5 cc 20 per cent chromic acid on Buehler Miracloth wheel at high (1750 rpm) speed.

(2) Final polishing

the above slurry (or same as in (3) above) on Buehler Miracloth wheel at slow (250 rpm) speed.

All specimens were electrolytically etched by the following procedures:

Metal	Etchant	Remarks
Platinum	20 cc HCl, 80 cc H_2O saturated with NaCl	6 volts-AC, 1 minute
Palladium	10 per cent HCl in ethyl alcohol	10 volts-DC, 30 seconds
Ruthenium	20 cc HCl, 80 cc H_2O saturated with NaCl	5-20 volts-AC, 1-2 minutes
Rhodium	Concentrated HCl	5 volts-AC, 1-2 minutes
Iridium	20 cc HCl, 80 cc H_2O saturated with NaCl	20 volts-AC, 1-2 minutes
Osmium	10 per cent HCl in ethyl alcohol	10 volts-DC, 30 seconds

The following solutions, 20 cc (H_2SO_4, HNO_3), 80 cc H_2O, and 10 per cent NaOH, were also suitable for etching the platinum-group metals. Etching conditions were 5-15 volts AC for 1-2 minutes for each of these solutions.

Considerable effort was spent to develop electrolytic polishing procedures for rhodium, iridium, and ruthenium. Each of the etching solutions was evaluated for suitability in electrolpolishing. Iridium formed a soluble compound in dilute and concentrated H_2SO_4. Although etching action was present, a maximum of metal was removed with a minimum of etching. The same was true for rhodium in 10 per cent NaOH, except the compound that was formed was not soluble. This latter compound could be removed from the specimen surface by frequent current surges. Conditions for maximum metal removal were 1-2 volts AC at room temperature. None of the other solutions were satisfactory for electrolytic polishing.

Surface replication is a specialized metallographic technique used in this program for the study of crack initiation and propagation in specimens while under load. Polished surfaces were replicated by pressing cellulose acetate, wet with acetone, against the surface of interest. After drying and stripping, replicas were mounted securely on glass slides and gold shadowed to provide a partially opaque surface for the metallographic examination. Fine structural detail could be retained using this technique.

Mechanical Evaluation

Mechanical properties evaluated in this research were tensile, creep, hardness, and bend properties.

Tensile Tests

Tensile properties of all the metals were determined in the range -196 to 1500 C. Platinum and palladium were studied in the range -196 to 1000 C, rhodium from -196 to 1250 C, ruthenium from 750 to 1500 C, and iridium from -196 to 1500 C. In establishing the temperature dependence of the properties of the metals, the only additional variable was testing atmosphere; grain size and strain rate were held constant. Substandard specimens, illustrated in Figure 1, were used in this phase of the work.

Tensile properties at temperatures up to 1000 C in air were determined for all five metals. Tests were performed on a standard hydraulic testing machine at a constant cross-head speed of 0.005 inch/minute (initial strain rate $\approx$ 0.0075 minute^{-1}). Load-extension curves were recorded autographically at all temperatures from a specially designed, wide-range extensometer attached to the specimen grips. Low temperature tests were conducted by immersing the specimen in liquid nitrogen. A potentiometer-controlled furnace was used for elevated temperature tests. Temperatures were controlled to $\pm$3 C from a thermocouple wired to the center of the specimen. Initial and final measurements of gage length were made from 10X projections of the reduced section of a combination or micrometer and traveling microscope

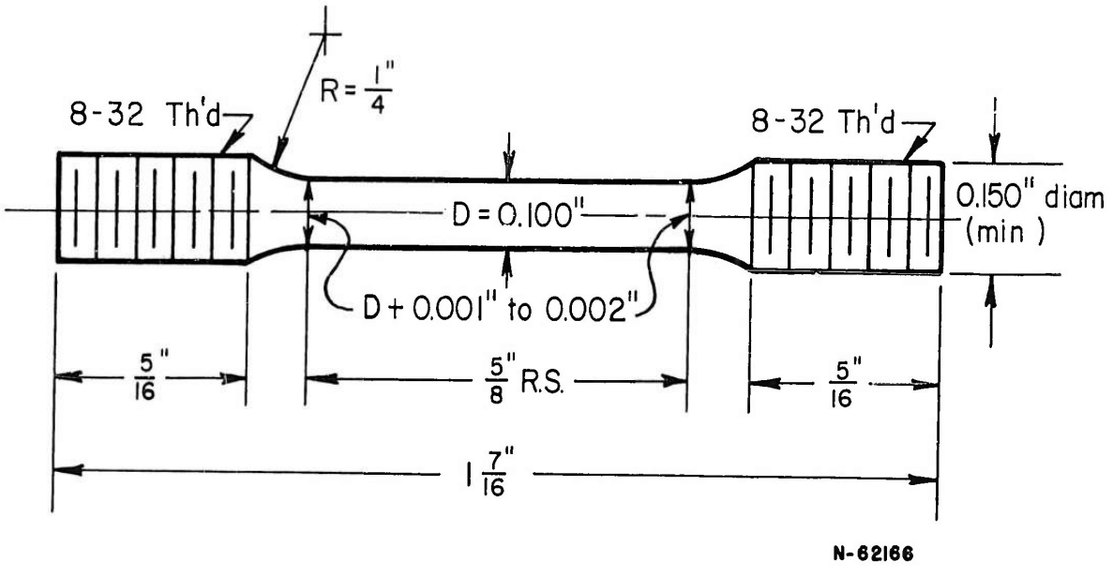

FIGURE 1. SPECIFICATIONS FOR MICRO TENSILE SPECIMEN

measurements, whichever was most appropriate for the particular measurement. Tension tests in the range 750 to 1500 C were conducted in a modified resistance heated high-temperature vacuum furnace. The load was applied hydraulically through an axial ram, where oil flow (and thus cross-head speed) was controlled by a variable speed motor. Loads were measured from an electric resistance load cell; extension was measured from an externally mounted dial indicator. Temperature control in these tests was ±5 C. Other testing and measuring details are the same as described earlier.

Three-inch long, 0.050-inch-diameter wire specimens were used to study the influence of strain rate and grain size on the room-temperature properties of rhodium and iridium. Reduced sections, 1/2 inch long, were prepared chemically by removing 0.001 to 0.002 inch from the diameter of the wire. Rhodium was polished 30 minutes at 1-2 volts AC in 10 per cent NaOH with frequent current surges to remove the reaction products. Iridium was polished about 30 minutes at 2 volts AC in 20 cc H_2SO_4 and 80 cc H_2O.

These room-temperature tensile tests were made in an Instron testing machine. The specimens were gripped in flat-face compression grips with crocus cloth inserts to prevent slipping. (Slipping in the grips at high loads and strains could not be avoided in several specimens.) Load extension curves were recorded autographically, with cross-head motion serving as the measure of extension. Tests were performed at 0.004, 0.02, 0.2, and 2 inches/inch/minute.

Stress-Rupture Tests

Short-time stress rupture properties of rhodium, iridium, and ruthenium were determined in vacuum in the range 1000 to 1500 C. Specimen dimensions have been illustrated in Figure 1. The high-temperature vacuum furnace used in the tensile study was further modified by the addition of a 9:1 ratio lever arm for creep tests. Applied loads, again, were measured from an electric resistance load cell and extension was measured from an externally mounted dial indicator. Temperature control, established by a transtat setting, was often only ±10 C for long-time tests.

Bend Tests

The bend ductility of all the platinum-group metals, except osmium, was established in the temperature range -196 to 600 C. Annealed specimens, approximately 1 x 1/4 x 0.04-inch, polished through 600-grit SiC papers were used to establish bend ductility by progressive bend tests. The minimum bend radius was determined as the bend die radius at which specimen failure is first observed, divided by the specimen thickness.

Specimens for low temperature tests were immersed in liquid nitrogen, dry ice and alcohol, or ice and water. High-temperature tests were performed in an oil bath heated by a potentiometer controlled furnace or in a vertical tube resistance furnace. Temperature control at all temperatures was at least ±3 C.

Hardness Tests

Vickers and Knoop hardness tests were used throughout the program in establishing recrystallization temperatures, work hardening behavior, alloy segregation, and specimen contamination and other appropriate properties. Loads from 5 kilograms to 10 grams were used in various phases of the work.

EXPERIMENTAL PROGRAM

Consolidation and Fabrication

The fabrication of ruthenium and osmium were of major interest, for at the initiation of the program neither of these metals were available in wrought form. Accordingly, about 50 per cent effort during the first 18 months was expended on studies of the sintering characteristics and fabricability of these metals.

Ruthenium

Powder Metallurgy. The initial consolidation of ruthenium was best accomplished by cold pressing at 15 to 20 tsi with a carbon tetrachloride binder, followed by presintering one hour at 1200 C in hydrogen. (Stearic acid and paraffin and carbowax were also used as binders; however, CCl_4 appeared more satisfactory.) Presintered densities ranged from 65 to 70 per cent of ideal. All powder metallurgy bars used in this work measured 1/4 x 1/4 x 6 inches.

The influence of sintering temperature on density, illustrated in Figure 2, was determined by progressive sintering of a single bar in the range 1200 to 1800 C, and another bar at 2000, 2100, and 2200 C. Sintering times of one hour were used in this work.

Typical microstructures of as-sintered ruthenium bars are shown in Figure 3.

Based on sintering tests, a schedule of 1 hour at 1200 C, followed by 1 hour at 2200 C, both in hydrogen, was selected for the consolidation of ruthenium bars for fabrication. This treatment resulted in a coarse grain size, approximately 0.1 millimeter in diameter. A deficiency of this particular schedule is that the beneficial effects of fine grain size on fabricability are compromised to achieve high sintered density.

Concurrent with this work at Battelle, Rhys of Mond Nickel Company, completed and published the results of an extensive study of the consolidation and fabrication of ruthenium.[1]* He found that fine powders (-330 mesh), high purity and high vacuum all promoted high sintered density and subsequent workability. The mode of compacting, die and plunger versus hydrostatic pressing, also influenced the properties of the material, but the properties generally were subject to the influence of purity and powder size. Hydrostatic pressing gave the best over-all results. Sintering time or temperature (if above 1400 C)

---

*References will appear at the end of this report.

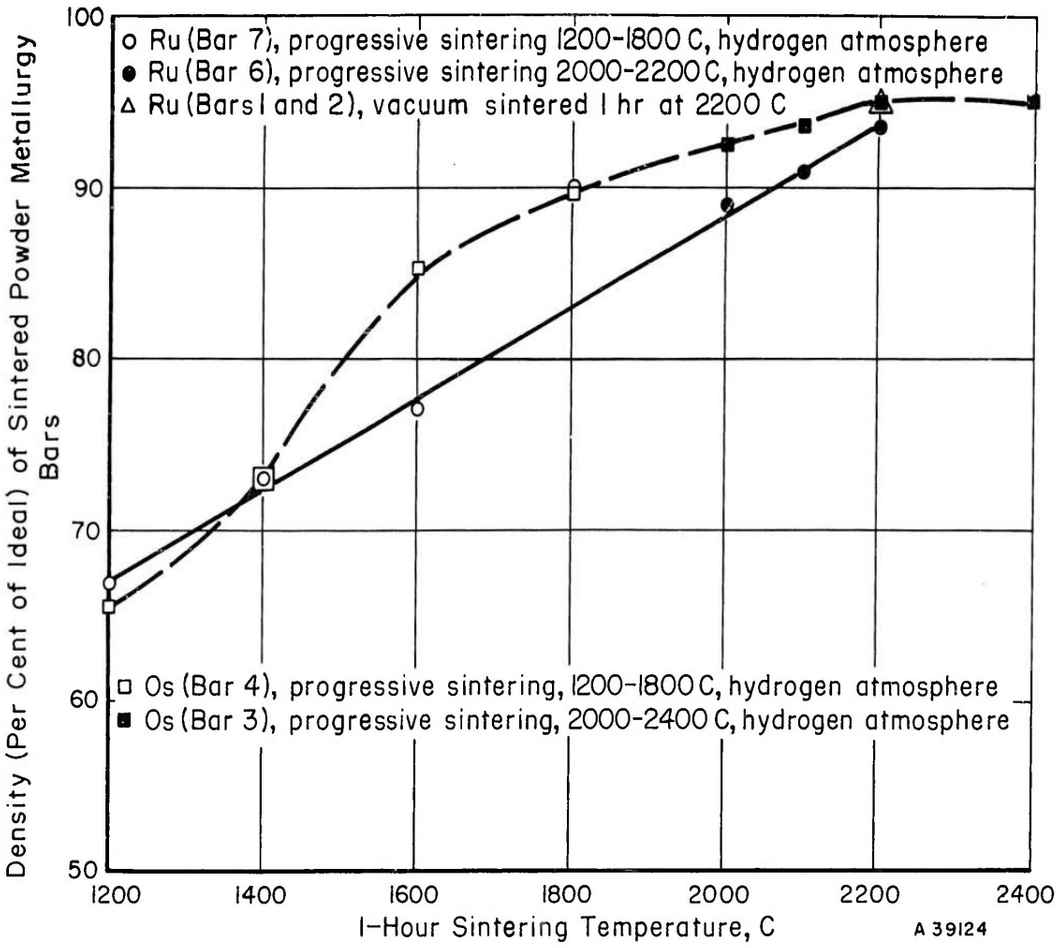

FIGURE 2. EFFECT OF SINTERING TEMPERATURE ON THE DENSITY OF RUTHENIUM AND OSMIUM POWDER METALLURGY BARS

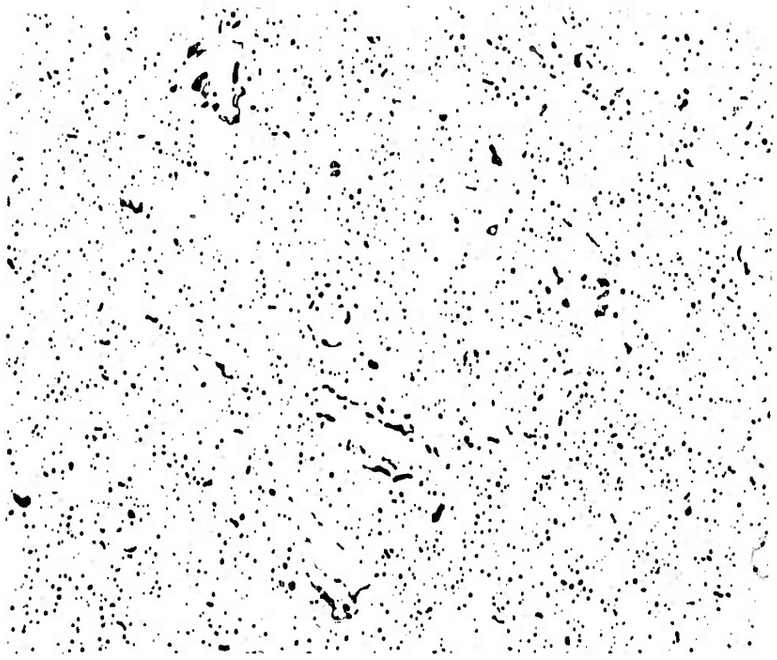

100X N56730

a. Ruthenium (Bar 6); Sintered Progressively 1 Hour at 2000, 2100, and 2200 C; Carbowax Binder; 93.5 Per Cent Ideal Density

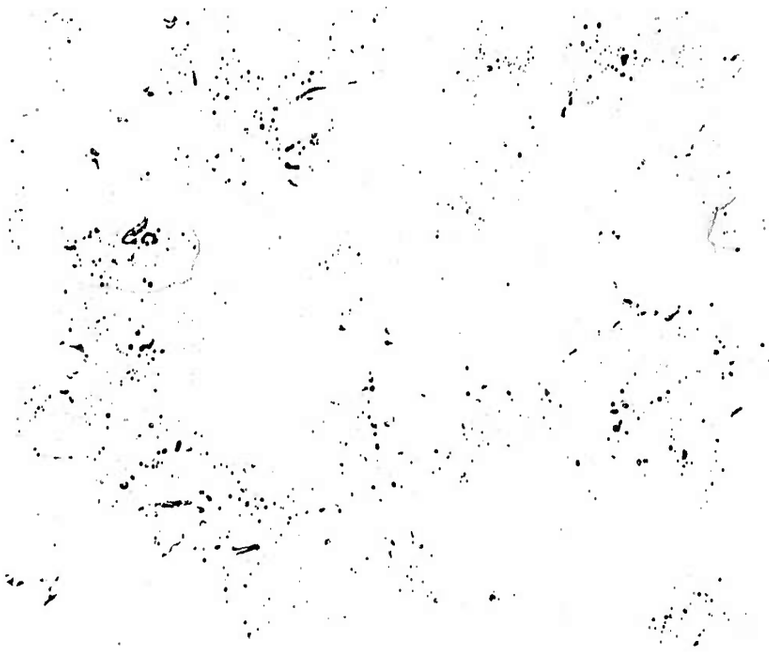

100X N56731

b. Ruthenium (Bar 8); Sintered Progressively 1 Hour at 2000, 2100, and 2200 C; CCl_4 Binder; 95 Per Cent Ideal Density

FIGURE 3. TYPICAL MICROSTRUCTURES OF SINTERED RUTHENIUM

had no appreciable effect on the sintered density. The results of Rhys' work are not directly comparable to the results of this program, as his material was of consistently higher purity than that used in this work.

Several fabrication schedules were investigated to produce wrought ruthenium for mechanical evaluation. These are listed in Table 3 with pertinent remarks. The only successful schedule for fabricating powder metallurgy ruthenium was swaging at 1800 C with intermediate sintering at 2200 C. This was selected for fabrication of all ruthenium for mechanical property evaluation. The density of typical samples after this fabrication schedule was 99.5 per cent of ideal.

The results of fabrication studies of powder metallurgy ruthenium were not in total agreement with the work of Rhys,[1] who found high-purity ruthenium prepared from fine powders could be successfully fabricated by forging, rolling, or swaging at temperatures as low as 1400 C. This emphasizes the significance of the size and purity of starting materials on the ductility of ruthenium.

Electron-Beam Melting. Recognizing the desirability of metal purity in fabrication, sintered ruthenium bars were electron-beam melted to remove volatile contaminants and possibly effect additional purification by zone refining. The reduction in gaseous impurities by electron-beam melting was illustrated in Table 2. Significant reduction in metallic impurities is doubtful.

TABLE 3. FABRICATION SCHEDULES FOR HYDROGEN SINTERED RUTHENIUM (>90 Per Cent Ideal Density)

Schedule	Remarks
Cold work with frequent annealing (analogous to successful procedures for the fabrication of rhenium)	Failed after less than 8 per cent reduction of the diagonals of a square bar.
Rod rolling at 1500 C, 10 per cent reduction per pass	Intergranular cracking observed after 24 per cent reduction. Cracks enlarged with subsequent reduction.
Pack rolling (evacuated stainless steel containers) at 1200 C, 5 per cent reduction per pass	Broke into short pieces in the pack.
Swaged from hydrogen at 1400 C, 10 per cent reduction per pass	Major diagonal reduced 25 per cent before rod failed; no surface cracking.
Swaged from hydrogen at 1800 C, 10 per cent reduction per pass to 30 per cent reduction; resintered at 2200 C; swaging continued at 1800 C to 65 per cent total reduction	Some single cracks, but no extensive cracking observed. Products were suitable for mechanical evaluation.

One electron-beam-melted sample, connected to unmelted rod, was swaged through two dies at 1600 C, when fracture occurred at the melted sintered interface. Subsequent rod rolling of the melted section at 1600 C resulted in serious cracking.

A second piece of electron-beam-melted ruthenium was flat rolled to 85 per cent reduction at 1200 C, in an evacuated stainless steel jacket. The resulting strip was crack free but roughened from the non-uniform deformation of the stainless steel. This material showed the best fabricability of all the ruthenium that was studied. No additional studies of electron-beam-melted ruthenium were conducted because of the development of successful fabrication techniques with powder metallurgy bars, and the high cost entailed in electron-beam melting.

Osmium

Powder Metallurgy. Osmium bars, 1/4 x 1/4 x 6 inches, were pressed at 20 tsi using a CCl_4 binder and presintered one hour at 1200 C to provide material for sintering and fabrication studies. The results of progressive sintering of osmium bars was shown in Figure 2. Osmium, like ruthenium, densifies continuously with increasing temperature up to about 2400 C. Sintering at higher temperatures, 2700 C, resulted in low density, about 80 per cent of ideal. Additional studies showed osmium bars were 92 per cent of ideal density after five hours at 1800 C, but the densification was not improved by an additional 7 hours' sintering

at 1800 C. Osmium bars for fabrication studies were sintered 5 hours at 1800 C to achieve reasonably high density consistent with fine grain size, about 0.01 millimeter in diameter. A typical microstructure of osmium after sintering at 1800 C is shown in Figure 4.

Only two attempts were made to fabricate powder metallurgy osmium. Pieces of sintered bar were sealed in evacuated stainless steel jackets, and flat rolled 26 passes (at 5 per cent per pass) at 1200 C. The osmium broke into small pieces in each pack and sustained almost no deformation; all the deformation was absorbed in the stainless steel jacket.

A second osmium bar was sealed in an evacuated molybdenum capsule and swaged at 1750 C. Again the osmium showed little ductility during working and was completely fragmented when removed from the capsule. No further attempts were made to fabricate powder metallurgy osmium.

Electron-Beam Melting. A single powder metallurgy osmium bar was electron-beam melted, encapsulated in an evacuated molybdenum tube, and swaged at 1600 C through 26 dies (at 10 per cent reduction per die). The osmium was broken into small pieces during working but did sustain some deformation. This was manifested as the slipping of large sections of material on a single set of planes, similar to the classical picture for the slip of zinc or cadmium single crystals. A piece of the deformed osmium is shown in Figure 5. Studies of the fabricability of osmium were concluded at this point.

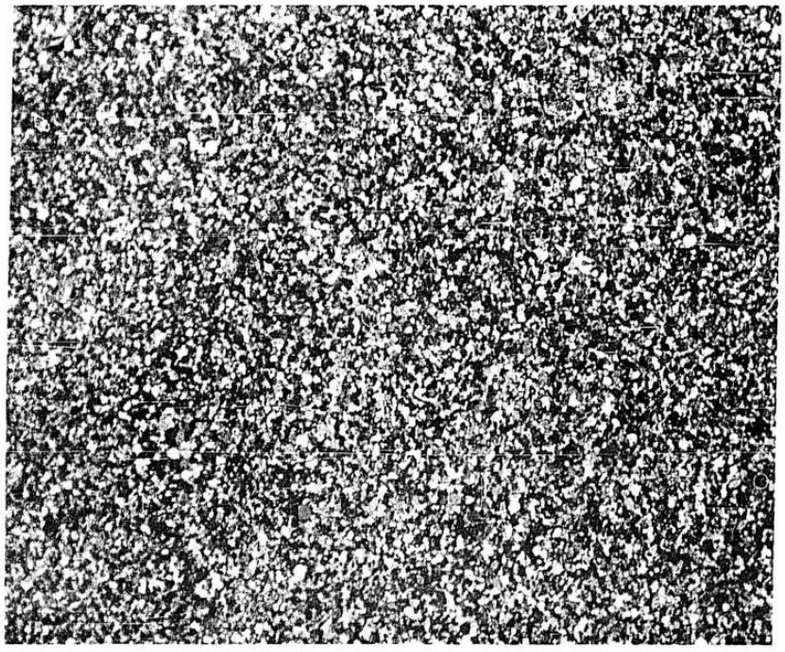

100X N57144

FIGURE 4. OSMIUM SINTERED 12.5 HOURS AT 1800 C

Os-1, polarized light, as polished.

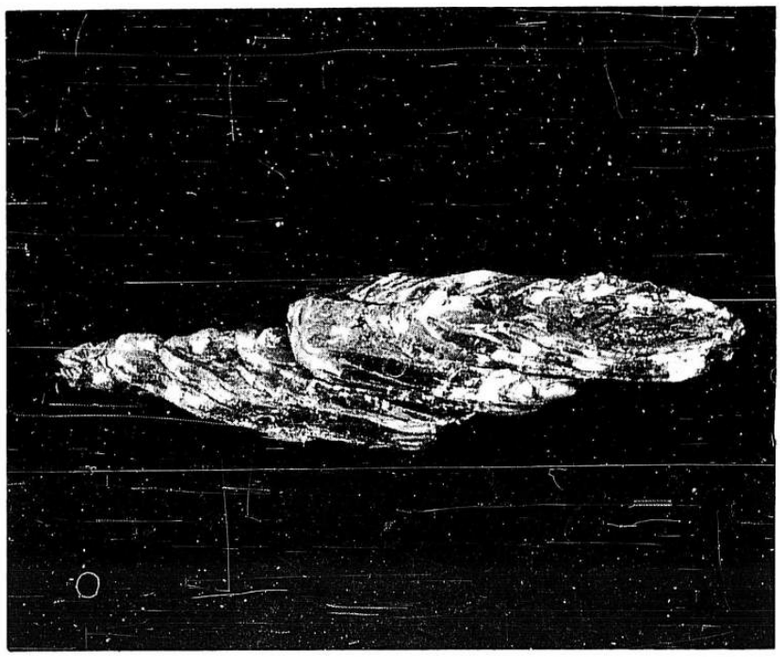

5X N62164

FIGURE 5. ELECTRON-BEAM-MELTED OSMIUM

Swaged at 1600 C (encapsulated in molybdenum).

Rhodium and Iridium

The initial stock of rhodium and iridium was supplied in wrought form; thus, subsequent fabrication, where necessary, was relatively straightforward. It was necessary, however, in several instances, to fabricate these metals from the as-melted condition. Melting was selected as a consolidation technique mainly because of lack of familiarity with powder-metallurgy techniques for these materials. The most suitable consolidation and fabrication techniques developed for rhodium and iridium are as follows: arc-melt on a "wire bar" copper crucible or drop-cast into a cylindrical copper mold to produce a cylindrical sample; swage the as-melted ingot at 1800 C, to a total of 20 per cent reduction in area, after which swaging is continued at successively reduced temperatures (the swaging temperature should be reduced roughly 100 C per three swaging dies, 10 per cent reduction per die). After sufficient reduction, a fibrous microstructure is developed resulting in improved ductility. At this point, it is possible to cold- or warm-work with intermediate stress-relief annealing. It is imperative, expecially in the case of iridium, that a large grained recrystallized structure be avoided after initial ingot breakdown is completed.

Arc-melted ingots of both rhodium and iridium can be hot forged and rolled or directly hot rolled; however, metal losses due to cracking during rolling are large during initial ingot breakdown. Metal recovery averaged about 50 per cent for direct hot rolling and 75 per cent for direct hot swaging. After ingot breakdown by either forging or swaging, both metals could be successfully hot rolled with little or no cracking.

Electron-beam-melted single crystals of both rhodium and iridium were cold-worked to determine the inherent ductility and fabricability of the metals. Single crystals of rhodium were cold-rolled and cold-swaged to approximately 90 per cent reduction without intermediate annealing. Iridium single crystals fractured after 20 to 30 per cent reduction by cold rolling. It is apparent from these results that grain boundary effects are highly detrimental to the ductility of rhodium. The ductility of iridium, although sensitive to grain boundary effects, appears to be inherently low or, more likely, very sensitive to small impurity concentrations. The factors influencing the ductility of these metals are discussed in greater detail later in this report.

A brief study was made of the sintering characteristics of powder metallurgy rhodium. Bars, 1/4 x 1/4 x 6 inches were pressed at 20 tsi with a CCl_4 binder, and presintered in hydrogen for one hour at 1200 C. Bars were then sintered progressively in hydrogen and vacuum at 1000 to 1700 C. The resultant variation of density with sintering temperature is illustrated in Figure 6. The maximum density, 85 per cent of ideal, was comparable to the density of ruthenium after a similar exposure, but lower than the density of osmium. Investigation of the sintering characteristics of rhodium was discontinued at this time because it was felt the results of further study would not justify additional effort in this area.

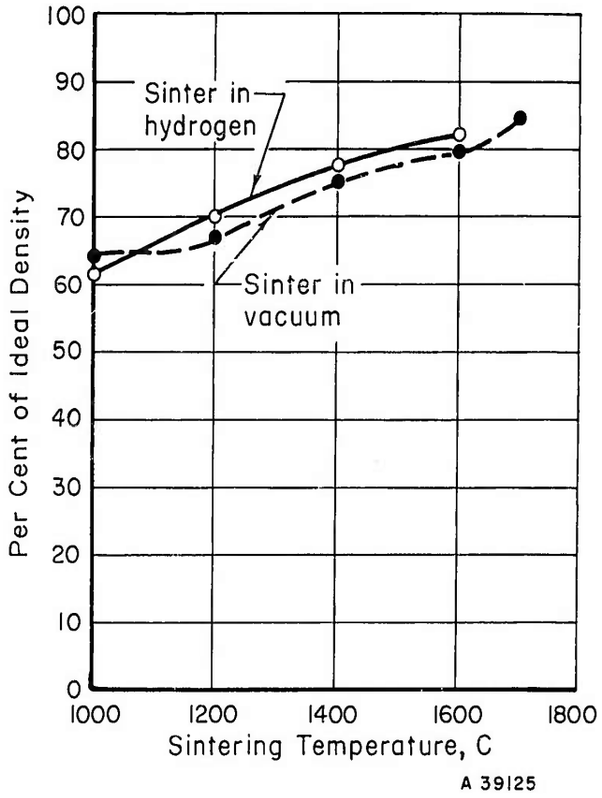

FIGURE 6. EFFECT OF SINTERING TEMPERATURE ON THE DENSITY OF RHODIUM

Sintering time 1 hour.

Annealing and High-Temperature Characteristics

The annealing characteristics, melting points, emissivities, and solid-state reactions of the platinum-group metals were investigated during the course of this program. Many of these studies, such as emissivity determinations, were brief, simply serving to supply information necessary for the performance of the major investigations.

Recrystallization Temperatures

The recrystallization temperatures of all the platinum-group metals, except osmium, were determined to aid in subsequent annealing treatments and also to identify the temperature range over which cold-work strengthening would be effective. The variation on the hardness of the worked metals with annealing temperature is shown in Figures 7 and 8. The annealing temperature for 50 per cent softening, and complete softening, of samples cold-worked to 50 per cent reduction, are listed below:

Metal	Condition	Softening Temp, C	
		50 Per Cent	Complete
Rhodium (commercial)	50 per cent warm worked (600 C)	650	800
Rhodium (electron-beam melted)	50 per cent warm worked (600 C)	700	800
Iridium (commercial)	50 per cent warm worked (900 C)	1200	1400
Ruthenium (electron-beam melted)	Worked 80 per cent at 1200 C	1175	1300
Platinum (commercial purity)	50 per cent cold worked	525	900
Palladium (commercial purity)	50 per cent cold worked	500	600

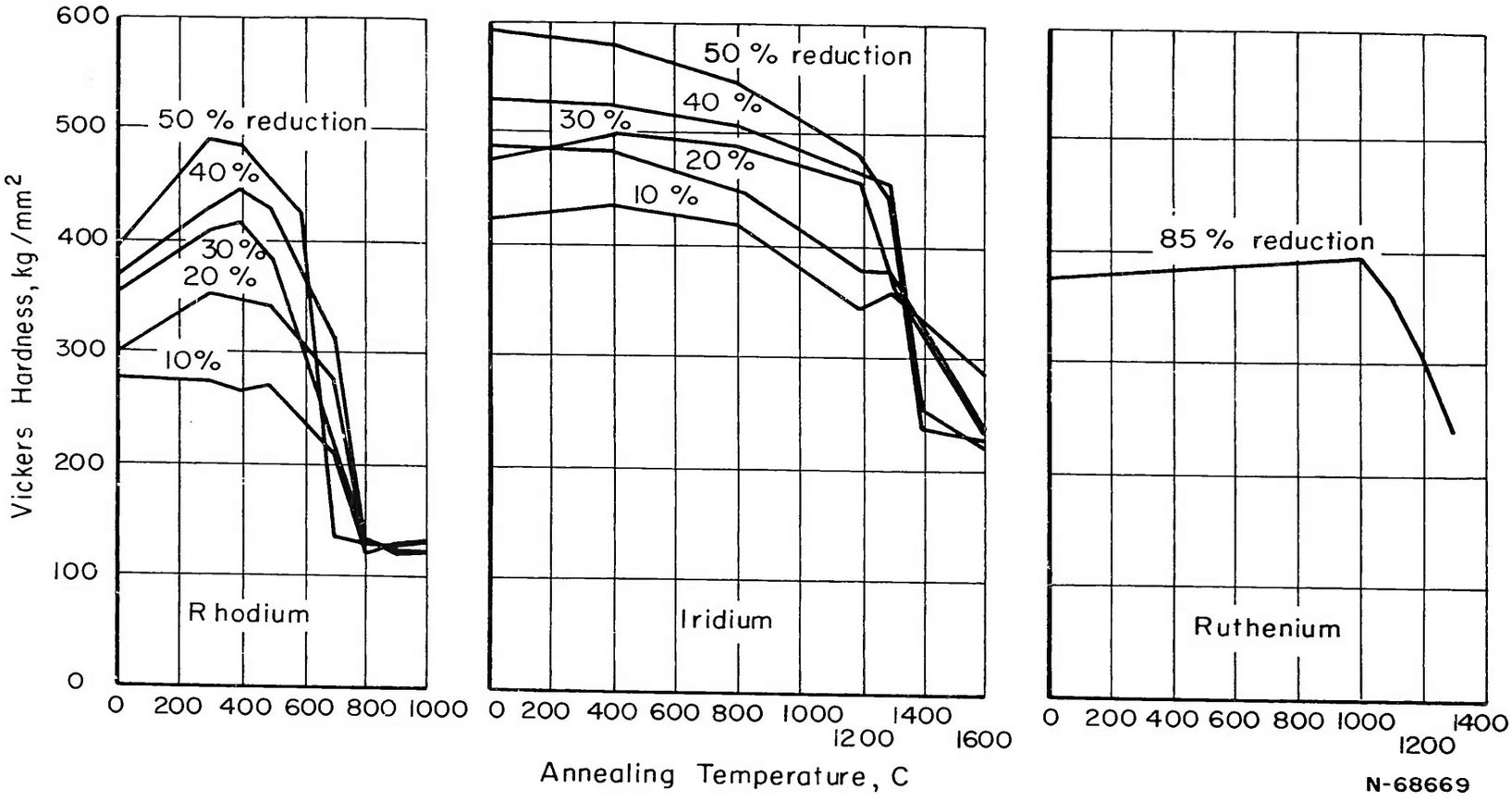

FIGURE 7. EFFECT OF COLD WORK ON THE SOFTENING BEHAVIOR OF THE REFRACTORY PLATINUM-GROUP METALS (5)

Annealing time, 1 hour.

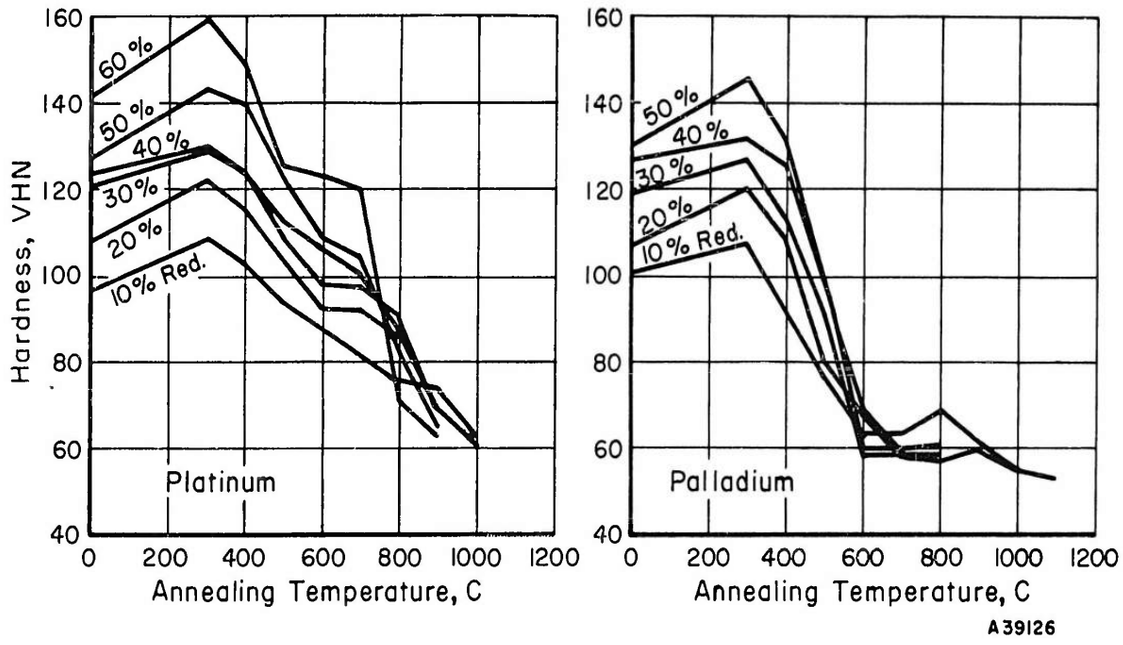

FIGURE 8. EFFECT OF ANNEALING TEMPERATURE ON HARDNESS OF PLATINUM AND PALLADIUM WARM ROLLED 10 TO 60 PER CENT REDUCTION

Annealing time 1 hour.

The recrystallization temperatures of the refractory platinum-group metals are high. Iridium and ruthenium are intermediate between molybdenum and tungsten, regarding recrystallization temperature, and, thus, would retain cold-work strengthening over a wide temperature range.

A striking feature of Figures 7 and 8 is the increase in hardness at low annealing temperatures found in platinum, palladium, and rhodium. Samples of chemically pure platinum and palladium were examined further to elaborate on this hardness variation. Softening curves for these metals are presented in Figure 9. Hardness peaks were not found in either high-purity metal. This was affirmed by careful examination of hardness variations at low annealing temperatures, 50 to 300 C (see Figure 10).

The data presented in Figure 9 show that the softening temperature of platinum and, perhaps, palladium is reduced by increasing the purity of the metal. The data for both metals are difficult to interpret because of the hardness variations at high annealing temperatures.

The hardness peaks in annealed rhodium also were examined in greater detail. A softening curve for electron-beam-melted rhodium, warm worked 50 per cent, showed no hardness peak at low temperatures, Figure 11. Careful study of hardness variations at low annealing temperatures did show signs of a hardness peak in another sample of electron-beam-melted rhodium swaged to 85 per cent reduction in area, as shown in Figure 12.

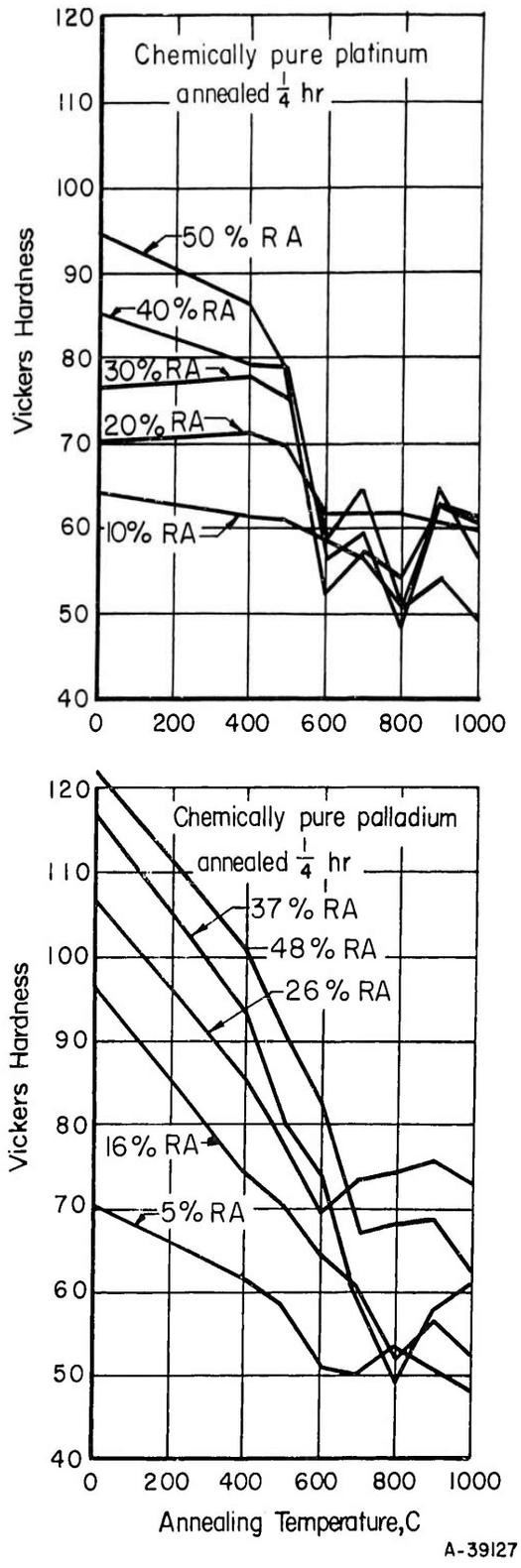

FIGURE 9. EFFECT OF ANNEALING TEMPERATURE ON THE HARDNESS OF COLD-ROLLED PLATINUM AND PALLADIUM

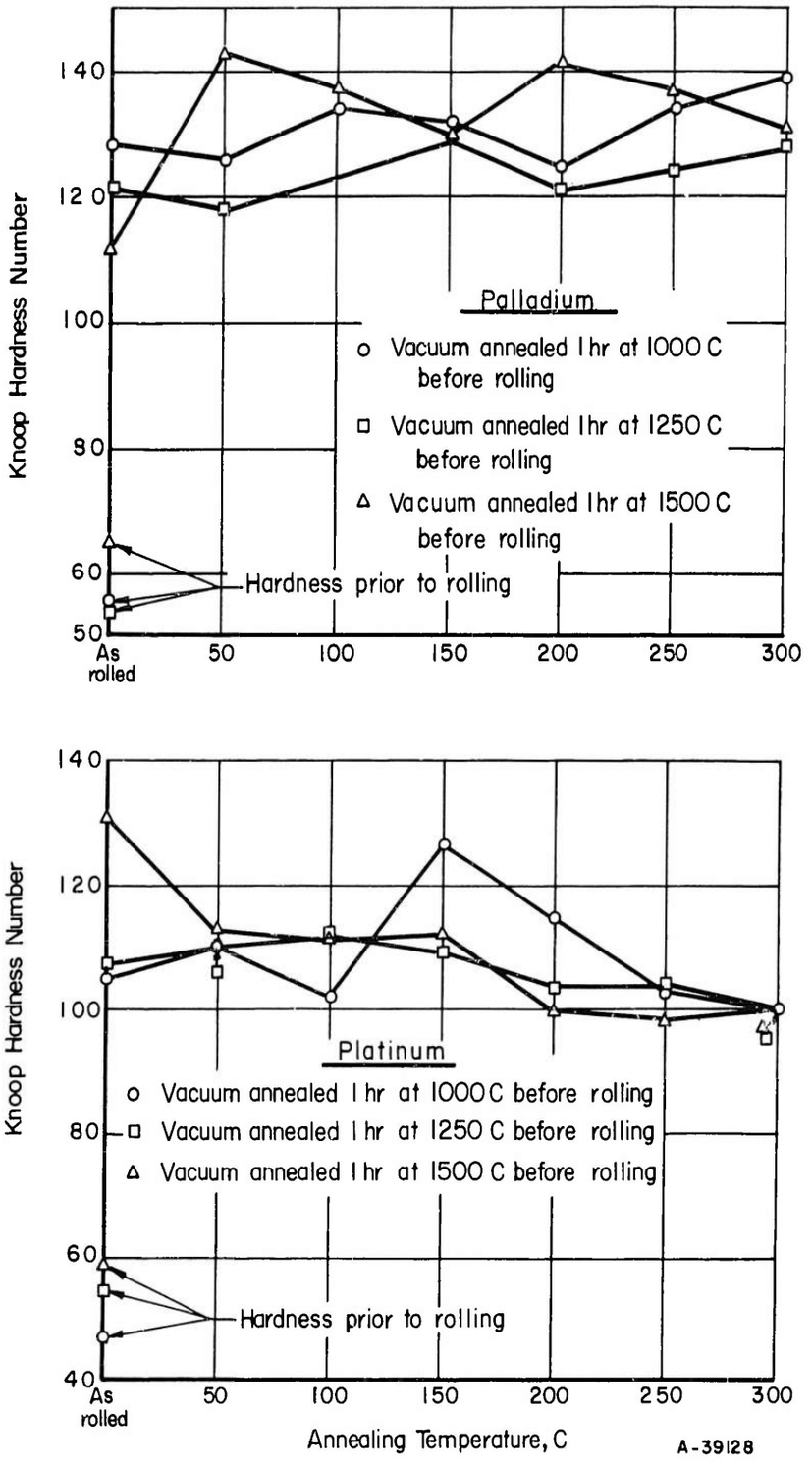

FIGURE 10. EFFECT OF ANNEALING TEMPERATURE ON THE HARDNESS OF CHEMICALLY PURE PLATINUM AND PALLADIUM COLD WORKED 50 PER CENT

Annealing Time 1 hour.

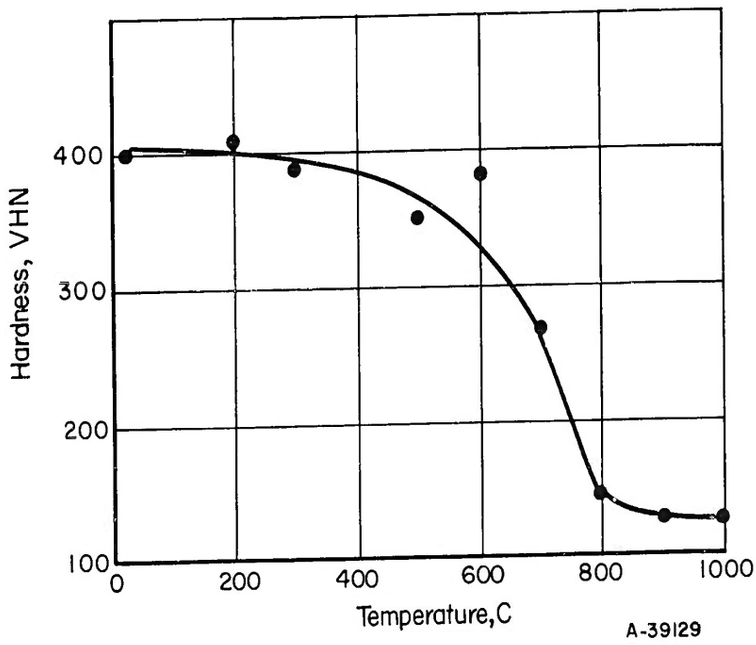

FIGURE 11. VARIATION OF HARDNESS WITH ANNEALING TEMPERATURE FOR ELECTRON-BEAM-MELTED RHODIUM, WARM WORKED 50 PER CENT

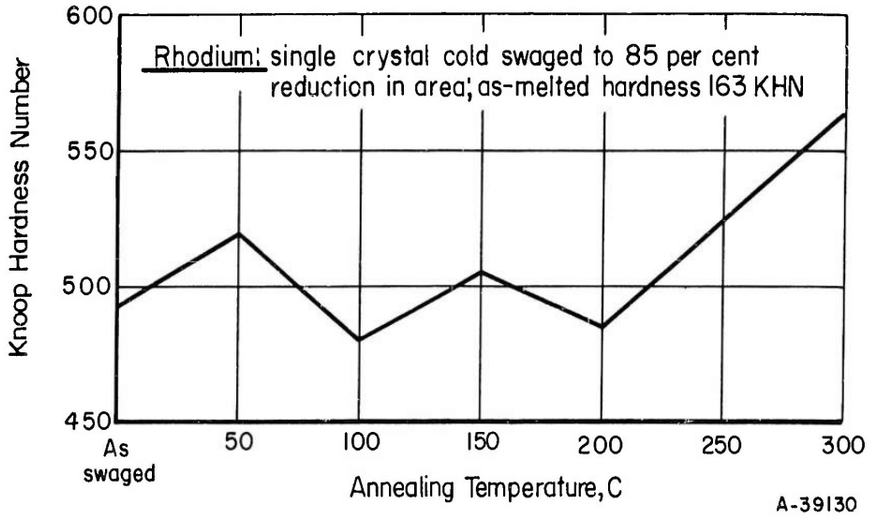

FIGURE 12. EFFECT OF ANNEALING TEMPERATURE ON THE HARDNESS OF COLD-SWAGED, ELECTRON-BEAM-MELTED RHODIUM

The results of these additional tests in rhodium are not incompatible. The data in Figures 7 and 8 showed the hardness peaks were sensitive to cold work, increasing the magnitude with increasing cold work. It is likely that working electron-beam-melted rhodium to 50 per cent reduction was not sufficient to activate the hardening mechanism, whereas, with additional working, some hardening was observed.

The hardening mechanism is not entirely clear at the present time. The hardening is attributed to a strain-aging mechanism in accordance with the observed dependence of hardening upon temperature, purity, and deformation. The active impurities have not been identified, but substitutional rather than interstitial impurities are suspect. This is supported by the similar gas contents of the two grades of platinum that were examined. Gas contents in ppm of the chemical purity and commercial purity platinum are: O_2:5, H_2:0.5 and O_2:5, H_2:0.1, N_2:<2, respectively. The strain-aging behavior could not be eliminated in rhodium although the gas content of rhodium is reduced significantly by electron-beam refining, as shown in Table 2. This last point could stand additional confirmation as there is no doubt that electron-beam refining retarded the hardening mechanism in rhodium.

These hardness peaks in softening curves for platinum, palladium, and rhodium were manifested as strain rate and temperature sensitivity in tensile property investigations. This will be discussed later in this report.

Melting Temperatures

During a study of the sintering characteristics of osmium and ruthenium discrepancies in the previously accepted melting points of the metals were noted. The melting temperatures had not been measured at the time of the work, but were estimated in the literature as 2700 C for osmium and 2450 C for ruthenium.[2] A recent investigation by Baird[3] has shown the melting temperatures of osmium and ruthenium are 3000 and 2250 C, respectively. In the present work, osmium bars sintered at temperatures as high as 2900 C showed no evidence of melting, whereas ruthenium showed definite evidence of melting at temperatures as low as 2250 C. In view of the apparent discrepancies, the melting temperatures of both metals were determined.

Powder metallurgy bars were self-resistance heated in a vacuum sintering bell. Temperatures were measured with an L & N disappearing filament optical pyrometer. True temperatures were read at the base of a 0.30-inch-diameter, 0.150-inch-deep hole drilled into the center of a presintered bar. Apparent temperatures were read from the surface of the bar adjacent to the hole.

The melting temperature of the metals was determined as the temperature at which a slight additional increase in current through the specimen resulted in a reduced temperature at the base of the hole. The apparent reduction in temperature is a result of liquid metal filling the hole, thus altering the black-body conditions. The melting points of osmium and ruthenium, based on three determinations for each metal by this technique, are 3010 ±10 and 2250 ±10 C, respectively. These are in close agreement with the values determined by Baird.[3]

Spectral Emissivities

The spectral emissivities of osmium and ruthenium were determined to aid in temperature measurement during annealing. Apparent and true temperatures were measured during sintering runs for each metal, by the method described previously. These data are presented graphically in Figures 13 and 14.

The straight lines described by the data were calculated by the least squares method. Equations of these lines are:

$$T_{app} = 0.840\ T + 157.8 \text{ Osmium}$$

$$T_{app} = 0.817\ T + 172.0 \text{ Ruthenium}$$

where the temperature is in degrees Kelvin. Applying Wein's law to the true and surface temperatures, and taking the ratio of radiant intensities from each source,[4] the following relations are derived for the spectral emissivities of osmium and ruthenium:

$$\text{Osmium} \qquad \log \epsilon_{\lambda = 0.655} = 9510 \left[\frac{157.8 - 0.160\ T}{T\ (0.840\ T + 157.8)} \right]$$

$$\text{Ruthenium} \qquad \log \epsilon_{\lambda = 0.655} = 9510 \left[\frac{172.0 - 0.183\ T}{T\ (0.817\ T + 172.0)} \right]$$

The variation of emissivity with temperature, calculated from these equations is illustrated in Figure 15. Both curves show an emissivity minimum at 2060 and 1910 K, for osmium and ruthenium, respectively. These minima are a result of substituting a straight line relation into the expression for spectral emissivity; however, the straight line relations are certainly supported by the data.

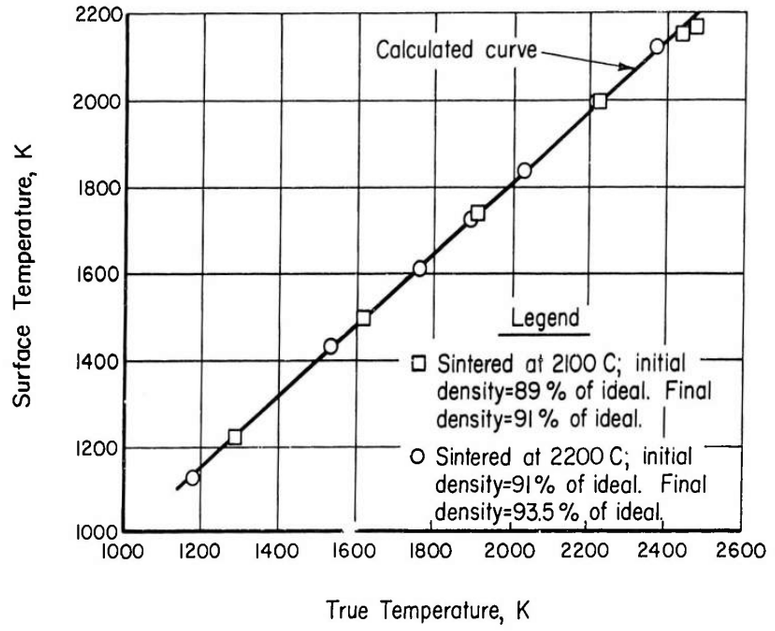

FIGURE 13. RELATION OF APPARENT TEMPERATURE TO BLACK-BODY TEMPERATURE FOR RUTHENIUM

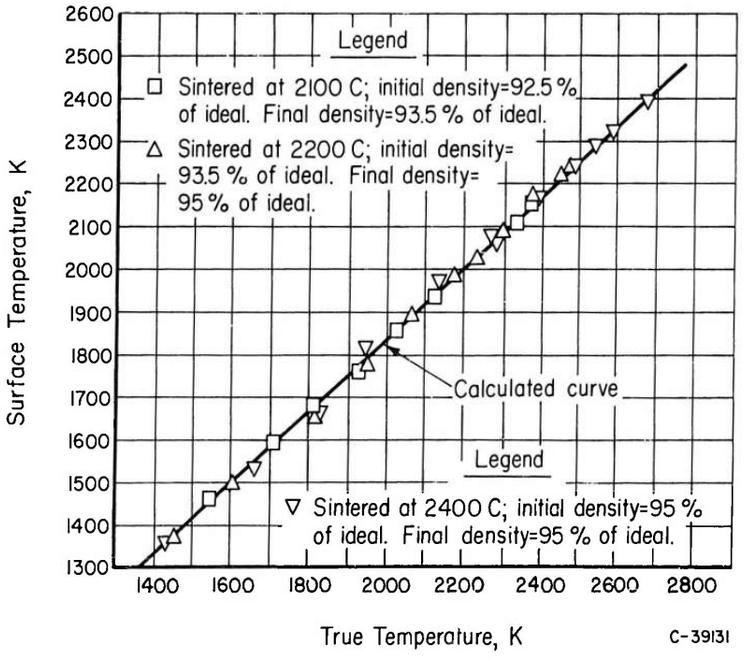

FIGURE 14. RELATION OF APPARENT TEMPERATURE TO BLACK-BODY TEMPERATURE FOR OSMIUM

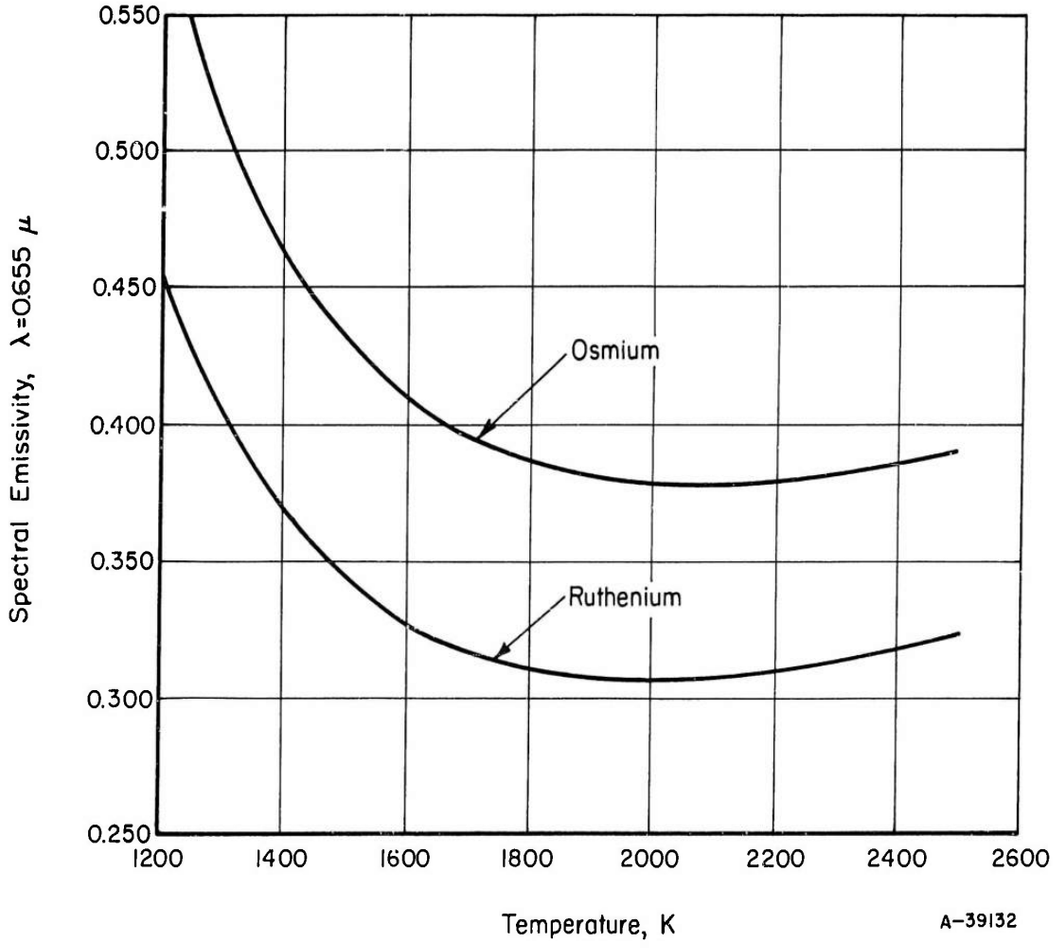

FIGURE 15. EFFECT OF TEMPERATURE ON THE EMISSIVITY OF RUTHENIUM AND OSMIUM

Compatability Studies

The high annealing and fabrication temperatures encountered with the platinum-group metals, and the lack of constitution data for these metals with other elements, led to many problems in the selection of containers for high-temperature treatments.

Seven common container materials, alumina, thoria, zirconia, graphite, molybdenum, tungsten, and tantalum, were considered. Small specimens of rhodium, iridium, and ruthenium were exposed for 3 hours at 1800 C in a hydrogen atmosphere in intimate contact with each of the selected materials. The refractories were in the form of high-purity, readily available powders, while the metals were either wire or thin foil. Of the nonmetals, only graphite showed no reaction with rhodium, iridium, ruthenium during exposure. This was ascertained by visual and metallographic examination. The rhodium appeared to have melted in contact with both alumina and thoria and was tightly bonded to a heavy layer of zirconia. Ruthenium also melted in contact with thoria and zirconia and had a hard alumina coating. Iridium was melted on contact with thoria and had hard coatings of zirconia and alumina. All of the oxides were densified as a result of exposure. The exact reactions responsible for these results were not determined. The oxide were of high purity, the silica content of the thoria and zirconia was less than 0.1 per cent. The analysis of the alumina is not known.

No melting occurred during exposure of the metals in contact with tantalum, molybdenum, and tungsten. There was, of course, some diffusion bonding, but, in each case, the container metal could be

stripped from the specimen by hand. Subsequently, rhodium, iridium, and ruthenium wrapped in tantalum foil were exposed 5 hours at 1900 C in vacuum. The tantalum-ruthenium sample melted during the exposure; however, tantalum-iridium and tantalum-rhodium showed only slight diffusion bonding.

These brief compatability studies provided the necessary information for selection of containers for most annealing treatments. In two cases, the results were misleading and led to specimen contamination. Rhodium samples, exposed at 1800 C in a hydrogen atmosphere for hot working, melted locally in contact with a molybdenum boat. This melting appeared to result from rhodium being in contact with both molybdenum and alumina sand from the refractory muffle. When the molybdenum boats were kept clean of foreign elements, especially alumina sand, no melting or bonding was observed.

In another case, rhodium in contact with molybdenum for 12 hours at 1650 C in hydrogen formed a liquid phase, that destroyed sections of the molybdenum boat. The rhodium-molybdenum contact area was less than 0.02 square inch and was free of foreign particles. No explanation can be given for this results.

Mechanical Property Evaluation

At the start of this work, virtually no information was available describing the mechanical properties of the refractory platinum-group metals. An exploratory study was conducted to establish strength-temperature relationships and deformation characteristics. Additional

studies, designed to elaborate on the results of the exploratory studies, were also conducted. These included investigations of strain and structure sensitivity, fracture initiation and propagation characteristics, and deformation systems. An attempt will be made here to give an integrated picture of the mechanical behavior of the metals.

Tensile Properties

Temperature Effects. The tensile properties of the five fabricable metals were determined in the range -196 to 1000 C in air. The vacuum tensile properties of rhodium, iridium, and ruthenium were determined in the range 750 to 1500 C. Tensile data are tabulated in Tables 4 and 5 and are presented graphically in Figures 16 through 21. The average grain sizes of the high-purity rhodium, iridium, and ruthenium were 0.26, 0.037, and 0.08 millimeter in diameter, respectively.

The strengths of the metals at moderate and high temperatures compare roughly as the melting points. At low temperatures, strength-temperature variations are more complex. The tensile strengths of platinum, palladium, and iridium do not decrease uniformly over the entire temperature range as would be expected. Tensile strength remains constant or increases slightly going from room temperature to 250 C. Similar behavior is observed in the yield strength variation of rhodium. Yield point phenomena were observed in commercial purity platinum and palladium at low temperatures, as indicated in Table 4. These anomalies are considered manifestations of the strain-aging behavior found in softening curves for most of the metals.

TABLE 4. TENSILE PROPERTIES OF THE PLATINUM-GROUP METALS IN AIR

Temp, C	Ultimate Tensile Strength, psi	Proportional Limit, psi	0.2% Offset Yield Strength, psi	Reduction of Area, per cent	Remarks
	Ruthenium, Sintered, Swaged 10% at 1400 C, Annealed 1 Hour at 1400 C				
750	34,400	--	--	0	Fractured in elastic range
1000	30,600	26,000	--	0	Fractured prior to 0.1% plastic strain
	Ruthenium, Sintered, Swaged 30% at 1800 C, Annealed 1 Hour at 1400 C				
750	42,400	26,600	32,200	0.1	
1000	31,400	26,900	28,600	12	
1200	>19,000	--	--	--	Pulled out of grips
	Rhodium, As-Received (High Purity), Annealed 1/4 Hour at 900 C				
-196	125,000	9,210	13,300	27.8	
25	102,500	7,170	9,670	22.5	
250	88,500	10,800	13,780	59,4	
500	48,800	8,380	10,900	32.4	
750	16,950	3,410	5,820	~90	
1000	12,320	3,500	4,930	--	Severe surface cracking noted
	Rhodium, Electron-Beam Melted, Swaged 80% at 900 C, Annealed 1/4 Hour at 800 C				
-196	149,000	46,800	53,400	--	
25	110,100	34,000	38,500	42	
250	91,000	37,400	41,500	55	
500	61,800	35,800	42,500	35	
750	32,600	31,500	--	~100	
1000	12,860	3,120	4,370	35	Slight surface cracking noted
	Palladium, As-Received (Commercial Purity), Annealed 1/4 Hour at 700 C				
-196	62,700	9,940	13,700[a]	80.7	
25	39,350	8,530	12,800	93.3	
250	42,000	13,250	13,250[a]	88	
500	9,990	5,990	7,550	98.1	
750	3,940	1,725	2,385	~99	
1000	1,840	572	700	--	Double neck observed
	Palladium, As-Received (Chemically Pure)				
-196	67,400	55,100	57,700	95	Specimens inadvertently tested in a
250	40,800	33,300	40,400	96	wrought condition
500	25,950	22,000	25,100	98	
	Iridium, As-Received (Commercial Purity), Annealed 1/4 Hour at 1350 C				
-196	57,900	14,700	18,700	3.5	Severe cracks
25	64,700	7,950	13,280	7.7	Ditto
250	72,200	9,370	12,750	8.9	"
500	27,900	9,510	13,400	8.4	"
750	47,200	8,970	11,180	62,8	"
1000	31,100	27,500	28,600	47.0	"
	Iridium, As-Received (High Purity), Annealed 1/4 Hour at 1500 C				
-196	103,200	--	--	--	Failed in threads
25	90,300	31,600	33,900	6.8	
250	102,000	37,200	41,800	11	
500	76,800	28,900	34,000	12.7	
750	65,000	15,300	20,600	51.0	Repeated yielding
1000	48,000	--	6,300	80.6	Ditto

TABLE 4. (Continued)

Temp, C	Ultimate Tensile Strength, psi	Proportional Limit, psi	0.2% Offset Yield Strength, psi	Reduction of Area, per cent	Remarks
	Iridium, Electron-Beam Melted, Swaged 80% at 1500 C, Annealed 1/4 Hour at 1500 C				
25	107,000	64,100	68,600	0	
500	78,100	50,300	55,200	7.6	
750	64,000	46,400	53,100	45.3	
1000	43,100	3,780	9,080	72.2	
	Platinum, As-Received (Commercial Purity), Annealed 1/4 Hour at 900 C				
-196	75,300	41,900	45,150	93.3	
25	35,500	22,800	22,800[a]	93.8	
250	34,300	19,200	19,200[a]	94.4	
500	16,300	10,720	12,250	97.5	
750	9,730	6,260	6,800	99.0	
1000	3,380	1,530	2,230	~100	
	Platinum, As-Received (High Purity), Annealed 1/4 Hour at 900 C				
-196	55,600	21,900	27,000	80	
25	19,650	5,800	7,100	96	
250	15,800	3,980	4,950	96.5	
500	11,100	2,630	4,200	~100	
750	6,300	--	--	99	

(a) Value given is stress at upper yield point.

TABLE 5. VACUUM TENSILE-TEST DATA FOR RHODIUM, IRIDIUM, AND RUTHENIUM

Specimen	Test Temp, C	Ultimate Tensile Strength, psi	0.2% Offset Yield Stress, psi	Reduction in Area, per cent	Elongation, per cent
Rh 3-1[a]	750	48,700	15,360	85	29
Rh 3-11[a]	1000	16,950	6,900	100	61
Rh 3-12[a]	1250	8,900	3,640	100	--
Ir 3-15[b]	1000	56,000	31,100	66	35
Ir 3-17[b]	1000	41,900	14,300	31	20
Ir 3-16[b]	1250	39,200	23,400	69	37
Ir 3-18[b]	1250	35,200	10,700	58	11
Ir 3-19[b]	1500	22,600	11,600	42	71
Ru 3-13[c]	1000	61,000	46,700	20	10[d]
Ru 3-14[c]	1250	28,500	25,500	10	4[d]
Ru 3-12[c]	1500	15,560	13,900	3	4[d]

(a) Annealed 1/4 hr at 900 C.
(b) Annealed 1 hr at 1500 C.
(c) Annealed 1 hr at 1400 C.
(d) Measured from change in total length divided by the length of the reduced section.

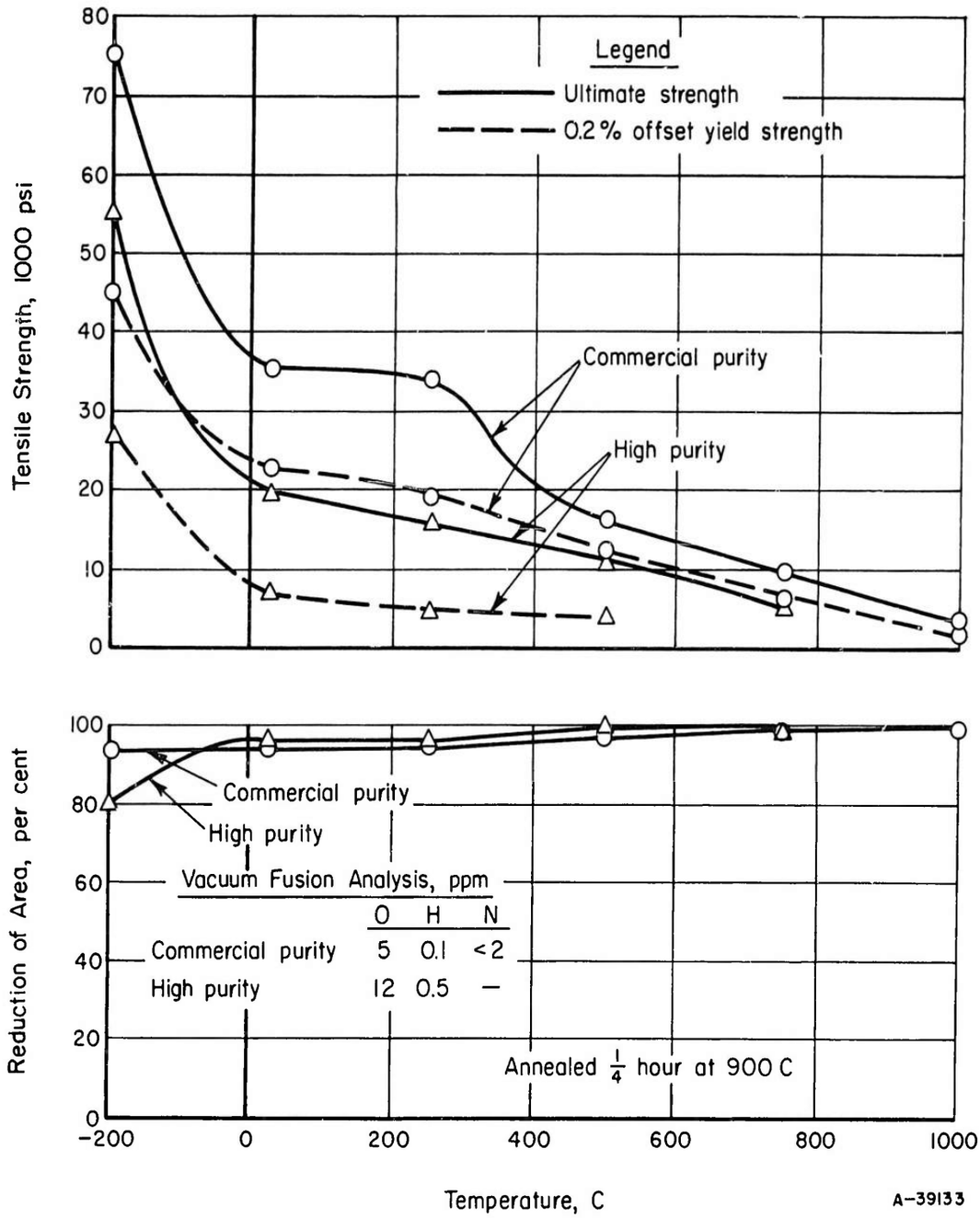

FIGURE 16. EFFECT OF TEMPERATURE ON THE TENSILE PROPERTIES OF ANNEALED PLATINUM

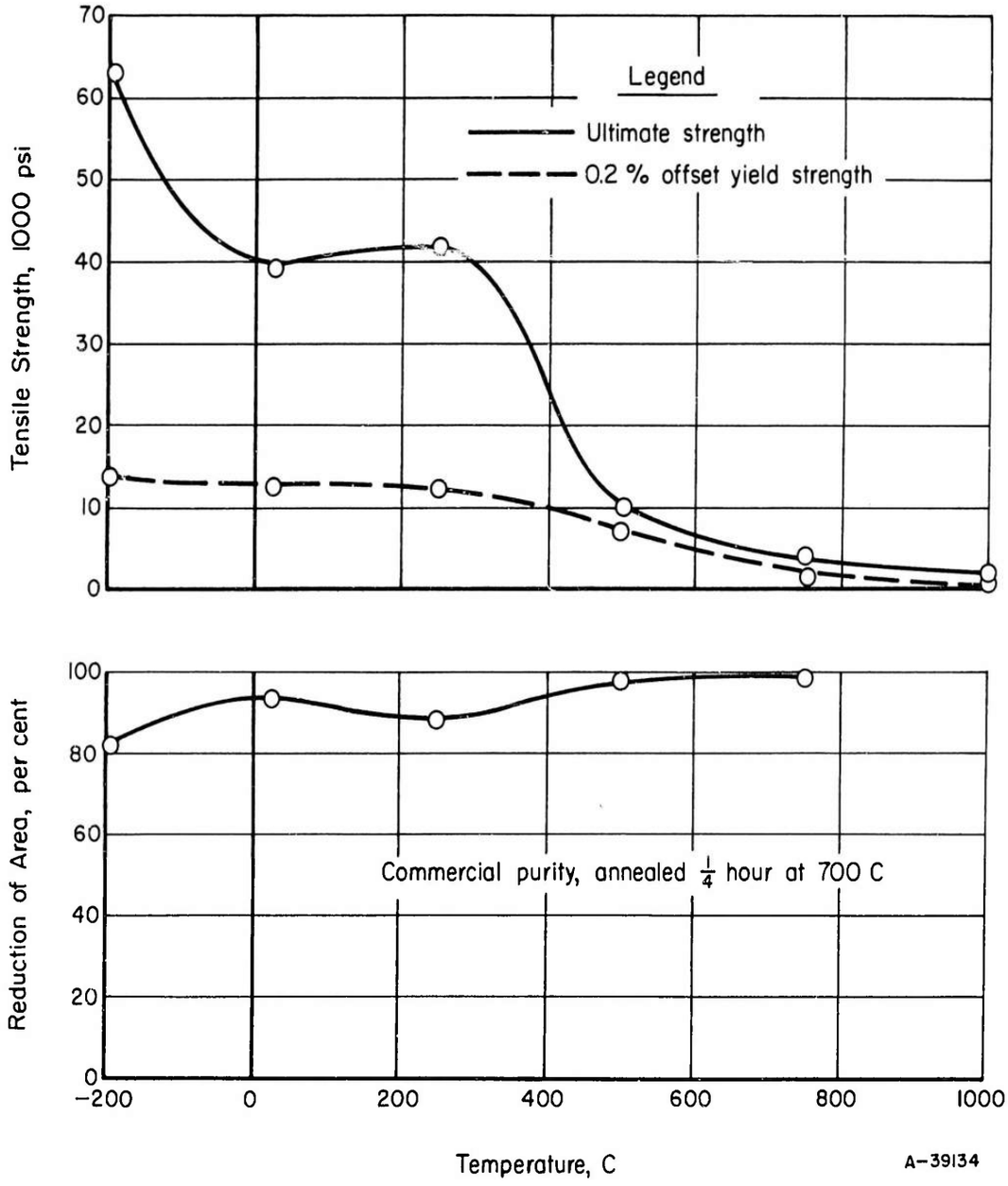

FIGURE 17. EFFECT OF TEMPERATURE ON THE TENSILE PROPERTIES OF ANNEALED PALLADIUM

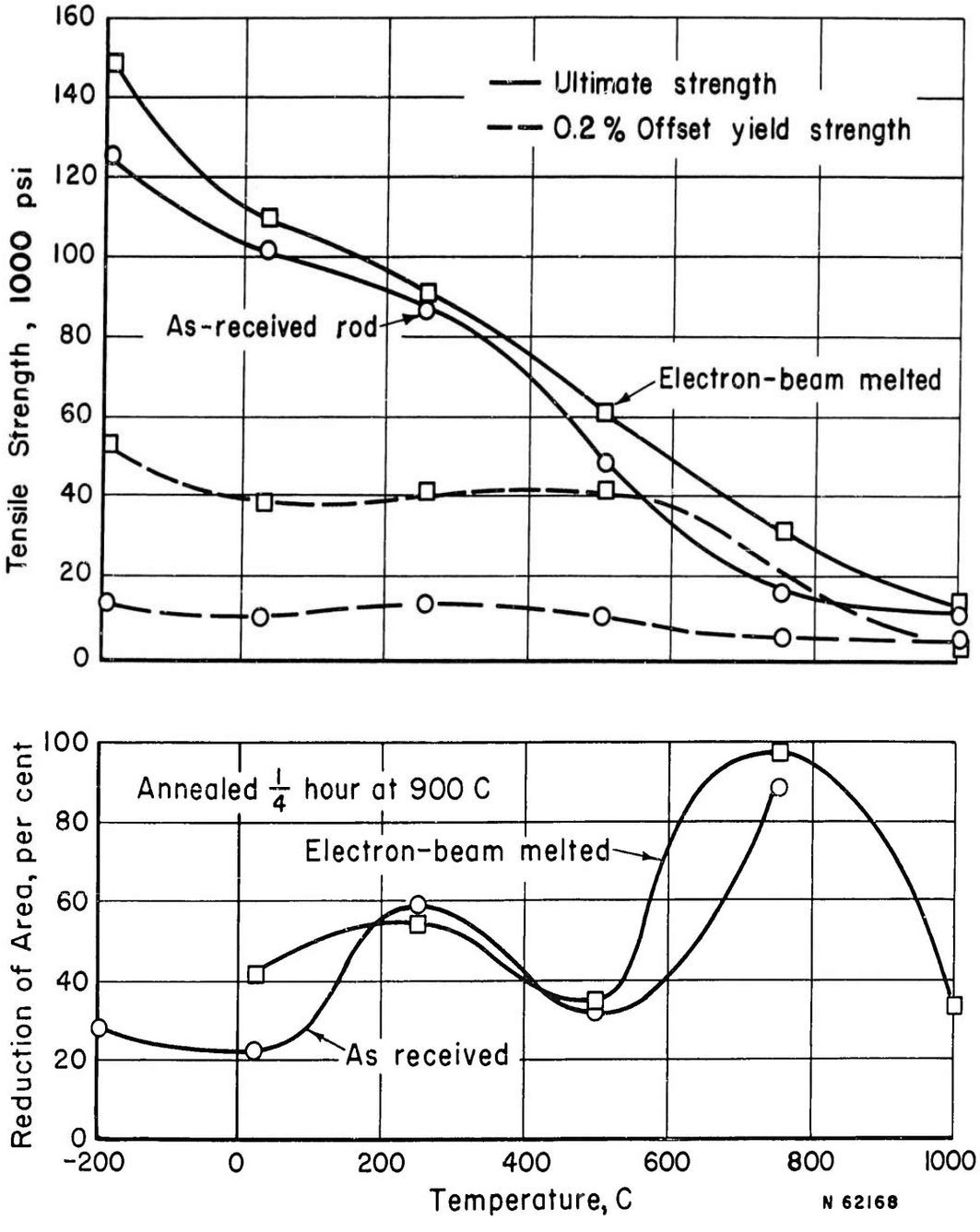

FIGURE 18. EFFECT OF TEMPERATURE ON THE TENSILE PROPERTIES OF ANNEALED RHODIUM

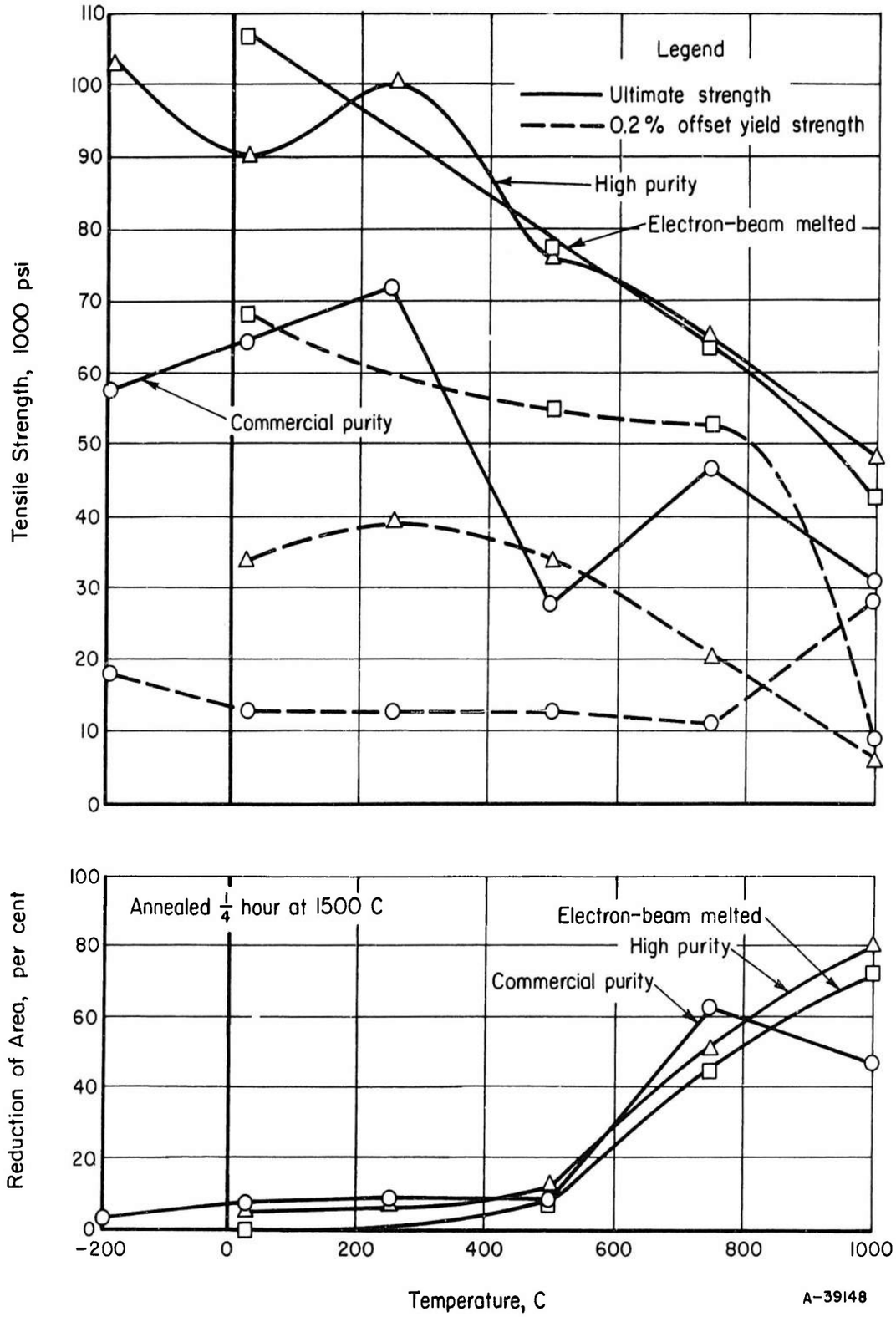

FIGURE 19. EFFECT OF TEMPERATURE ON THE TENSILE PROPERTIES OF ANNEALED IRIDIUM

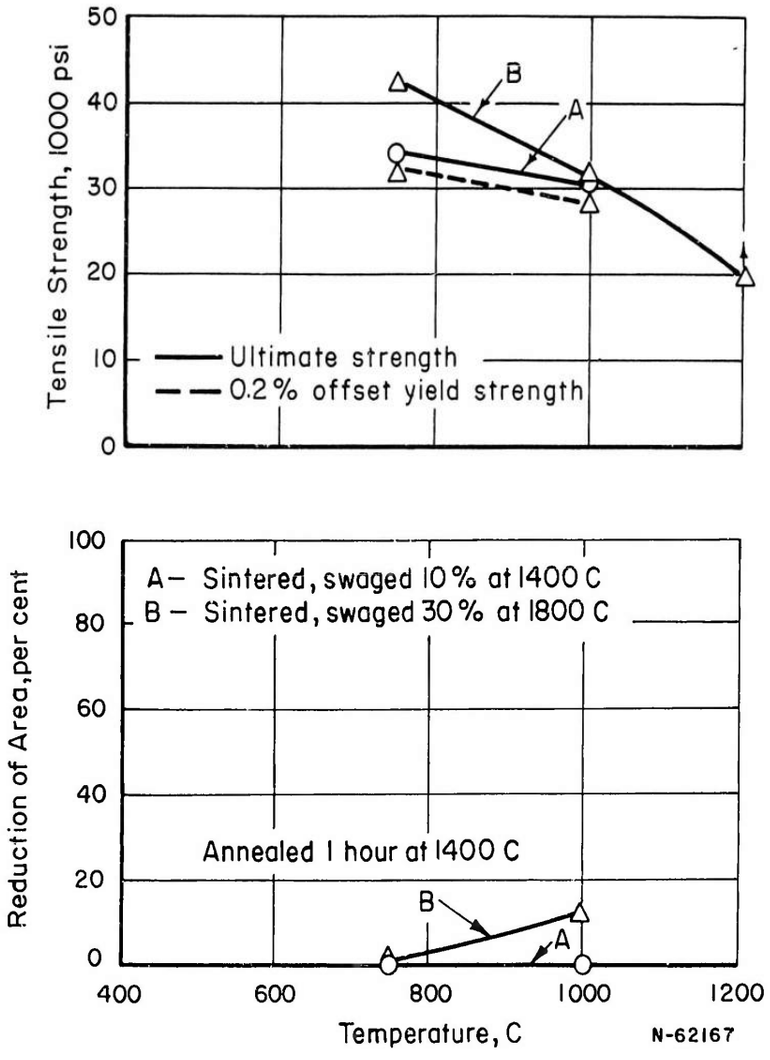

FIGURE 20. EFFECT OF TEMPERATURE ON THE TENSILE PROPERTIES OF ANNEALED RUTHENIUM

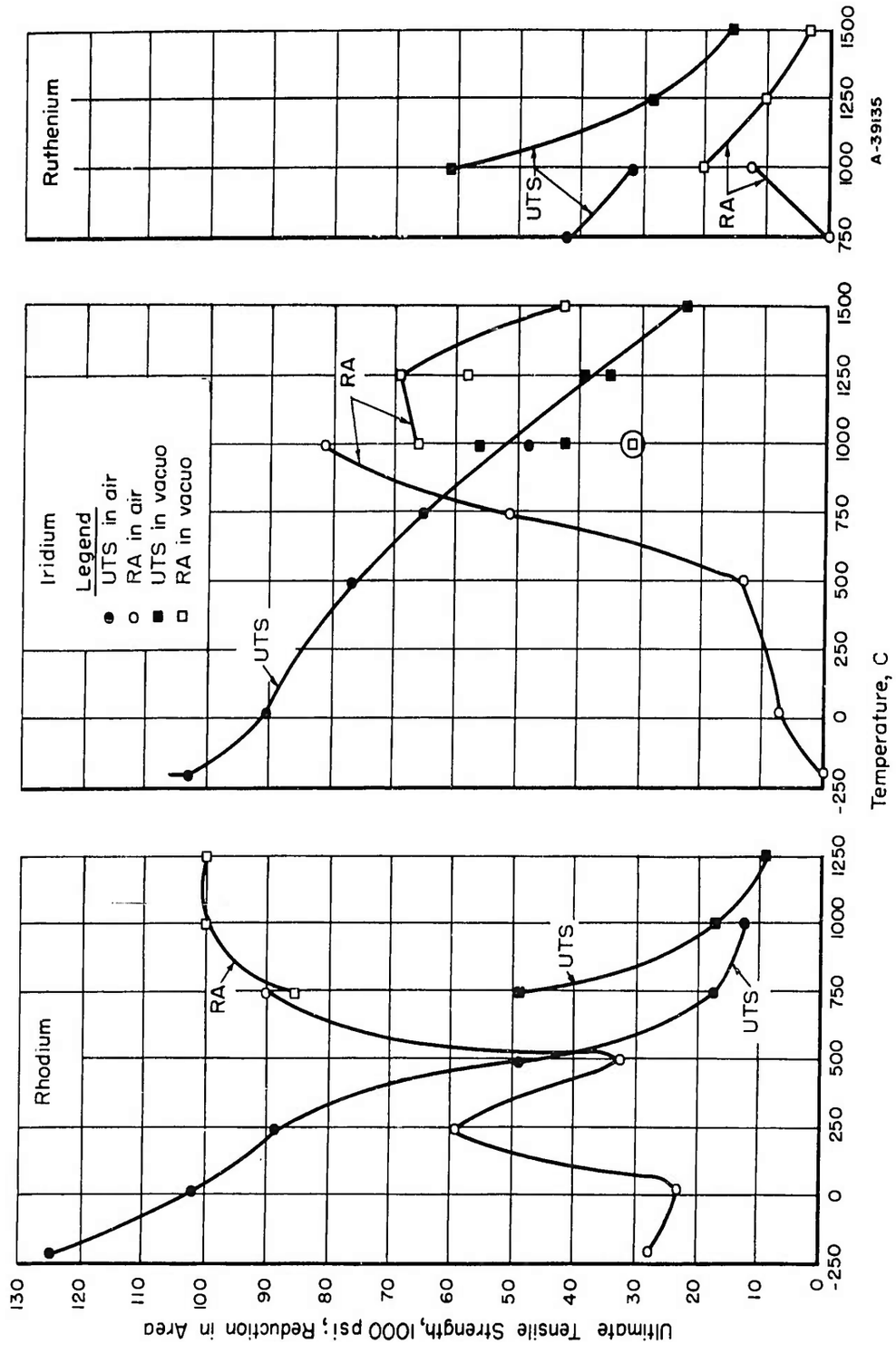

FIGURE 21. EFFECT OF TEMPERATURE AND TESTING ATMOSPHERE ON THE TENSILE PROPERTIES OF RHODIUM, IRIDIUM, AND RUTHENIUM

The strength of rhodium and iridium appear sensitive to purity, but in an inverse way. As gas and substitutional impurity levels are reduced, the flow stress is increased, This is observed over a wide temperature range and is not likely a result of scatter or experimental technique.

The data for commercial iridium illustrate the necessity for sound, crack-free material in studying brittle materials. The strength variations for this material are due almost entirely to internal defects.

The ductility of the metals is of particular interest. Ordinarily, face-centered cubic metals have high ductility and a high tolerance for impurities. Platinum and palladium conform to this generalization; however, rhodium and iridium are characterized by moderate and low ductility, respectively. The range of impurity levels covered in this program had no significant effect on the ductility of these metals.

Metallographic examination showed rhodium failed by intergranular cracking at -196 and 25 C and iridium failed partially or completely by intergranular fracture over the entire temperature range, -196 to 1500 C. Examples of intergranular failure are shown in Figure 22. Ruthenium, another low-ductility metal, also failed by intergranular failure in all tensile tests.

The tensile data shown in Figure 22 suggest the strength of rhodium and ruthenium may be influenced by testing atmosphere. Strengths are higher in vacuum than in air,at temperatures where comparable data are available. The strength increase of rhodium is associated with a retardation of recrystallization in the vacuum tested sample. The

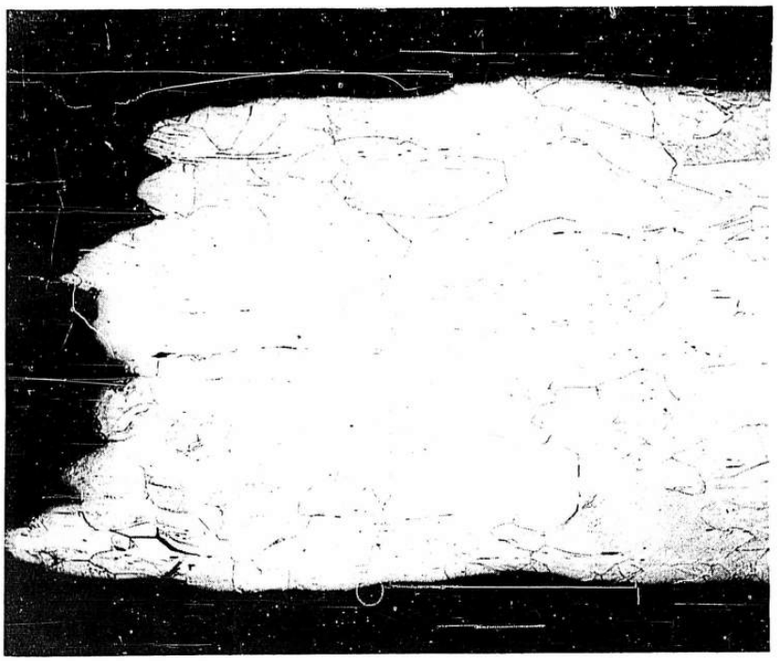

45X N57901

a. Rhodium, Annealed 1 Hour at 900 C, Tensile Test at 25 C

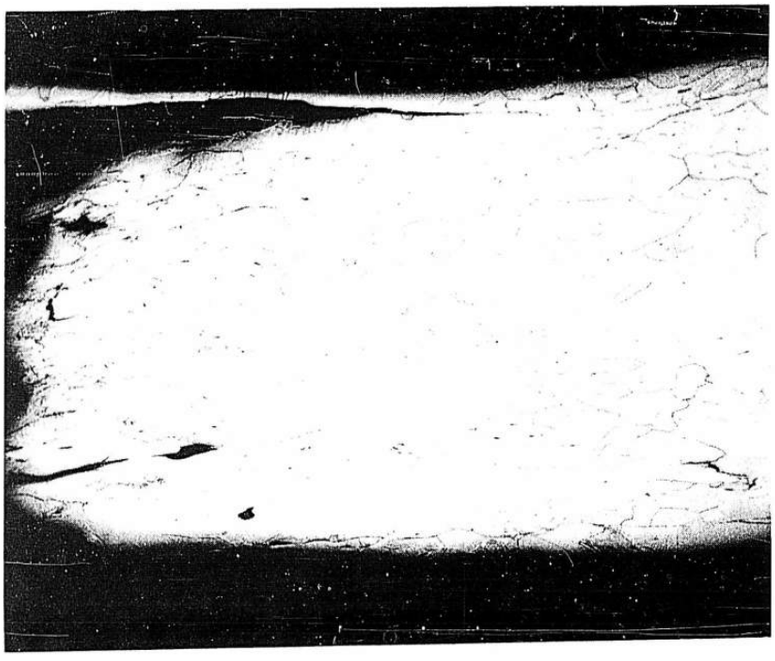

45X N57898

b. Iridium, Annealed 1 Hour at 1500 C, Tensile Test at 500 C in Air

FIGURE 22. INTERGRANULAR FRACTURE IN RHODIUM AND IRIDIUM TENSILE SPECIMENS

atmosphere effect in ruthenium could not be correlated with microstructure. The reduction in the ductility of iridium above 1000 C, Figure 22, is associated with an increased tendency toward intergranular failure. The reduction in ductility of ruthenium above 1000 C could not be correlated with microstructure.

Metallographic examination of broken tensile specimens revealed signs of deformation twinning. Temperature ranges where twinning was observed are as follows:

Rhodium	-196 to 500 C
Iridium	-196 to 500 C
Platinum	-196 to 25 C
Palladium	-196 to 250 C
Ruthenium	750 to 1000 C

Examples of what appears to be deformation twins in rhodium and iridium were shown in Figure 22. The twinning was not examined by other techniques.

The tensile data obtained for the platinum-group metals are of additional value when compared with comparable data for other metals. A comparison of the strengths of several high-melting metals is shown in Figure 23. The high-melting platinum-group metals are stronger than the well-known refractory metals. This may be related in part to a higher intrinsic strength of close-packed lattices. Platinum and palladium, both close-packed elements, however, do not compare favorably on a strength basis with the refractory metals.

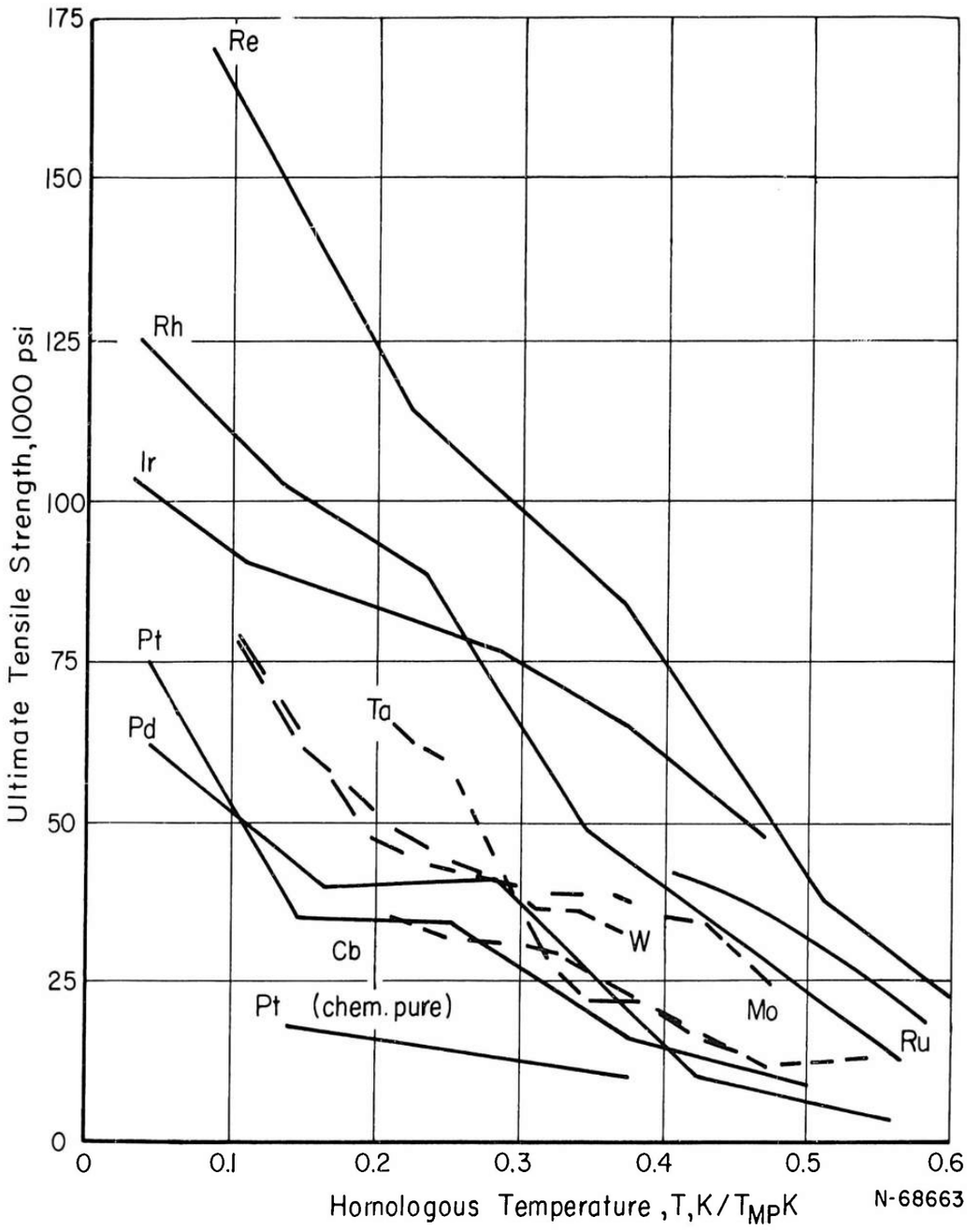

FIGURE 23. TENSILE STRENGTH VERSUS TEMPERATURE FOR ANNEALED REFRACTORY METALS [5]

The strengths of the platinum-group metals are compared with several face-centered cubic metals in Figure 24. The strength ranking of the metals is roughly in line with melting points except for platinum and palladium, which are considerably weaker than would be expected. The reason for this is not apparent.

The comparisons shown in Figures 23 and 24 must be considered in light of variations in purity, grain size, and strain rate. Nevertheless, it appears that the strength of rhodium and iridium agree with predictions based upon melting points; whereas, the strength of platinum and palladium represent a significant departure from expected behavior.

Grain Size and Strain Rate Effects. The influence of grain size and strain rate on the mechanical properties of rhodium and iridium were evaluated to provide additional information on the observed strain-aging effects.

Cold drawn 0.050-inch-diameter wire, prepared from the available high-purity material, was used in this study. Three microstructural conditions: stress relieved, and fine- and large-grained recrystallized structures, and four strain rates, 0.004, 0.02, 0.2, and 2 inches/inch/minute were considered. The annealing schedules and associated grain sizes are as follows:

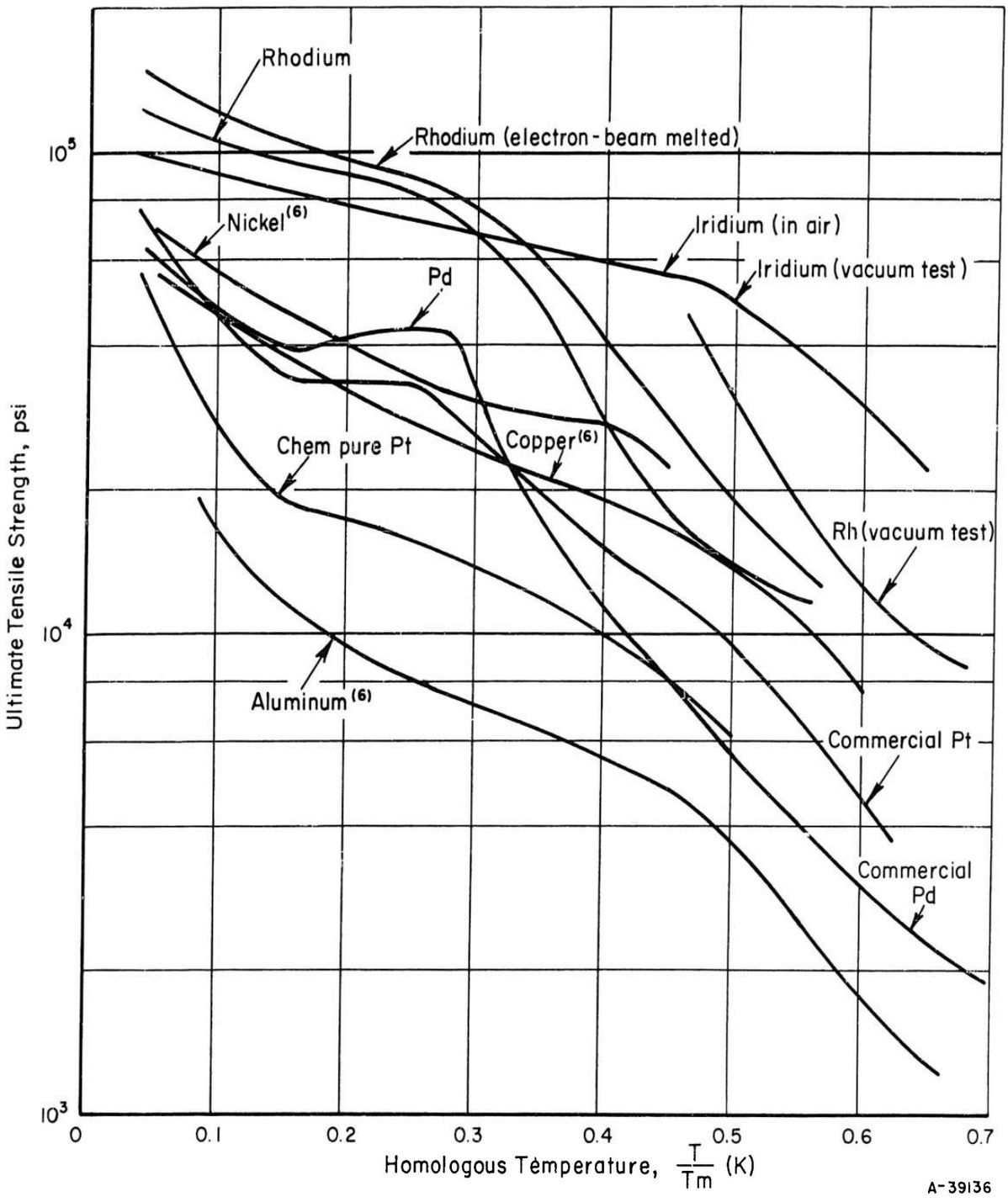

FIGURE 24. TEMPERATURE-STRENGTH RELATIONS OF SEVERAL HIGH-PURITY FACE-CENTERED CUBIC METALS

Metal	Microstructural Condition	Annealing Schedule	Average Grain Diameter, mm
Rhodium	Stress relieved	1 hour at 500 C	--
	Fine grained, annealed	1 hour at 700 C	0.035-0.05
	Coarse grained, annealed	1 hour at 1000 C	0.07
Iridium	Stress relieved	1 hour at 1000 C	--
	Fine grained, annealed	1 hour at 1400 C	0.05
	Coarse grained, annealed	1 hour at 1500 C	0.07

All tests were performed at room temperature.

Tensile data for rhodium and iridium in three microstructural conditions and at several strain rates are presented in Table 6. These data are illustrated graphically in Figures 25 and 26.

The strength of both metals is sensitive to grain size and strain rate. The influence of these variables is more pronounced in iridium than in rhodium. Both metals show low flow stresses under certain conditions, indicating that grain boundaries do not offer appreciable resistance to plastic flow. The low flow stresses indicate dislocation locking is absent in the annealed samples.

The strain rate sensitivity also was manifested as a yield point discontinuity in rhodium annealed at 700 C and tested at 0.02 and 0.2 minute^{-1}. The yield point, illustrated in Figure 27, was not observed in any other rhodium samples. The important features of this yield point are listed below:

TABLE 6. TENSILE DATA FOR RHODIUM AND IRIDIUM IN SEVERAL MICROSTRUCTURAL CONDITIONS

Microstructure	Initial Strain Rate, minutes^{-1}	Proportional Limit, psi	Ultimate Tensile Strength, psi	Elongation, per cent in 1/2 inch[a]	Strain-Hardening Exponent at $\epsilon = 0.08$[b]	Remarks
			Rhodium			
Stress relieved, annealed 1 hr at 500 C	0.004	149,000	226,000	6	--	
	0.02	36,200	235,000	12	0.08	
	0.2	149,000	188,000	3	--	
	0.2	93,000	170,000	2.5	--	
	2.0	172,000	193,000	8	--	
ASTM Grain Size No. 6-7, annealed 1 hr at 700 C	0.004	15,900	129,000	27	0.31	No yield point
	0.02	15,800	118,000	--	0.40	Yield point, slip in grips
	0.2	34,000	113,000	--	0.35	Yield point, slip in grips
	0.2	20,000	115,000	44	0.47	Yield point
	2.0	45,000	120,000	--	0.31	No yield point, slip in grips
ASTM Grain Size No. 5, annealed 1 hr at 1000 C	0.004	11,700	87,000	26	0.4-0.5	
	0.02	11,700	87,000	28	0.4-0.5	
	0.2	17,900	89,000	30	0.41	
	0.2	15,900	91,000	27	0.54	
	2.0	34,500	94,000	45	0.48	
			Iridium			
Stress relieved, annealed 1 hr at 100 C	0.02	104,000	192,000	11[c]	0.22	
	0.2	96,000	212,000	15[c]	0.22	
	2.0	100,000	167,000	2[c]	0.22	
ASTM Grain Size No. 6, annealed 1 hr at 1400 C	0.02	51,000	128,000	4[c]	--	
	0.2	79,000	165,000	8[c]	0.21	
	2.0	73,000	147,000	8[c]	0.21	
ASTM Grain Size No. 5, annealed 1 hr at 1500 C	0.02	17,400	67,300	2[c]	0.47	
	0.2	14,500	83,000	8[c]	0.43	
	2.0	110,000	176,000	8[c]	0.24	

(a) Determined from autographic record; no value can be given where slipping in grips is observed.
(b) Exponent is determined as the slope of the true stress-true strain curve at 0.08 true strain.
(c) Measured from broken tensile specimens.

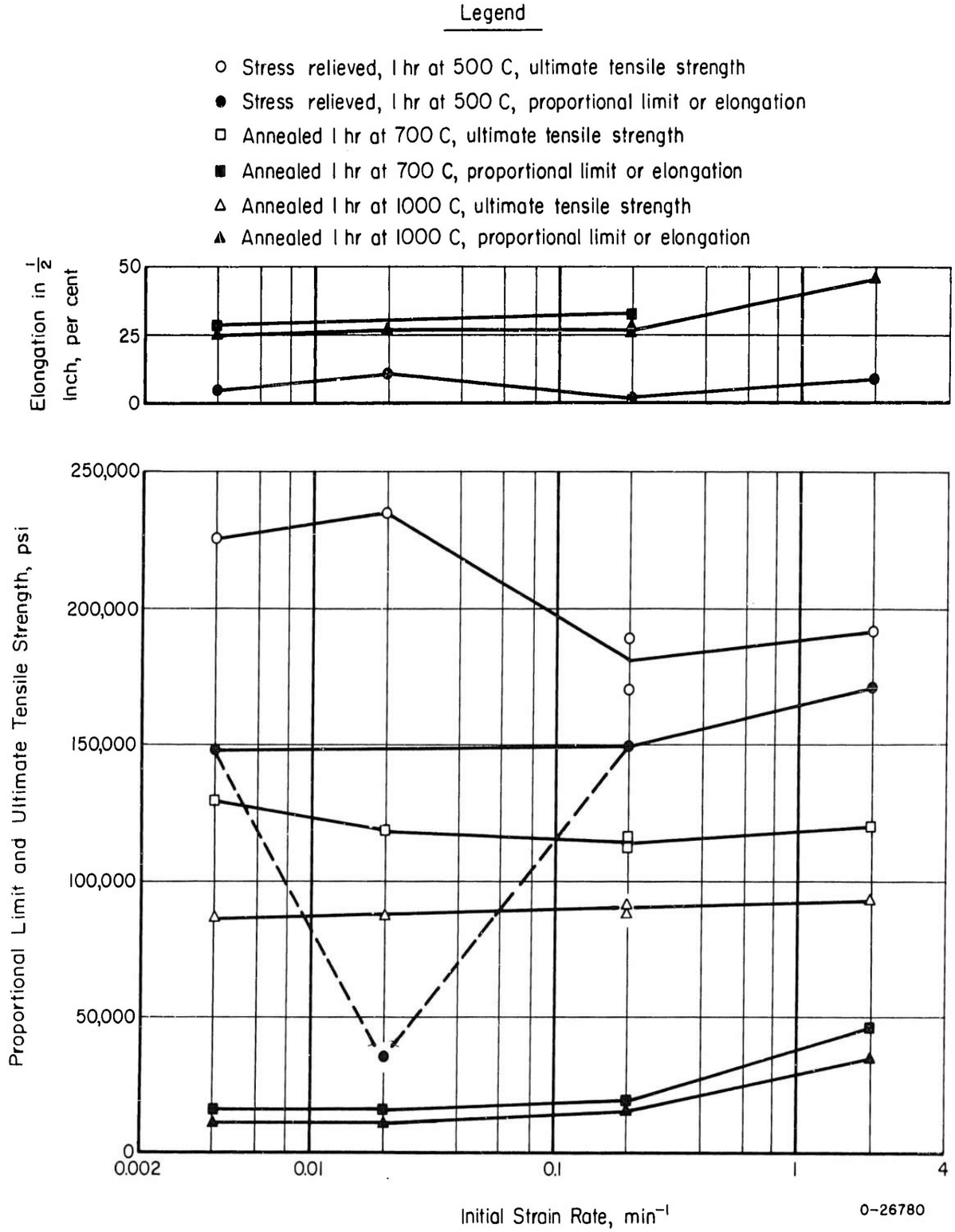

FIGURE 25. EFFECT OF INITIAL STRAIN RATE ON THE TENSILE PROPERTIES OF RHODIUM

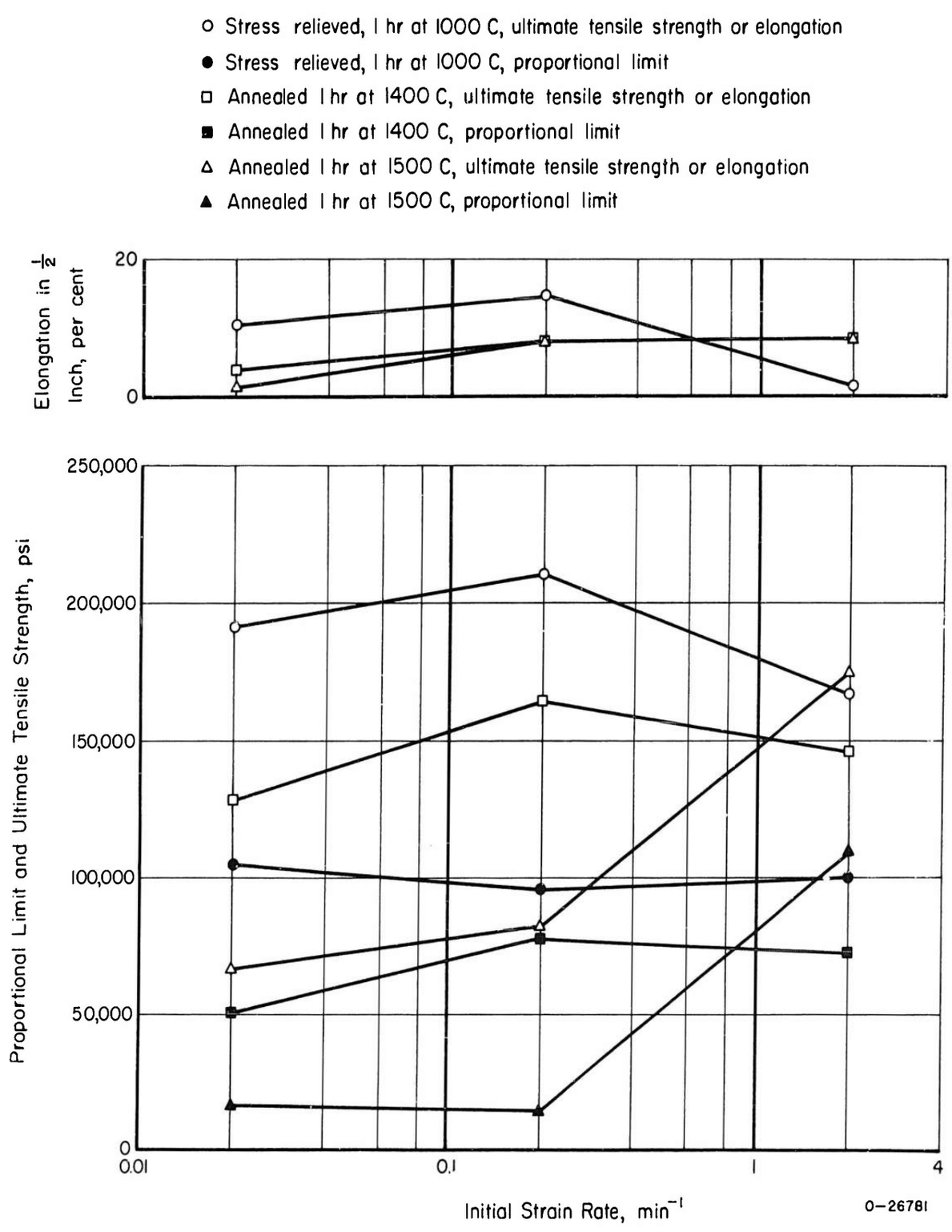

FIGURE 26. EFFECT OF INITIAL STRAIN RATE ON THE TENSILE PROPERTIES OF IRIDIUM

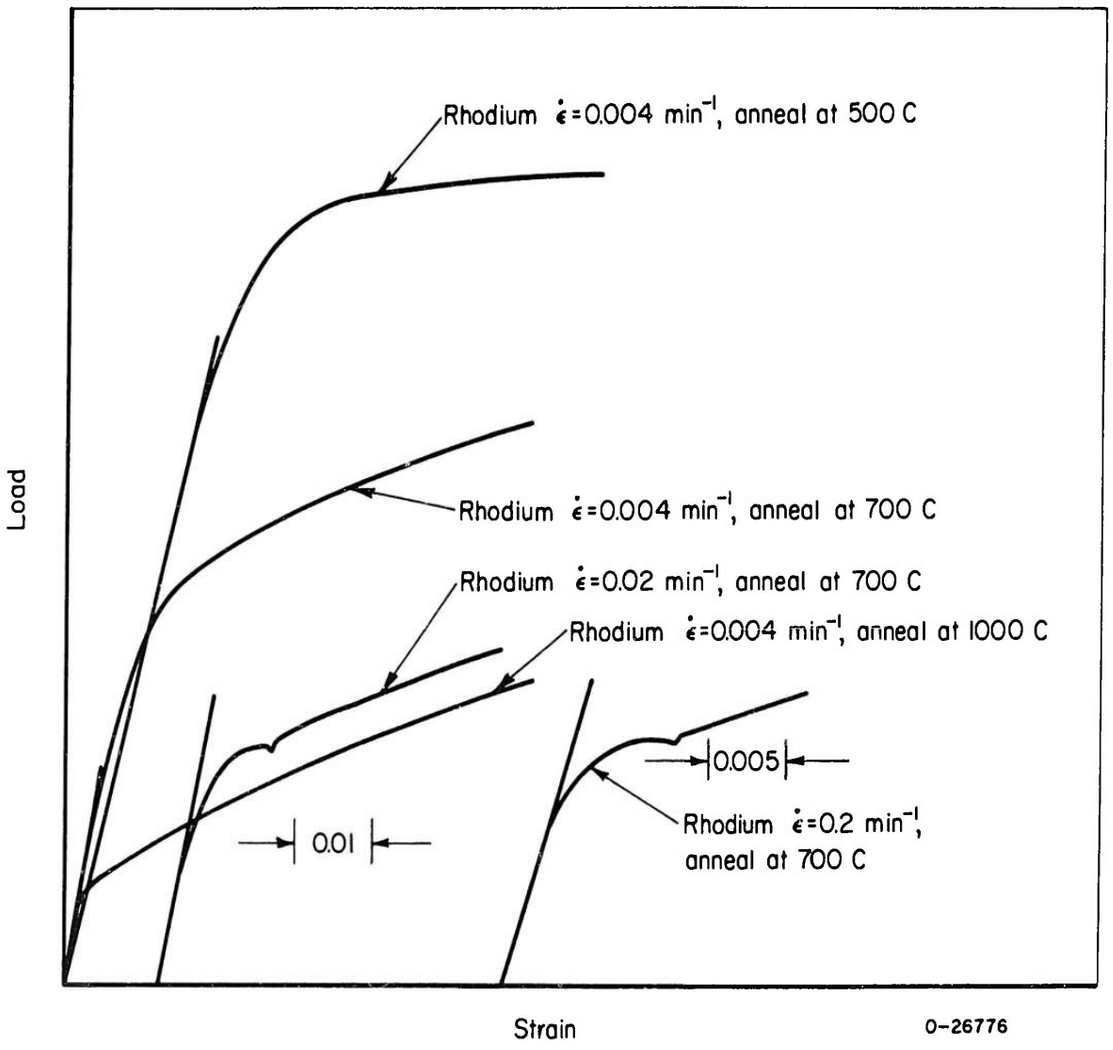

FIGURE 27. TYPICAL LOAD-STRAIN CURVES FROM TENSILE TESTS OF RHODIUM

(1) The pre-yield strain is high, about 0.5 per cent; an indication the yield behavior is activated by deformation.

(2) The yield behavior is sensitive to strain rate and grain size; indicating temperature sensitivity and a mechanism dependent upon impurity distribution.

These features preclude the action of a hardening mechanism involving solute atoms surrounding dislocations at equilibrium or segregation of solute atoms to stacking faults. The data show substantial agreement with a strain-aging picture involving the interaction of moving solute atoms with moving dislocations, described by Cottrell.(7) The operation of this mechanism, or any hardening mechanism involving solute atom-dislocation interactions, indicates that rhodium, unlike most face-centered cubic metals, is very sensitive to impurities.

The strain rate and grain size effect found in iridium most likely arises from impurities. The hardening mechanism appears different in iridium than in rhodium, for, in the former, the initial flow stress is increased significantly by reduction in grain size and increase in strain rate. It may be, of course, that the hardening mechanisms are identical in both metals, but more pronounced in the iridium.

Both rhodium and iridium work harden rapidly as illustrated by the data in Table 6 and by the true stress-true strain curves in Figures 28 and 29. The rate of hardening is sensitive to the initial

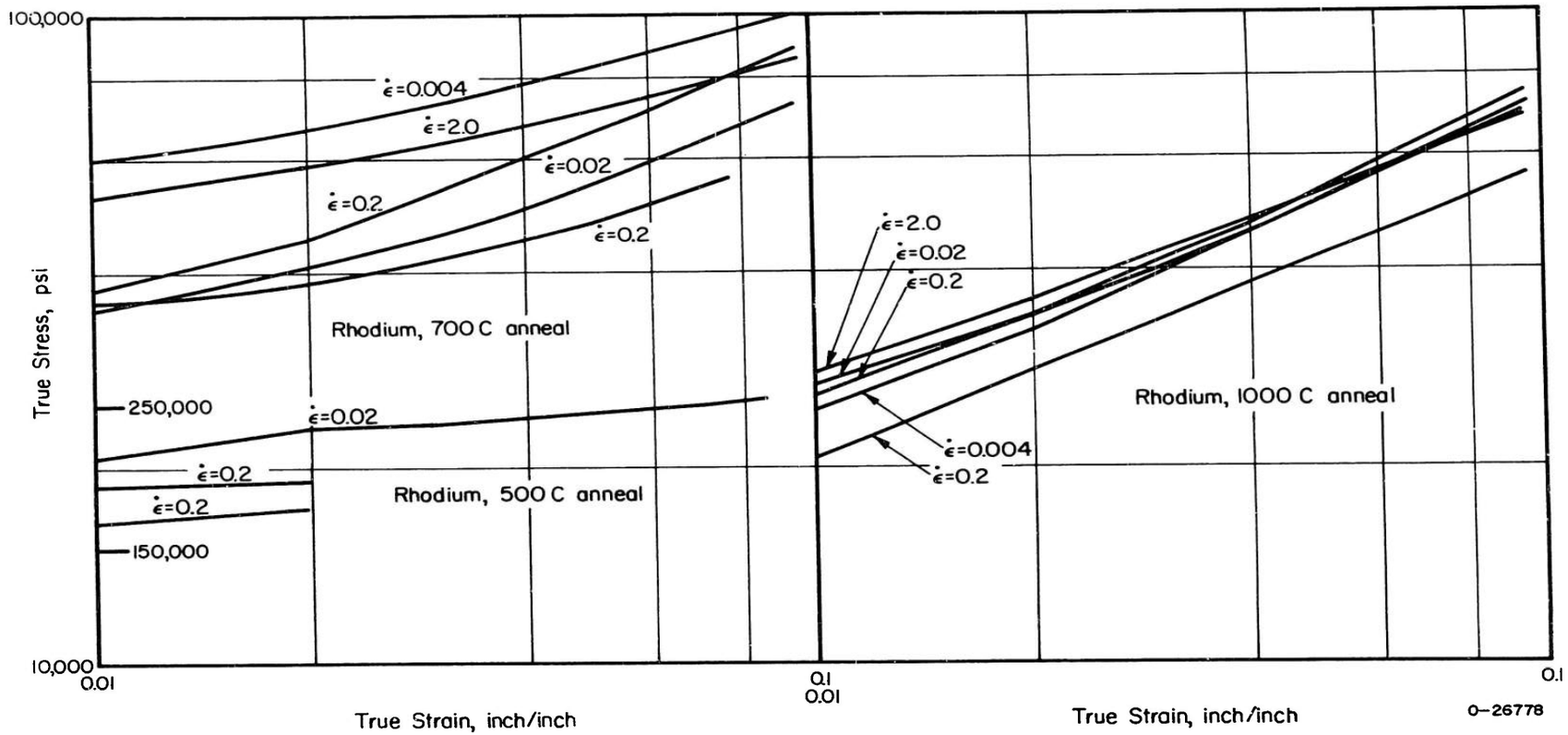

FIGURE 28. TRUE-STRESS TRUE-STRAIN CURVES FOR RHODIUM AT SMALL STRAIN

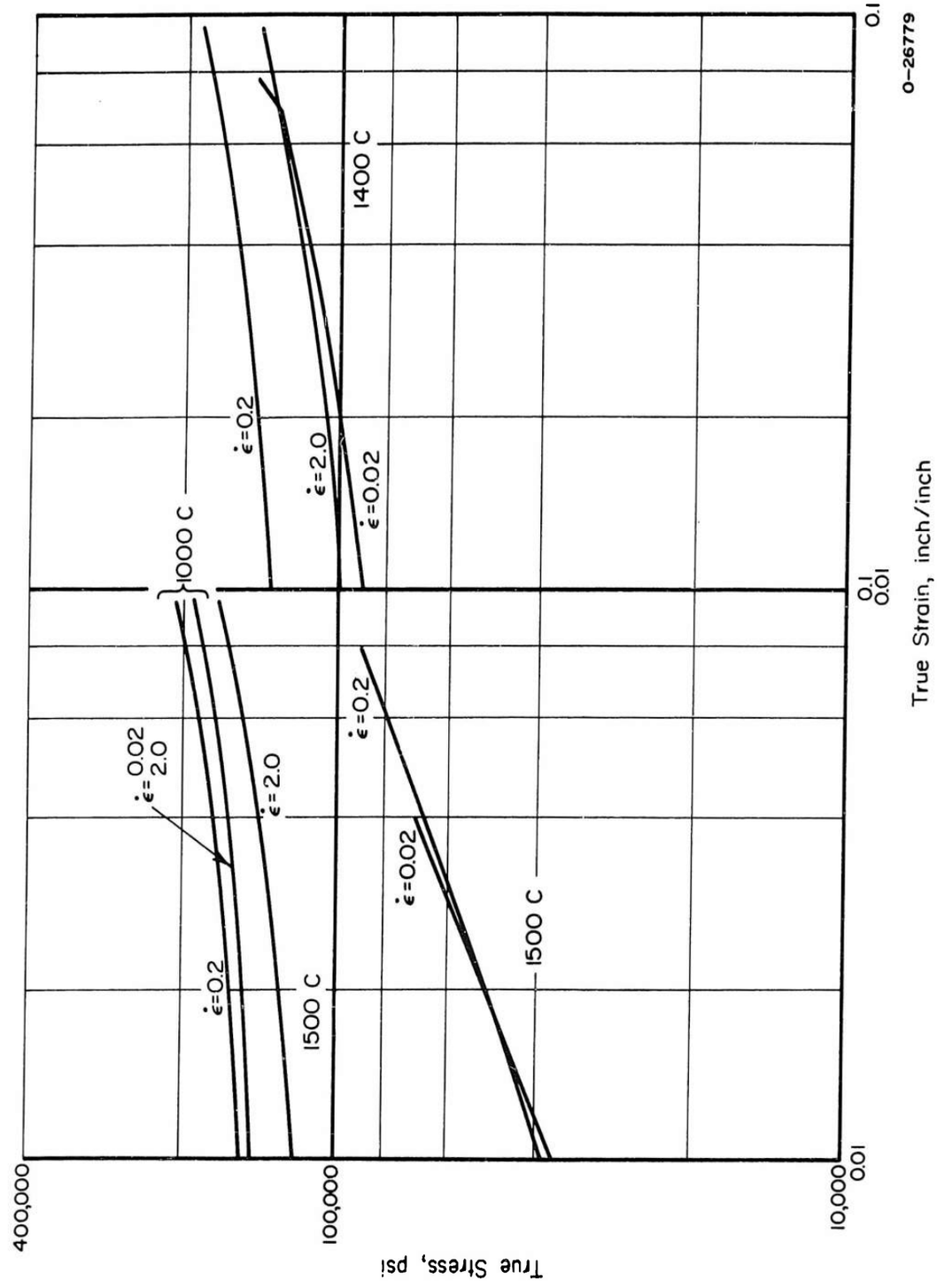

FIGURE 29. TRUE-STRESS TRUE-STRAIN CURVES FOR IRIDIUM AT SMALL STRAINS

flow stress and, thus, to grain size. Rapid hardening has also been observed in cold-working studies made in connection with the recrystallization temperature work as illustrated in Figure 30. Bale[8] suggests work hardening in ultrahigh purity rhodium arises from the operation of unusual slip systems.

Consideration of several properties of rhodium and iridium in light of current theories of metal deformation serves to clarify the observed work-hardening behavior. Seeger,[9] in discussing the work hardening of face-centered cubic metals, shows there are three stages of work hardening. In the rapid hardening stage, Stage II, the rate of work hardening is $\theta_{II} \simeq 10^{-3}$ G, where G is the shear modulus in the glide plane. This rapid hardening stage is due, presumably, to the continuous formation of Lomer-Cottrell barriers to dislocation motion. The end of the rapid hardening stage is reached when the energy supplied to a blocked dislocation is sufficient to cause cross-slip. The magnitude of this energy is related to the separation of the extended dislocations held up at the barrier and, thus, is related to the stacking-fault energy of the metal.

Rhodium and iridium both have high elastic moduli; the bulk moduli for several face-centered cubic metals are listed below:

Metal	Elastic Modulus, 10^6 psi
Aluminum	9
Copper	16
Nickel	30
Platinum	21
Palladium	16
Rhodium	45
Iridium	76

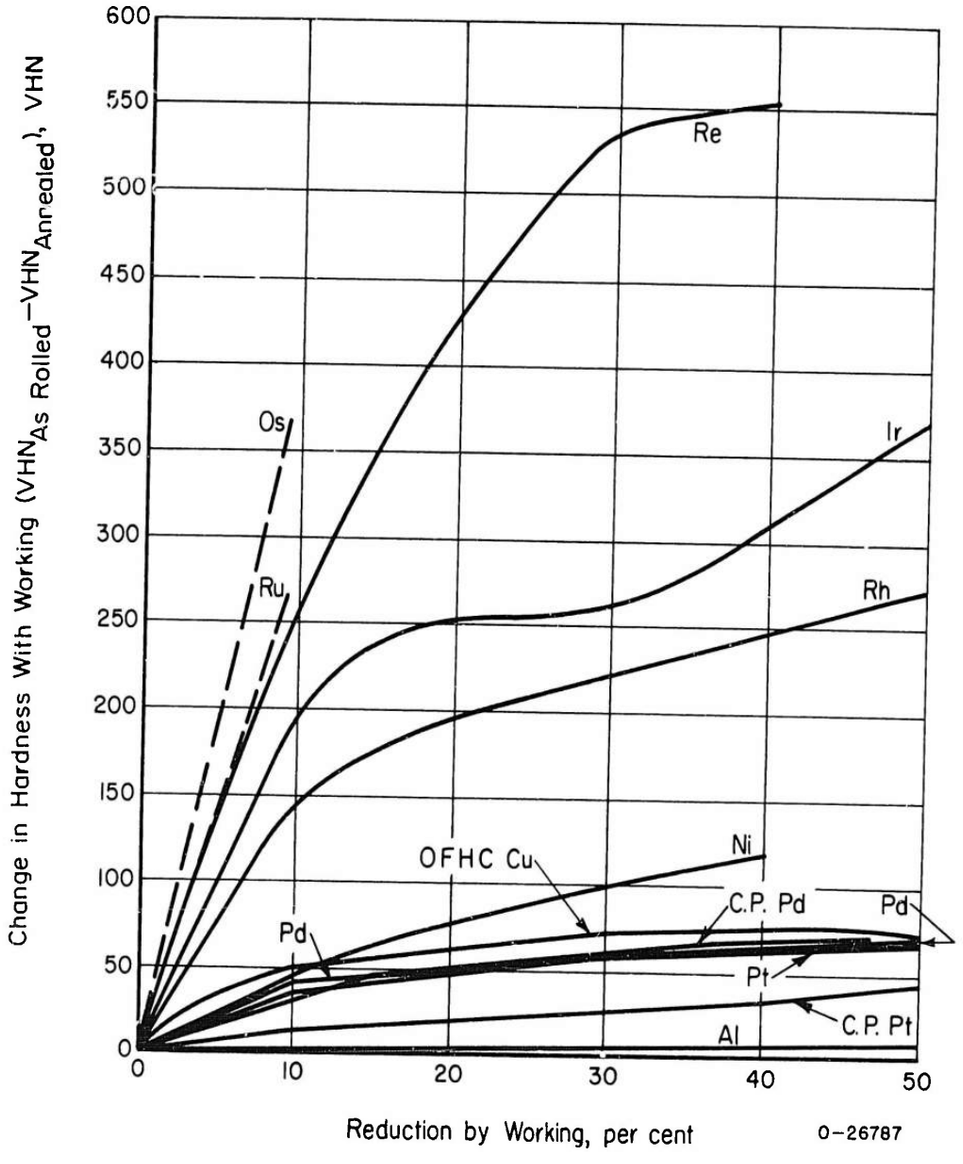

FIGURE 30. CHANGE IN HARDNESS WITH COLD WORKING FOR SEVERAL FACE-CENTERED-CUBIC METALS

Although the moduli of rhodium and iridium in the glide plane are not known, it is assumed that the order of magnitude difference of moduli of the metals will be the same in the glide plane as in the aggregate. Then it would be expected rhodium and iridium single crystals would work harden 1.5-5 and 2.5-8 times more readily, respectively, than other face-centered cubic metals.

Although stacking-fault energies have not been measured, they are expected to be low. This is suggested by the frequency of annealing twins in these metals, especially iridium, shown in several photomicrographs.

Theory would predict that metals with high shear moduli would show rapid work hardening and that this rapid work hardening would persist to higher stresses the lower the stacking-fault energy.(9) Based on these considerations, rapid work hardening would be expected in rhodium and iridium.

Improvements in the tensile ductility of rhodium and iridium were sought by stress-relief annealing after cold work. This technique has proved successful in improving the ductility of molybdenum and tungsten. In the present case, the strength of both metals was increased significantly by stress relieving, rather than recrystallizing, after cold work. The ductility of iridium also was increased slightly, but the ductility of rhodium was reduced by this treatment.

Slip Plane Determinations

The active slip planes of rhodium and iridium were determined by examination of slip traces in grains (in a polycrystal) of known orientation.

The rhodium sample was cut from an electron-beam-melted rod as a 1/4 x 1/4-inch cube. The iridium sample was ground to 3/4 x 1/4 x 1/4 inch from an arc-cast ingot reduced 5 per cent at 1500 C and vacuum annealed 1 hour at 2100 C. Care was taken during grinding to insure all corners were square and opposite edges parallel. The iridium and rhodium samples were annealed 1 hour at 2100 and 1800 C, respectively, after grinding, mounted on bakelite, and polished and deeply etched to reveal the structure to the naked eye. The crystallographic orientation (relative to a side of the sample) of selected grains was determined by standard Laue back reflection techniques. The selected grains of both samples are shown in Figure 31; the poles of the surface of these grains in a standard sterographic triangle are shown in Figure 32.

After orientation, the specimens were repolished to remove etch pits, lightly etched, carefully broken from the mounts, and squeezed in a bench vise to a total of 2 per cent compression. At this point, slip traces were visible to the naked eye. The angles between the slip traces and the side of the specimen used as a reference line for the crystallographic orientations were measured at 100X from the ground glass screen of a metallograph, by rotating a corner of the specimen into coincidence with a rectangle scribed on the ground glass screen. The angles between the slip trace and the reference line were taken as the average of 5 to 10 measurements. At least two, and usually three or four, separate slip traces were found in each grain.

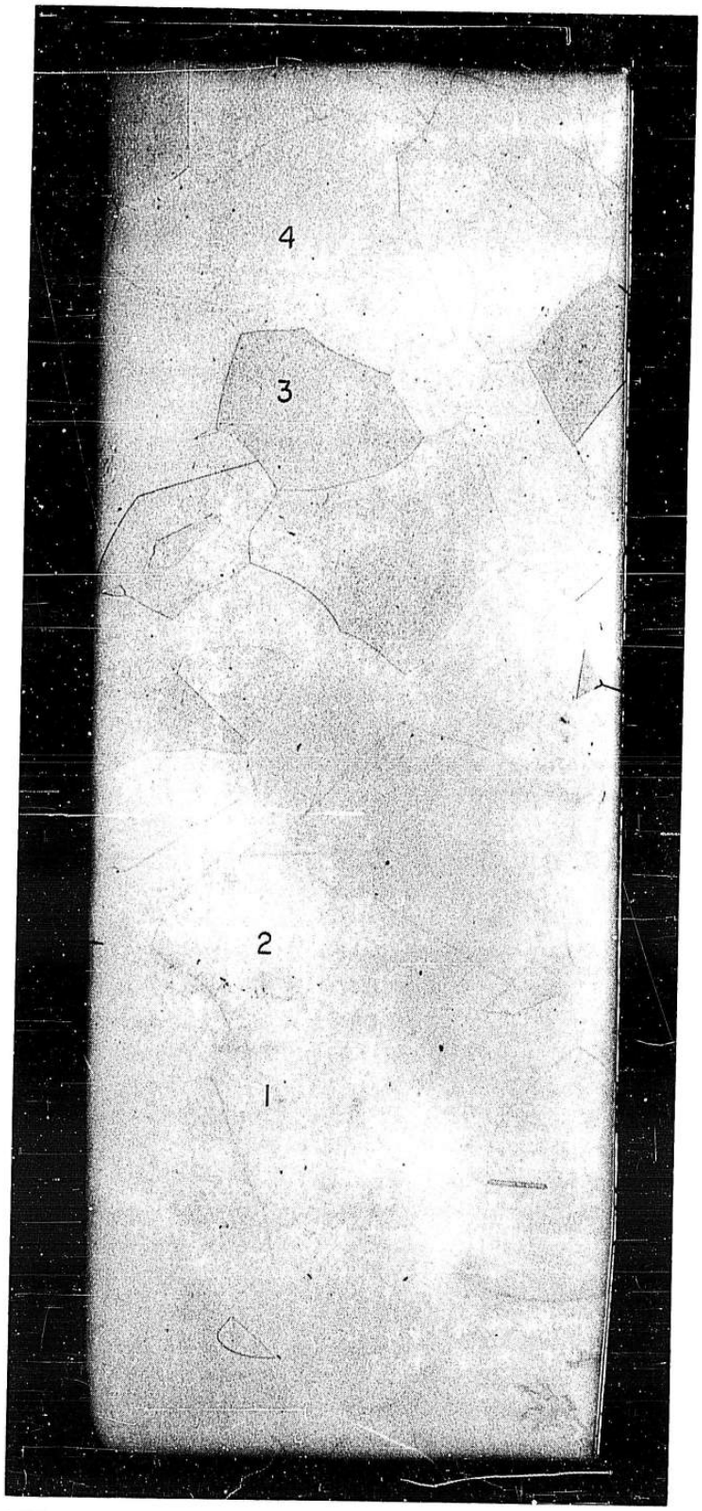

15X N78978

FIGURE 31a. PHOTOMACROGRAPH OF IRIDIUM SAMPLE FOR SLIP PLANE DETERMINATIONS

Numbered grains were oriented by back-reflection techniques.

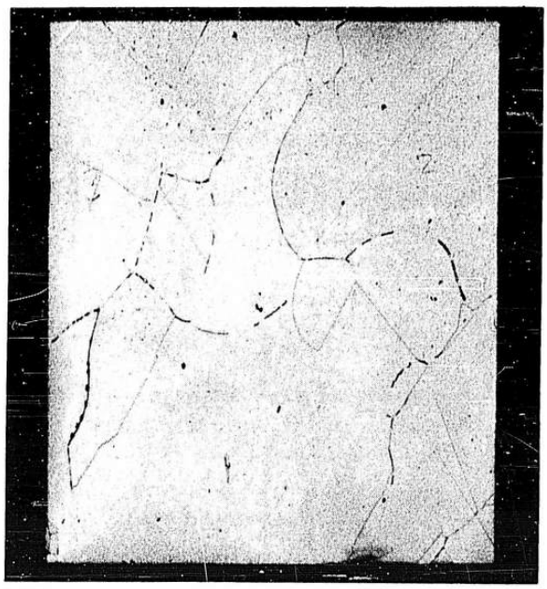

FIGURE 31b. PHOTOMACROGRAPH OF RHODIUM SAMPLE FOR SLIP PLANE DETERMINATIONS

Numbered grains were oriented by back-reflection techniques.

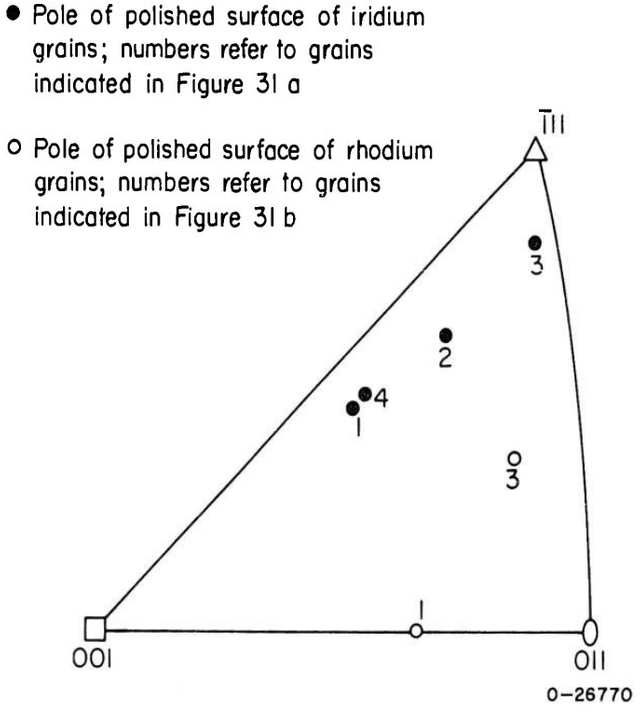

FIGURE 32. CRYSTALLOGRAPHIC ORIENTATIONS OF SELECTED RHODIUM AND IRIDIUM GRAINS

The planes responsible for the slip traces were determined by constructing the locus of poles of planes responsible for each trace and superimposing the loci over the stereographic projection for each grain. The results of this procedure are illustrated in Figures 33 and 34. In iridium, all traces can be accounted for by slip on $\{111\}$ planes, within experimental error. In rhodium, the results are more complicated. In grain No. 1, three slip traces appear to result from $\{111\}$ slip, but the plane responsible for the fourth trace could not be identified. In grain No. 3, the angles between slip traces are consistent with $\{111\}$ slip, but the loci of planes responsible for the slip do not match up with $\{111\}$ poles or the poles of any other single set of low indice planes. The loci of poles can be matched with the $\{111\}$ poles by an 18-degree rotation of the reference line. This rotation is about 1.5 times the estimated experimental error.

Because of the confusion in specifying the active slip planes of rhodium, the relationship between slip traces and annealing twins was carefully examined. Hall[10] reports the $\{111\}$ planes are twin planes and twin boundary planes of coherent twins in face-centered cubic metals. This was ascertained by examining the relation between twin boundaries and slip traces in oriented grains of rhodium and iridium, as illustrated in Figure 35. Slip traces parallel to twin boundaries in other grains, shown in Figure 36, also were found, providing additional proof of slip on $\{111\}$ planes in both metals.

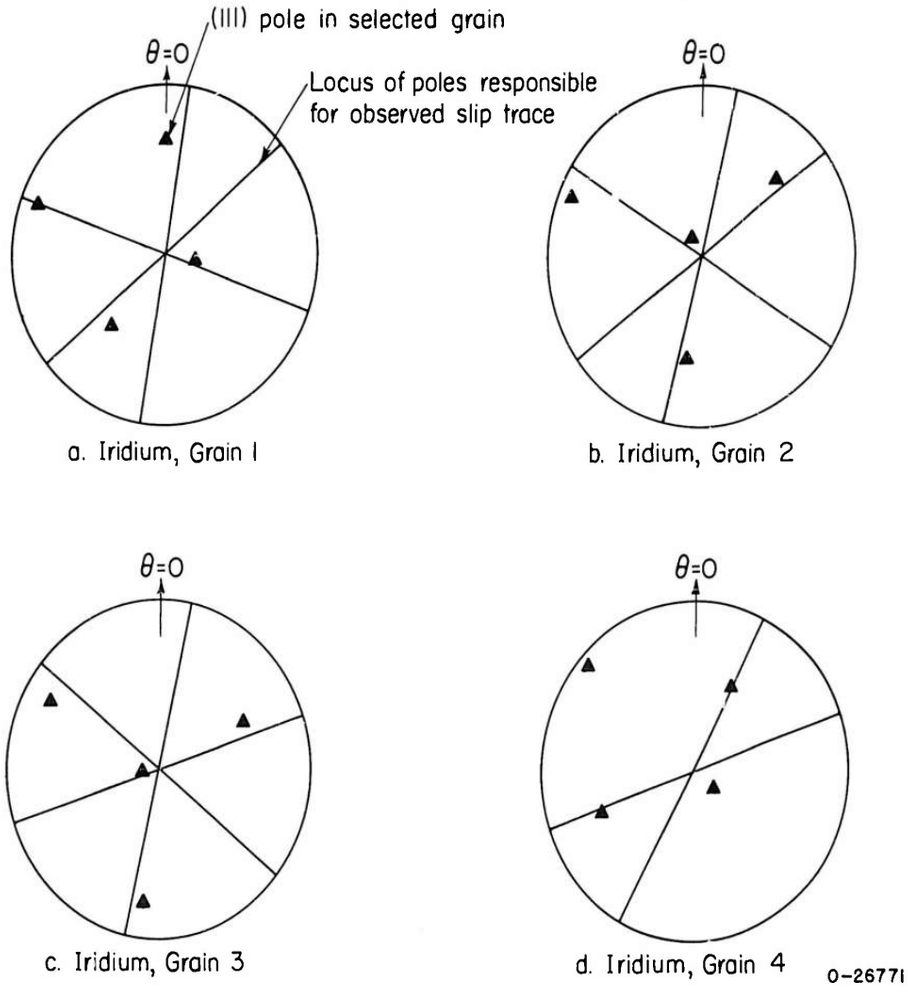

FIGURE 33. STEREOGRAPHIC PROJECTIONS OF {111} POLES OF IRIDIUM GRAINS, OVERLAID WITH THE LOCI OF POLES OF PLANES RESPONSIBLE FOR OBSERVED SLIP TRACES

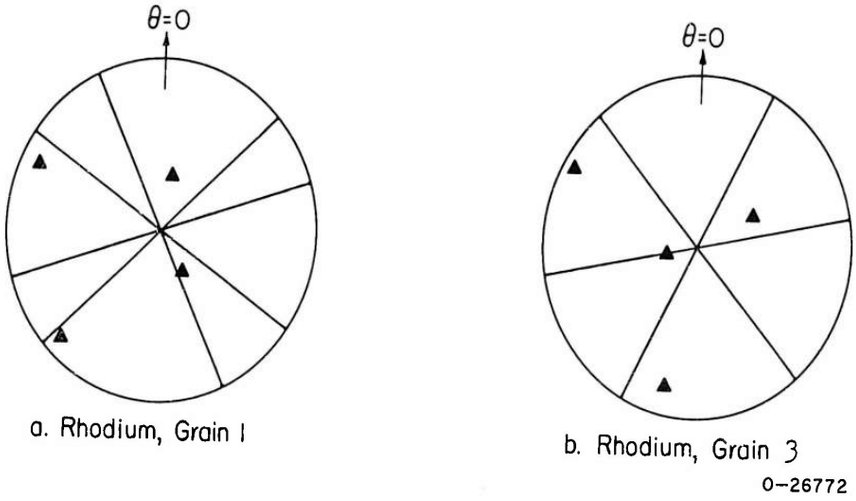

FIGURE 34. STEREOGRAPHIC PROJECTIONS OF ⟨111⟩ POLES OF RHODIUM GRAINS, OVERLAID WITH THE LOCI OF POLES OF PLANES RESPONSIBLE FOR OBSERVED SLIP TRACES

500X

a. Rhodium

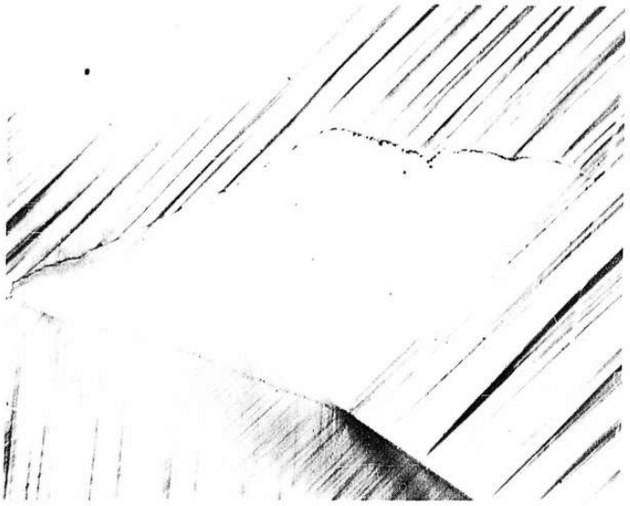

150X

b. Iridium, Oblique Lighting

FIGURE 35. PHOTOMICROGRAPHS OF COHERENT TWIN BOUNDARIES PARALLEL TO $\{111\}$ SLIP TRACES IN ORIENTED GRAINS OF RHODIUM AND IRIDIUM

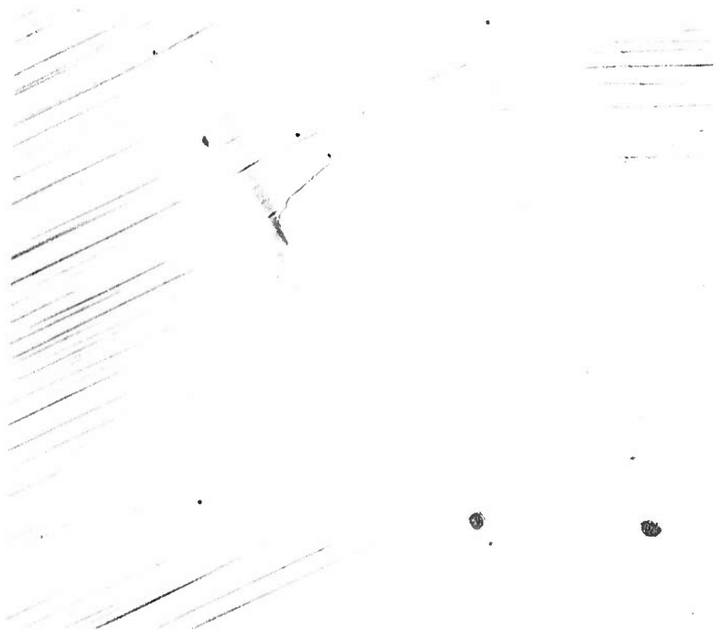

200X N79799

a. Rhodium

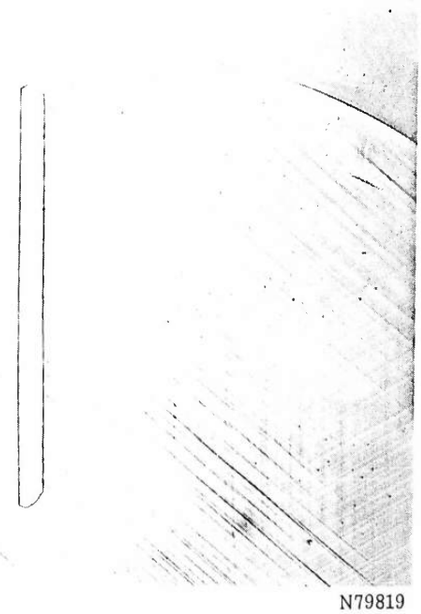

150X N79819

b. Iridium, Oblique Lighting

FIGURE 36. PHOTOMICROGRAPHS OF COHERENT TWIN BOUNDARIES PARALLEL TO SLIP TRACES IN RHODIUM AND IRIDIUM GRAINS OF UNKNOWN ORIENTATION

Single Crystal Studies

Single crystals of rhodium and iridium were prepared by electron-beam melting. As-received rods of each metal, 0.150-inch diameter and 6 inches long, were melted three times at zone traverse speeds of 2 inches per hour. The as-melted rods had irregular cross sections, diameters varied from 0.060 to 0.160 inch, and were composed of single crystals, 1/4 to 1 inch long, strung out along the rod.

Two 1-1/2-inch-long samples of each metal were cut for tensile specimens. Metallographic examination of the rhodium samples showed they were polycrystalline and, thus, not suitable for tensile testing as single crystals. Metallographic and X-ray examination of the iridium samples showed they were single crystals over the entire reduced section. The iridium crystals were oriented with a $\{100\}$ pole parallel to the longitudinal axis of the specimen.

Attempts to produce single crystals by electron-beam melting larger diameter rods of each metal were unsuccessful. Four melting passes at 1 inch per hour were used, but the bars were polycrystalline after each pass. These bars were hot rolled at 1500 C to 0.050-inch-thick strip for future study.

The iridium single crystals were tensile tested at room temperature at an initial strain rate of 0.0075 $minute^{-1}$. The samples were metallographically polished for observation of slip traces; however, sections of the reduced sections were roughened with emery paper for the application of etched foil strain gages. One specimen, Ir-3, was extended to 0.5 per cent strain and unloaded; the other sample, Ir-4, was tested to failure. Resolved stress-strain curves for each specimen are presented in Figure 37.

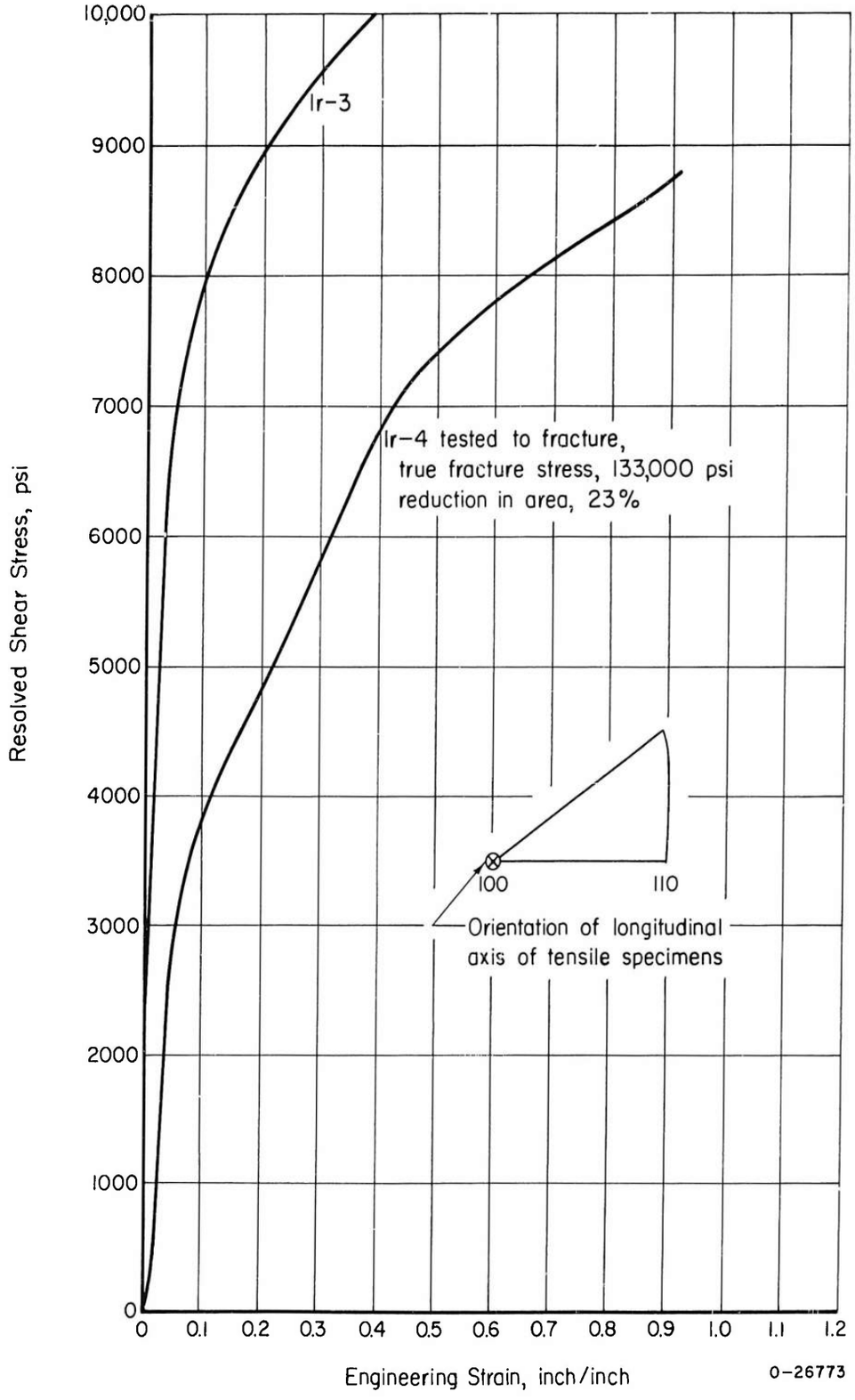

FIGURE 37. RESOLVED SHEAR STRESS-STRAIN CURVES OF IRIDIUM SINGLE CRYSTALS

The work hardening behavior of the samples differ markedly. It is likely that multiple slip occurred more readily in Specimen Ir-3 than in Specimen Ir-4, due to slight orientation differences, resulting in more immediate hardening. Critical resolved shear stresses for slip are approximately 2400 and 5400 psi for Ir-4 and Ir-3, respectively.

Specimen Ir-4, tested to failure, showed brittle cleavage failure at 135,000 psi and 13 per cent extension. The cleavage face is shown in Figure 38. This is the first known example of cleavage failure in a pure face-centered cubic single crystal. The gross cleavage occurred on a (100) plane; however, from the "river"-like fracture surface, it appears the microscopic cleavage may have occurred on other planes.

Cracking also occurred at the ends of slip traces as shown in Figure 39. These cracks are composed of segments lying in $\{100\}$ planes. Cracks of this type were only observed in areas that had been roughened with emery paper, suggesting that a notch effect may have been instrumental in crack initiation. Metallographic examination of the interior of specimens revealed several small cracks in a (100) orientation. These cracks lay entirely within the specimen, as illustrated in Figure 40. The geometry of the cracks relative to the observed slip traces conforms to a picture of crack initiation, resulting from stress concentrations at a pile up of dislocations at the intersection of two active slip planes.(11)

The second single crystal, Ir-3, was inadvertently broken during metallographic polishing to remove slip traces. This specimen also failed by cleavage on a (100) plane.

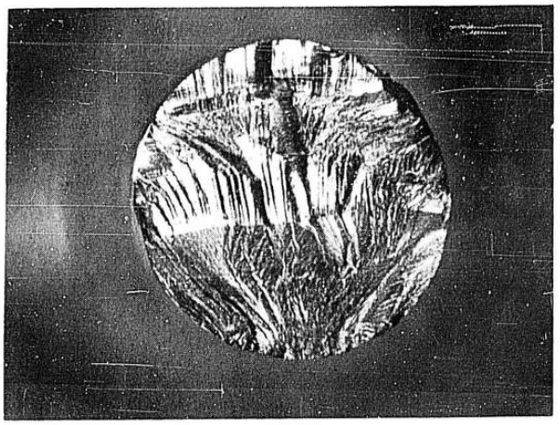

20X N71334

FIGURE 38. FRACTURE SURFACE OF AN IRIDIUM SINGLE CRYSTAL

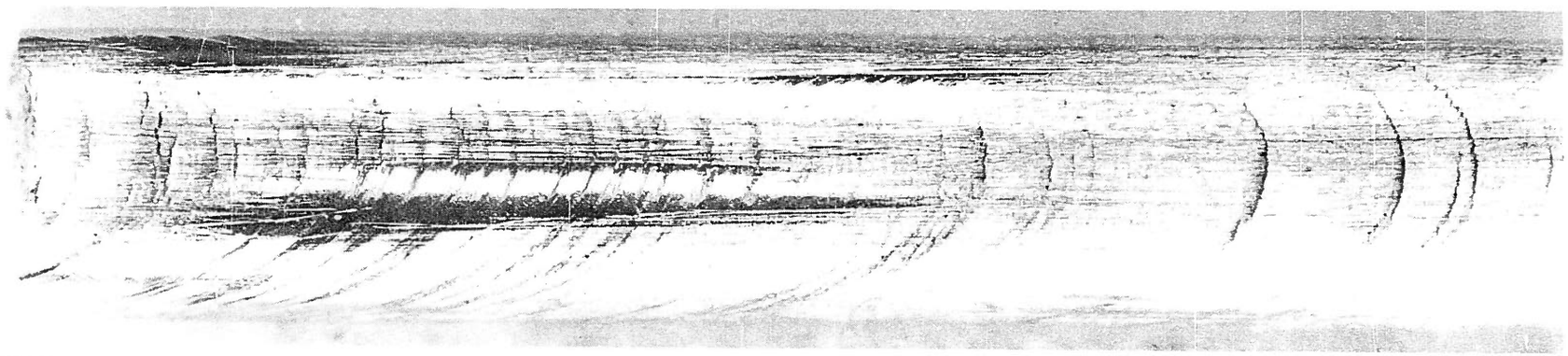

20X

N71335

FIGURE 39. SURFACE OF AN IRIDIUM SINGLE CRYSTAL AFTER FAILURE IN TENSION

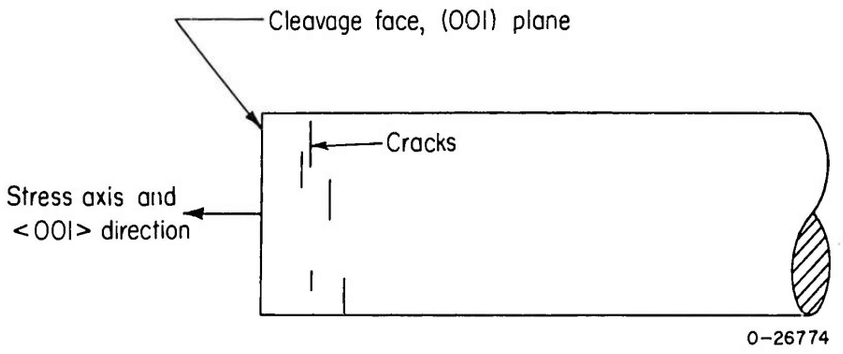

FIGURE 40. SCHEMATIC PICTURE OF INTERIOR CRACKS IN AN IRIDIUM SINGLE CRYSTAL BROKEN IN TENSION

Bend Ductility Studies

The temperature variation of bend ductility of all the metals is illustrated in Figure 41. Rhodium, platinum, and palladium are ductile at temperatures as low as -196 C. Iridium has a ductile-brittle transition at about 400-500 C; however, this is apparently reduced significantly by metallographic polishing of the stressed surface. Ruthenium is brittle in the temperature range that was studied (250-400 C).

The improved ductility of iridium resulting from metallographic polishing is likely a result of removal of stress concentrators at the specimen surface. The effect of microstructure on ductility agrees with the tensile data that have been reported, and can be understood in terms of rate of fracture propagation. This latter point will be discussed in a succeeding section of this report.

Intergranular separation was the failure mechanism for rhodium and iridium over the temperature ranges that were studied.

Fractographic Studies

The fracture surfaces of broken samples of rhodium and iridium were examined to find the cause of intergranular failure. Electron-beam-melted strips of both metals were strain annealed to develop a large grain size. Strain annealing was accomplished by alternate bending and annealing at 1800 and 2100 C for rhodium and iridium, respectively. Grains about 1 to 2 millimeter diameter were grown in this manner. Broken iridium tensile specimens that had shown low ductility also were strain annealed to enlarge the grain size.

Legend

○ Iridium, partially recrystallized, 1 hr at 1300 C
□ Iridium, stress relieved, 1 hr at 1000 C
△ Iridium, annealed, 1 hr at 1500 C
○□△ – Surfaces metallographically polished through red rouge
▲ Iridium
● Platinum and Palladium
■ Rhodium
▼ Ruthenium
▲●■▼ – Ground through 600-grit SiC paper; fully recrystallized

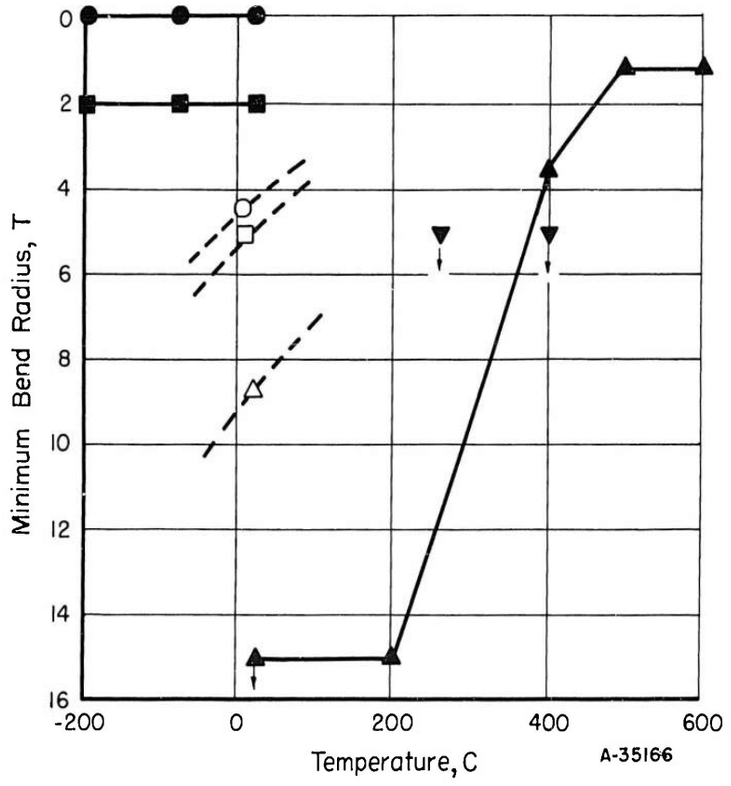

FIGURE 41. EFFECT OF TEMPERATURE ON THE BEND DUCTILITY OF ANNEALED PLATINUM-GROUP METALS

The samples were broken by hand and the fresh fracture surface examined under the microscope. All failures occurred at grain boundaries. Every sample examined showed precipitation in the grain boundary. Examples of the precipitates in electron-beam-melted rhodium and iridium and commercially produced iridium are shown in Figures 42 through 44.

That precipitation was not observed during routine examination of broken tensile specimens probably arises from the fine grain size of the tensile specimens, the sparseness of the precipitate, and the difficulty in finding metallographically "flat" surfaces. The difficulty in finding flat surfaces is a result of deformation of the grain boundary, illustrated by the fractographs of rhodium, Figure 44.

No attempt was made to identify the elements responsible for precipitation although this would be most desirable.

Fracture Initiation Studies

The influence of microstructure on the initiation and propagation of fracture in rhodium and iridium was studied ultilizing bend testing techniques. The bend test lends itself readily to fracture studies, as the maximum tensile stresses are concentrated on the free surface of the specimen. Thus, in all likelihood, fracture will initiate on this exposed surface permitting detailed examination of conditions leading up to fracture.

Strips of commercially prepared iridium and arc-melted rhodium were rolled from a hydrogen furnace at progressively decreasing temperatures (starting at 1600 C) to 0.050-inch-thick strip. The rolling schedule was adjusted to produce final samples with about

250X N78208

a. EBM Iridium, Rolled to Strip, Strain Annealed to Enlarge Grain Size

250X N78213

b. EBM Iridium, Tensile Tested; Strain Annealed to Enlarge Grain Size

FIGURE 42. FRACTOGRAPHS OF ELECTRON-BEAM-MELTED IRIDIUM

250X N78211

FIGURE 43. FRACTOGRAPH OF COMMERCIAL IRIDIUM

Tensile tested, strain annealed to enlarge grain size.

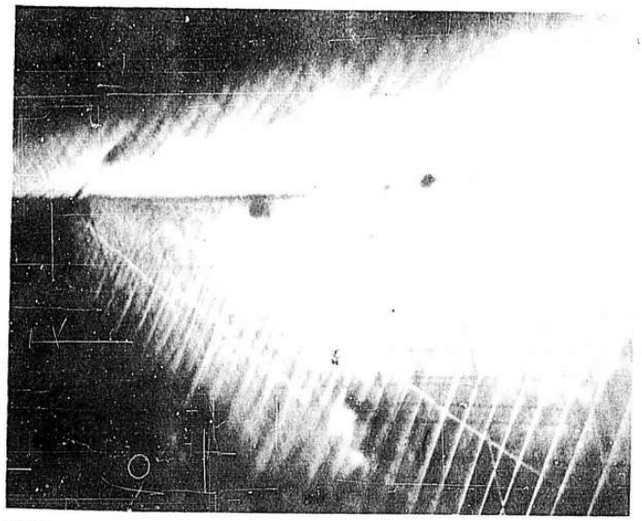

370X

a. Rhodium, Location 1, Oblique Lighting

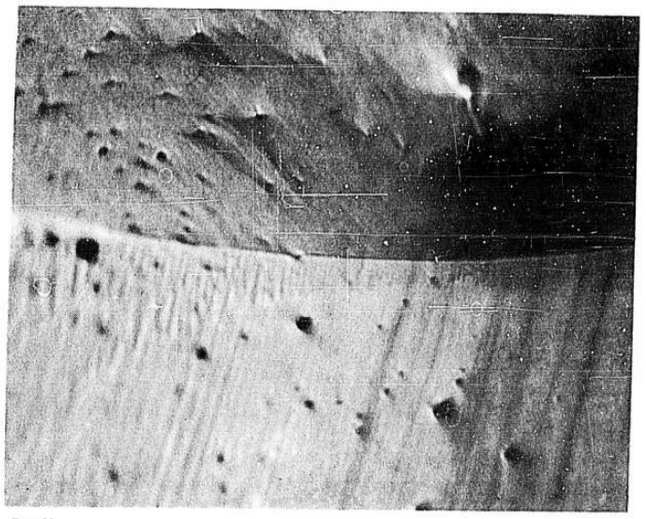

500X

b. Rhodium, Location 2, Oblique Lighting

FIGURE 44. FRACTOGRAPHS OF ELECTRON-BEAM-MELTED RHODIUM

50 per cent warm work and a fibrous microstructure. Four specimens of each metal were finish ground to remove oxide films, imbedded impurity particles, and surface cracks, and to provide flat surfaces for subsequent metallographic polishing.

After metallographic polishing the strips were vacuum annealed to produce the following microstructures:

(a) worked-stress-relieved,

(b) partially recrystallized,

(c) fully recrystallized, moderate, equiaxed grain size, and

(d) fully recrystallized, large, equiaxed grain size.

The heat treatment schedules were determined from annealing studies of both metals.

The specimens were repolished after annealing to remove the structure revealed by vaporization during annealing and finally etched to reveal the microstructure.

Specimens were bent in a specially designed, four-point loading bend jig until the limit of the jig was reached, and were then bent in a bench vise. Bending was continued until visible fracture had occurred.

Cellulose acetate replicas were made after each increment of bending strain. (The strain increments would vary depending upon the predicted ductility of the specimen.) This technique consisted of wetting the specimen surface thoroughly with reagent-grade acetone and pressing a strip of cellulose acetate firmly against the wetted surface. This technique is especially useful for replicating surfaces with a

single radius of curvature; but, as double curvature develops in the tension surface of the specimen, the procedure become somewhat more difficult to use.

Because of the large number of replicas obtained (25 to 100 per specimen) only selected ones were gold shadowed for metallographic examination. Replicas of each specimen were examined (going back on strain) to determine the origin and path of fracture.

The iridium samples used in studies of fracture initiation failed by intergranular separation, regardless of microstructure. Failures were generally initiated at a grain boundary at an edge of the sample. Fracture proceeded by propagation of the major fracture from the edge of the specimen, and by the joining of small grain boundary cracks, 1 or 2 grains long, in the center of the stressed surface with the major crack.

The stability of small grain-boundary cracks, and the rate of propagation of the major crack were influenced by microstructure. In stress-relieved and partially recrystallized iridium, many cracks formed early in the deformation process but grew very little during subsequent deformation and did not contribute to the final fracture.

This point is illustrated in Figures 45 and 46, depicting stress-relieved and partially recrystallized iridium samples, respectively. In stress-relieved iridium, failure was initiated away from the edge of the specimen, as shown in 45b. Several other cracks, in addition to the major one, are evident. Final failure, Figure 45c, occurs by the growth and joining of cracks. Slip is concentrated at two points along the

a. As Polished

150X

b. After Moderate Bending Strain; Crack Not Visible to Naked Eye

150X

c. Crack First Visible to Naked Eye

150X

FIGURE 45. CRACKING IN STRESS-RELIEVED IRIDIUM UNDER BENDING STRESS

Specimen annealed 1 hour at 1000 C.

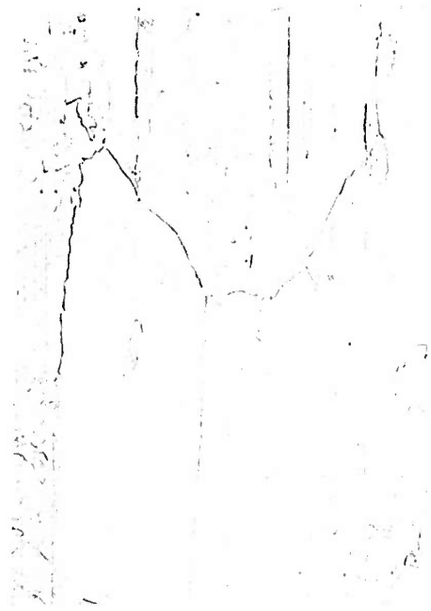

150X

As Polished

150X

b. About One-Half Total Deformation

150X

c. About Two-Thirds Total Deformation

150X

d. Completion of Deformation, Cracks First Visible to the Naked Eye

FIGURE 46. CRACKING IN PARTIALLY RECRYSTALLIZED IRIDIUM UNDER BENDING STRESSES

Specimen annealed 1 hour at 1300 C.

major crack, but there appears to be no slip around other smaller cracks. In fact, there is very little deformation apparent in this surface although local elongations near the fracture average about 10 per cent.

The stability and slow growth of cracks is illustrated by photomicrographs of the partially recrystallized iridium specimen, Figure 46. In this specimen, three apparently nonconnected cracks are formed at the boundaries of adjacent grains early in the deformation, Figure 46b. The deformation at this stage is less than half the total deformation required to produce a crack visible to the naked eye. The joining and growth of the three cracks is shown in Figure 46c. The deformation at this point is about two-thirds of the total deformation. The appearance of this crack at the final stage of deformation is shown in Figure 46c. At this stage, visible failure had occurred in another portion of the specimen.

Intergranular failure in fully annealed iridium is illustrated in Figures 47 and 48. The fine-grained sample, annealed at 1500 C, failed more rapidly than either of the previous two samples. The difference between the specimen in Figure 47b and 47c is a single strain increment, whereas the difference between Figure 46b and 46d (partially recrystallized sample) is 16 strain increments. Some few stable cracks were observed in the fine-grained iridium sample.

Failure of the large-grained iridium sample, Figure 48, occurred after slight deformation and entirely within one strain increment. That is, the deformation imparted to the sample during one strain increment was sufficient to cause total failure. No stable cracks were

a. As Polished

150X

b. At Strain Just Preceding Visible Failure

150X

c. Cracks First Visible to the Naked Eye

150X

FIGURE 47. CRACKING IN ANNEALED IRIDIUM UNDER BENDING STRESSES

Specimens annealed 1 hour at 1500 C.

150X

FIGURE 48. CRACKS IN LARGE GRAINED IRIDIUM AFTER FAILURE

Specimen annealed 1 hour at 1800 C.

observed except in the region adjacent to the fracture. This specimen is the only iridium sample where the fracture propagated through the entire specimen.

One important feature of the micrographs of annealed iridium, Figures 47 and 48, is the high incidence of annealing twins. Another feature is the relatively small amount of slip that is apparent in the deformed structure. Local elongations were about 10 per cent in all but the iridium specimen annealed at 1800 C. The elongations in this sample were less than 5 per cent.

Only two rhodium samples, stress-relieved and fine-grained recrystallized, were studied. The work on iridium indicated these two structures were most interesting for examination.

Fracture initiation and propagation in the two specimens occurred by different mechanisms. The recrystallized rhodium failed by intergranular separation as has been found in the past. This is illustrated in Figure 49. There appears to be a single trace of cleavage failure, shown to the right of center in Figure 49b. There is no apparent slip in the grains near the fracture nor is there any readily identified origin of the grain-boundary cracks.

The cracks in annealed rhodium appear to resist growth as strain is increased, as was the case with iridium. It was possible to continue bending the annealed specimen after visible failure had occurred without causing complete rupture into two pieces.

650X

a. Rhodium, Cracks First Visible to Naked Eye

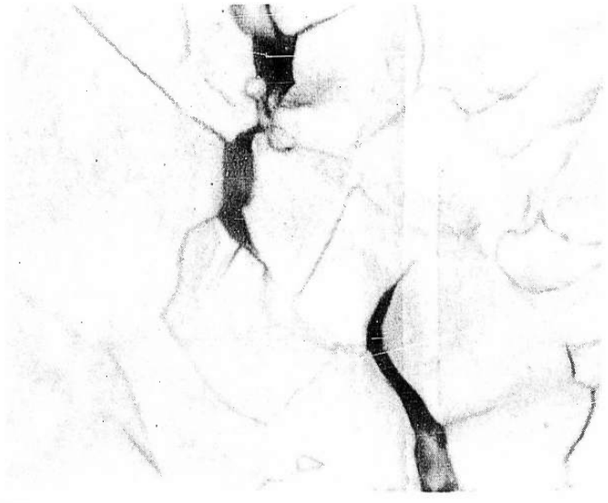

1250X

b. Rhodium, Cracks First Visible to Naked Eye

FIGURE 49. INTERGRANULAR FRACTURE IN ANNEALED RHODIUM

Specimen annealed 1 hour at 1000 C.

Fracture appeared to initiate and propagate by separation along slip planes in stress-relieved rhodium. The tip of the major crack in stress-relieved rhodium is shown in Figure 50. Above the tip is a cracked region not yet joined with the major fracture. The tip of the crack is shown again at higher magnification in Figure 50b. The advancing crack is made up of a series of small cracks. (The thin, vertical line near the center of the picture is caused by acetone from the previous replica accumulated in the crack.) Figure 50c is the same as Figure 50b except for the use of oblique lighting, which shows that cracks occur along slip markings and are presumably in the slip plane.

The results of this phase of the work have shown that iridium fails by intergranular separation in both the worked and annealed conditions. The reason for grain-boundary separation is not apparent from these studies. The mechanism of fracture in rhodium is sensitive to microstructure. Worked rhodium fails by separation along slip planes, while annealed rhodium fails by intergranular cracking.

The influence of microstructure on the ductility and crack stability of iridium appears to be simply a result of changes in grain boundary area. In large-grained samples, the boundary area is small, the density of precipitates is high and the ductility is low. In fine-grained material, the grain boundary area is larger, particle density is lower, and the ductility is higher. The stability of cracks arises mainly from changes in particle density and the associated grain boundary weakening or strengthening.

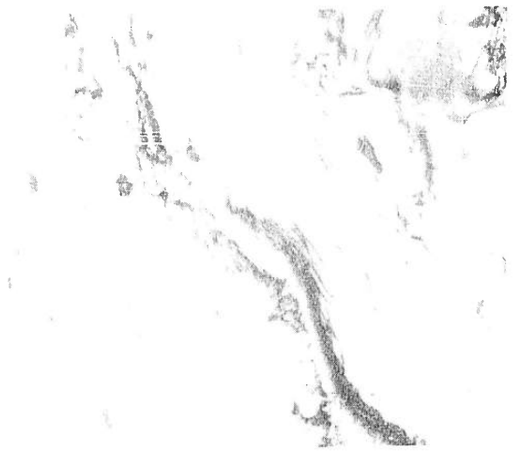

a. Tip of First Visible Crack

200X

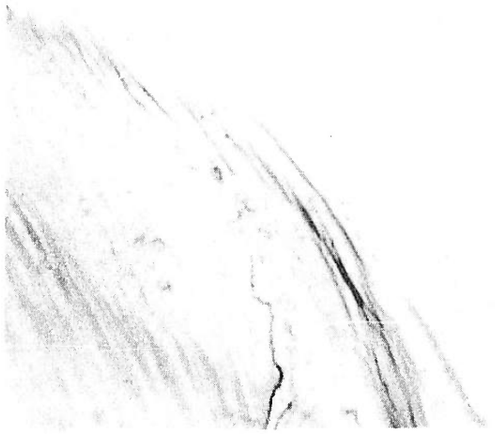

b. Tip of Crack in (a) Above at 1000X

1000X

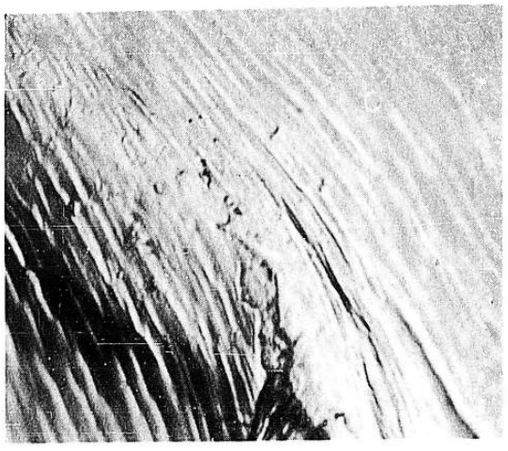

c. Same as (b) Above, Oblique Lighting

FIGURE 50. SHEAR FRACTURE IN STRESS-RELIEVED RHODIUM

Specimen annealed 1 hour at 500 C.

The initiation and propagation of fracture in arc-melted ruthenium was also studied, but not in detail. One half of an arc-melted button of ruthenium was polished and etched for metallographic examination. The sample was compressed in a bench vise along parallel, flat sides ground perpendicular to the polished surface. Cellulose acetate replicas of the polished surface were made before and during compression.

The cracking was predominantly cleavage, with some intergranular failure at the specimen edges. Cracking also occurred in connection with deformation twins as illustrated in Figure 51, a through e. (The dirt particles in this figure are caused by the use of standard-grade, rather than reagent-grade, acetone in preparing the replicas.)

The chronological order of deformation twinning and crack formation is not entirely clear from this study, although it appears that cracks are nucleated at the ends of growing twins, Figure 51c.

One of the few areas of the ruthenium showing intergranular failure also showed precipitation in the grain boundary, illustrated in Figure 52.

The results of this brief study of fracture in ruthenium were somewhat upsetting, for all previous examinations of broken specimens showed complete intergranular cracking.

Stress-Rupture Properties

The short-time stress-rupture properties of rhodium, iridium, and ruthenium were evaluated in vacuum at the following temperatures:

Rhodium - 1000 and 1250 C

Ruthenium and Iridium - 1000, 1250, and 1500 C.

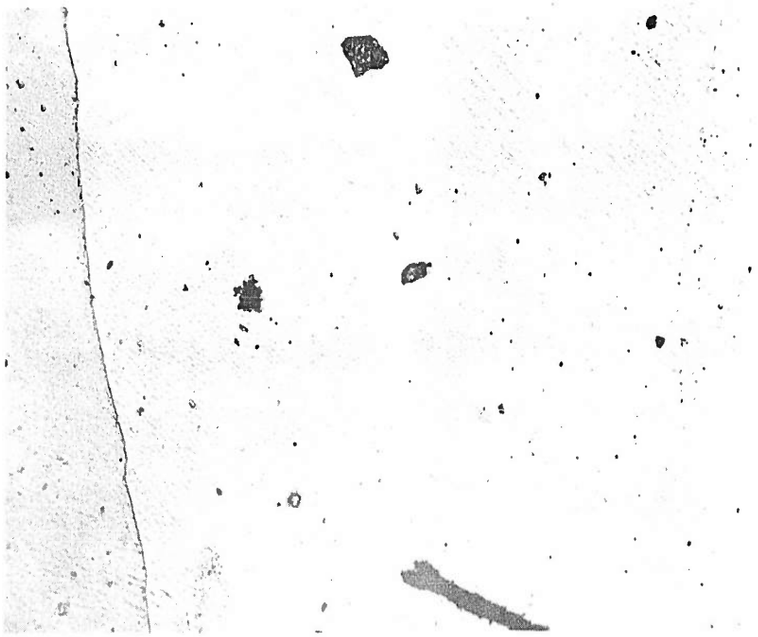

150X N75978

FIGURE 51a. GOLD SHADOWED REPLICA OF THE POLISHED SURFACE OF ARC-MELTED RUTHENIUM, AS MELTED

Oblique lighting.

150X N75979

FIGURE 51b. SURFACE REPLICA AFTER ABOUT 0.2 PER CENT STRAIN IN COMPRESSION

Oblique lighting.

150X N75977

FIGURE 51c. SURFACE REPLICA AFTER ABOUT 0.8 PER CENT STRAIN IN COMPRESSION

Oblique lighting.

150X N75970

FIGURE 51d. SURFACE REPLICA AFTER ABOUT 1.6 PER CENT STRAIN IN COMPRESSION

Oblique lighting.

150X N75982

FIGURE 51e. SURFACE REPLICA AFTER ABOUT 2 PER CENT STRAIN IN COMPRESSION

Oblique lighting.

500X N75915

FIGURE 52. FRACTURE SURFACE OF ARC-MELTED RUTHENIUM

This study was of an exploratory nature, designed to assess the load-bearing capacity of the metals for comparison with other high-temperature materials and to provide a basis for possible further studies.

The stress-rupture data are presented in Table 7 and Figures 53, 54, and 55. Vacuum tensile data are included, taking the rupture time for tensile tests as the time to attain maximum load. There is no correlation of ductility with applied stress or time to rupture, except possibly for iridium at 1500 C which shows a linear reduction in ductility with decreasing applied stress. Similarly, there appears to be no relation between ductility and temperature for any of the metals, although the ductility of iridium is lower at 1250 C than at 1000 or 1500 C. The ductility levels in the short-time stress-rupture tests are about the same as the high-temperature tensile ductility values.

The variation in rupture time with applied stress is strongly dependent upon temperature, especially in the case of iridium and ruthenium. This dependence can be correlated with microstructure. At low temperature, where there is deformation but no recrystallization, see Figure 56, rupture time is relatively independent of applied stress. At higher temperatures, where recrystallization or grain growth occurs during testing, rupture time is strongly dependent upon applied stress. Typical microstructure of iridium, tested in this latter temperature range, are shown in Figures 57 and 58.

The similarity of the stress-rupture properties of iridium at 1250 and 1500 C is surprising in view of the strong temperature dependence of properties of the other metals. This similarity may be

TABLE 7. STRESS-RUPTURE PROPERTIES OF RHODIUM, IRIDIUM, AND RUTHENIUM IN VACUUM

Specimen[a]	Test Temp, C	Applied Stress, psi	Rupture Time, minutes	Reduction in Area, per cent	Elongation in 1/2 In., per cent
Rhodium A-5	1000	16,800	11	97	60[b]
Rhodium A-6	1000	13,200	119	99	71[b]
Rhodium A-4	1000	11,200	811	98	59[b]
Rhodium A-3	1250	9,800	30	99	42[b]
Rhodium A-7	1250	10,900	52	97	120[c]
Rhodium A-2	1250	8,100	399	95	39[b]
Iridium 3-4	1000	54 000	73	84	44
Iridium 3-3	1000	50,000	3115	79	24
Iridium 3-2	1000	49,000	3805	85	34
Iridium 3-20	1250	29,500	22	26	20
Iridium 3-7	1250	27,600	33	30	33
Iridium 3-8	1250	22,600	191	37	16
Iridium 3-5	1250	32,700	826	35	15[c]
Iridium 3-11	1500	19,800	221	46	45
Iridium 3-13	1500	22,600	313	58	51
Iridium 3-10	1500	16,200	889	29	22
Iridium 3-9	1500	14,100	1086	18	24
Ruthenium 3-5	1000	47,400	137	13	5[b]
Ruthenium 3-4	1000	46,700	1427	17[d]	[e]
Ruthenium 3-1	1000	45,200	1835	5	2[b]
Ruthenium 3-16	1250	28,700	8	18	7[b]
Ruthenium 3-7	1250	23,900	33	6	2[b]
Ruthenium 3-8	1250	19,000	78	6	2[b]
Ruthenium 3-19	1250	16,700	283	7	2[b]
Ruthenium 3-15	1500	12,500	13	1	3[b]
Ruthenium 3-188	1500	9,500	55	5	4[b]
Ruthenium 3-17	1500	7,300	159	(f)	5[b]

(a) Rhodium, annealed 1/4 hr at 900 C; iridium, annealed 1 hr at 1500 C; ruthenium, annealed 1 hr at 1400 C.
(b) Calculated from total change in length divided by the length of the reduced section.
(c) Uncertain because of difficulty in measurements.
(d) Average value; specimen had elliptical cross section in the neck.
(e) Specimen was bent when removed from the furnace; measurement was not possible.
(f) Final diameter was larger than initial diameter.

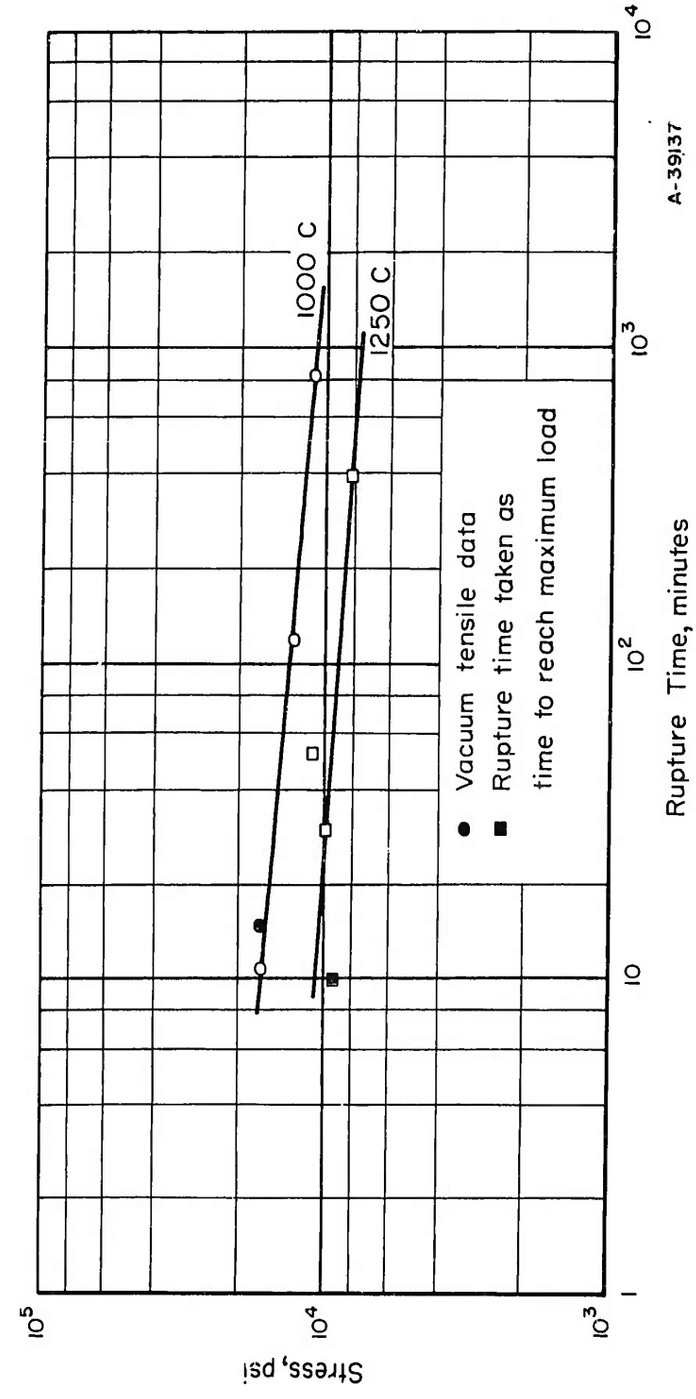

FIGURE 53. VACUUM STRESS-RUPTURE PROPERTIES OF RHODIUM AT 1000 AND 1250 C

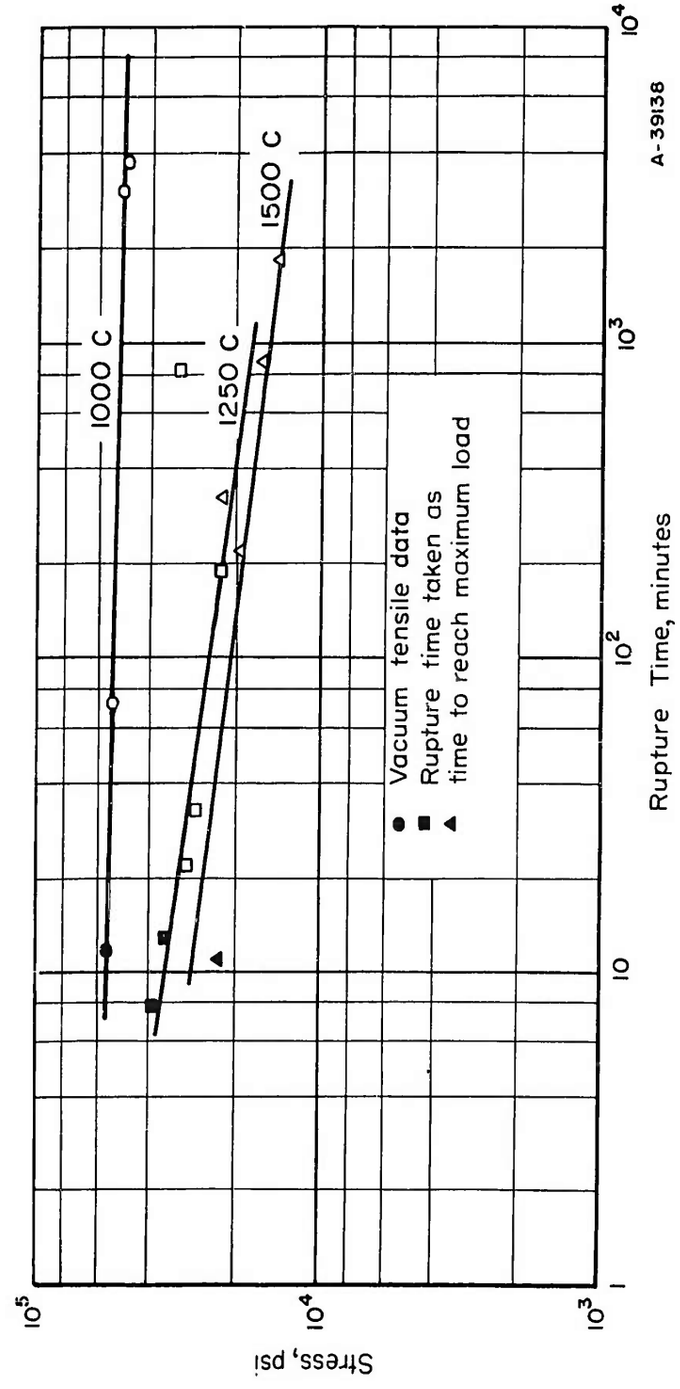

FIGURE 54. VACUUM STRESS-RUPTURE PROPERTIES OF IRIDIUM AT 1000, 1250, AND 1500 C

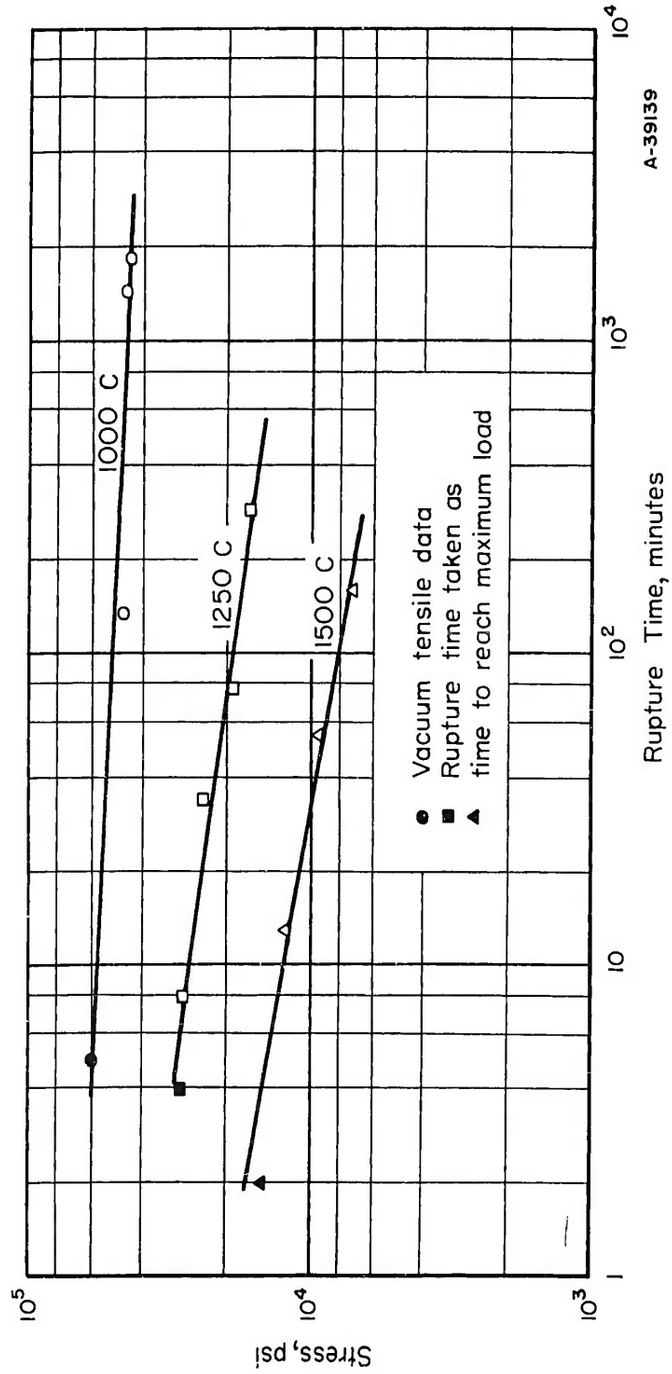

FIGURE 55. VACUUM STRESS-RUPTURE DATA FOR RUTHENIUM AT 1000, 1250, AND 1500 C

250X N75740

FIGURE 56. IRIDIUM (3-4)

Annealed 1 hour at 1500 C, vacuum creep test at 1000 C, stress 53,800 psi, rupture time 73 minutes.

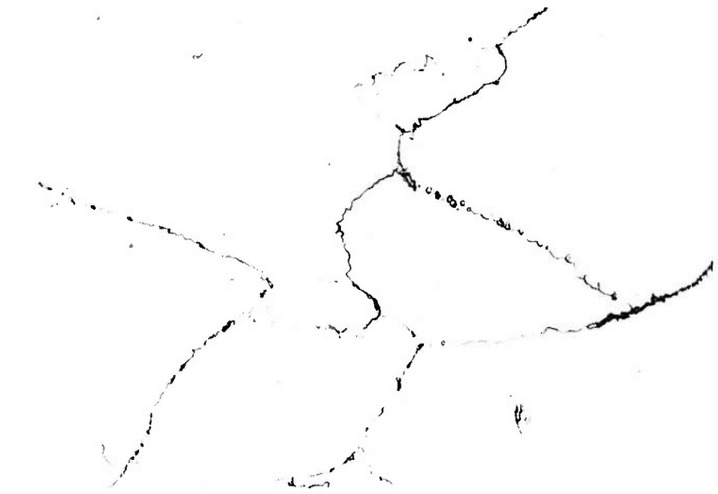

250X N75748

FIGURE 57. IRIDIUM (3-20)

Annealed 1 hour at 1500 C, vacuum creep test at 1250 C, stress 29,500 psi, rupture time 22 minutes.

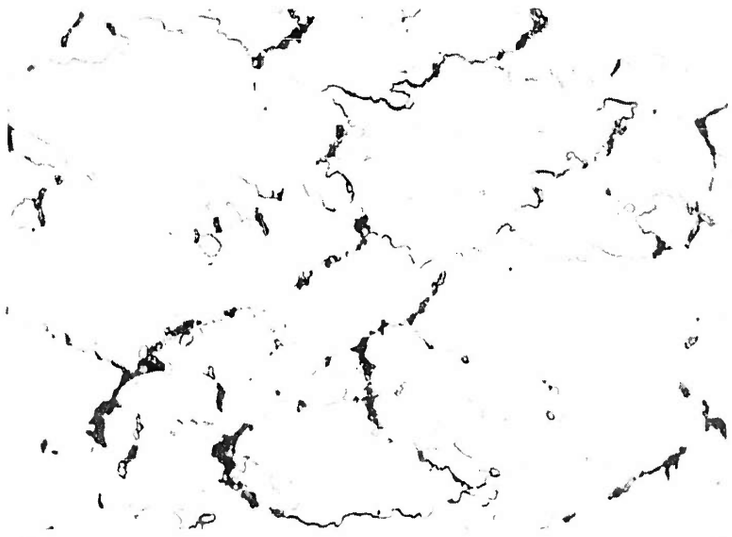

250X N75746

FIGURE 58. IRIDIUM (3-11)

Annealed 1 hour at 1500 C, vacuum creep test at 1500 C, stress 19,800 psi, rupture time 221 minutes.

related to microstructure. Typical structures of iridium creep tested at 1250 C show little deformation of the grains and apparent recrystallization or grain growth during testing. Tensile samples tested at this temperature showed granular deformation and no recrystallization, as illustrated in Figure 59. The only sample tested at 1250 C that deviated appreciably from the straight line describing the stress-rupture properties at 1250 C also showed some granular deformation and partial recrystallization, as illustrated in Figure 60.

All of the iridium and ruthenium samples tested in this program failed partially, or totally, by intergranular failure.

The stress-rupture and tensile data for rhodium and iridium are presented in a Larson-Miller-type plot in Figure 61. The rupture time for tensile tests was taken as the time to reach maximum load.

The data for ruthenium describe a single straight line with no inflection point marking a transition from low to high temperature deformation. This inflection point, or equicohesive break, is common in plots of this type, generally occurring at a parameter value calculated from data obtained at roughly one half the melting temperature of the material. The equicohesive break is illustrated by the data for rhodium. Its absence from the data for ruthenium is not understood.

These time-temperature parameter curves for rhodium and ruthenium should prove useful in predicting the high-temperature properties of the metals. Unfortunately, it was not possible to construct such a curve for iridium from the available data.

250X N75750

FIGURE 59. IRIDIUM VACUUM ANNEALED 1 HOUR AT 1500 C

Vacuum tensile test at 1250 C; UTS - 39,000 psi;
RA-69 per cent; elongation in 1/2 in. -37 per cent.

250X N75743

FIGURE 60. IRIDIUM (3-5)

Annealed 1 hour at 1500 C, vacuum creep test
at 1250 C, stress 32,700 psi, rupture time
826 minutes.

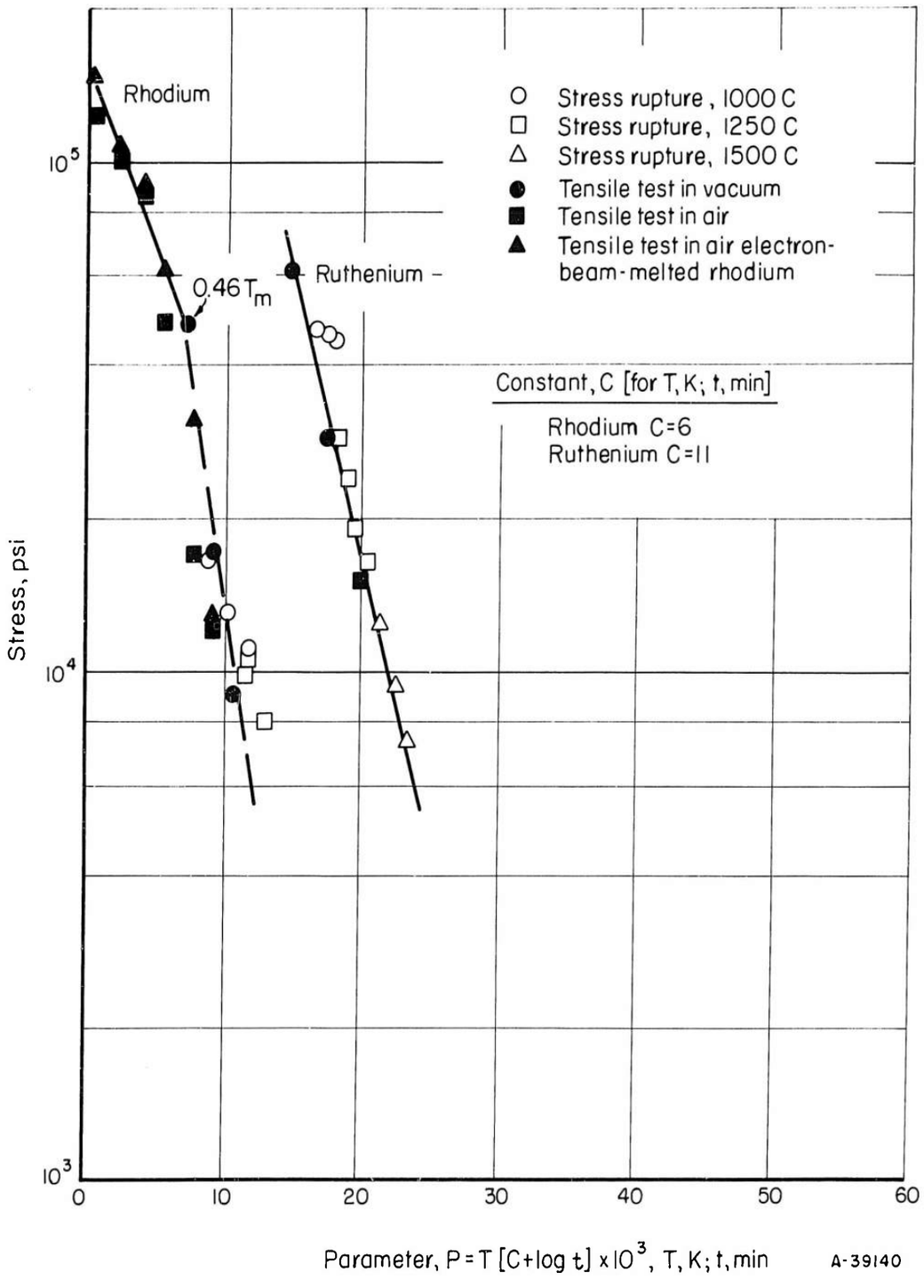

FIGURE 61. PARAMETRIC PLOT OF STRESS-RUPTURE AND TENSILE DATA FOR RHODIUM AND RUTHENIUM

Alloy Program

Alloys of the platinum-group metals with themselves were studied in this program. These studies were designed to show variations in basic metallurgical properties with alloying. One phase was a screening program utilizing 20, 40, 60, and 80 weight per cent additions of the platinum-group metals to rhodium, iridium, ruthenium, and osmium as bases. The other phase was a detailed study of rhodium-, iridium-, and ruthenium-base alloys containing 2.5 and 5.0 atomic per cent additions of the other platinum-group metals.

Screening Program

Rhodium, iridium, ruthenium, and osmium alloys containing 20, 40, 60, and 80 weight per cent additions of the other platinum-group metals were prepared as arc-melted 10-gram ingots. The hardness, microstructure, fabricability, and oxidation resistance of each alloy was evaluated. Hardness was evaluated in the as-cast and annealed conditions, fabricability was determined by forging and rolling at 1500 C (1800 C for osmium-containing alloys), and oxidation resistance was evaluated by 24-hour exposures at 800 and 1250 C in flowing air.

All alloy specimens were annealed at 1400 C in a hydrogen atmosphere. One-half of each ingot was exposed in a high-purity zirconia crucible, free of silica, boron, or phosphorus. The crucibles rested on a K-30 alundum brick. Metallographic examination of the annealed samples showed most rhodium-base alloys, high palladium content alloys, and some platinum-containing alloys were contaminated during

annealing. The contaminant appeared as a continuous, or semi-continuous grain-boundary phase, of high hardness. The depth of contamination extended well below the surface of the specimen. None of the annealed specimens had reacted with the crucible. The most likely source of contamination is silicon, arriving at the specimen in the vapor phase. Both the K-30 brick and the furnace muffle were potential sources of silicon.

Qualitative spectrographic analyses of a contaminated platinum specimen showed the silicon content was 0.003 to 0.1 per cent, less than the solubility limit of silicon in platinum at 825 C (the highest temperature where solubility data are available). If silicon is excluded from consideration, the source of contamination is not clear.

Fabricability screening studies were necessarily conducted at high temperatures because of the poor fabricability of the alloy bases. The pure platinum-group metals and their alloys are unique in that hardness does not correlate well with fabricability. For example, a Vickers hardness less than 100 normally indicates that a metal can be cold worked. Data presented thus far for rhodium illustrates that this "rule of thumb" does not hold for the platinum-group metals.

Hand forging with a 5-pound hammer in air was the first fabrication step. Alloys that forged successfully were subsequently hot rolled to 0.040-inch-thick strip or failure, whichever came first. All osmium-containing alloys were fabricated under a specially constructed mobile tent, that was exhausted at the top. The worker wore a gas mask for respiratory and eye protection. These measures were necessary and

satisfactory to protect the workers and keep the surrounding area free of toxic OsO_4 vapor. Each fabricated specimen was photographed with a 35-mm camera for a permanent record.

The oxidation screen program was accomplished by exposing half-buttons, in groups of about 25, for 24 hours in flowing air at 800 and 1250 C. Osmium-containing alloys were inadvertently exposed at 1200 C (rather than 1250 C). All of the oxidation specimens, except for samples of pure metals, were metallographic specimens that had been removed from the mounts. Specimens were placed, polished face up, on thin quartz rods, resting on high-purity aluminas and contained in a dished-out K-30 brick. Some of the initial exposures showed the alumina sand adhered lightly to the specimens in the absence of the quartz rods. The air flow rate in all tests was 2 standard cubic feet per hour.

The results of the hardness, microstructural, and fabricability studies are summarized in Table 8. The variation of as-cast hardness with composition for all of the alloys is illustrated in Figure 62. The maximum hardening results from osmium and ruthenium additions, in that order. Rhodium and iridium are generally ineffective as hardeners. There appears to be a general correlation of hardness with microstructure, the highest hardness generally occurring in two-phase alloys. Surprisingly, none of the metals, with the exception of osmium, are hardened appreciably by the addition of 20 weight per cent alloying elements. In fact, in most cases, hardness is initially diminished by the alloy addition. This behavior is understandable in the iridium-base alloys because of the high hardness of the pure metal

TABLE 8. HARDNESS, PHASE RELATIONS, AND FABRICABILITY OF AS-CAST AND ANNEALED PLATINUM-GROUP METAL ALLOYS

Alloy	Hardness, VHN, 5-Kg Load		Weight Loss After Four Melts, per cent	Phase Relations and Microstructure			Fabricability
	As Cast	Annealed		As Cast	Annealed 48 Hours at 1400 C		
					White Light	Polarized Light	
Rhodium	194	151	--	Single phase; coarse equiaxed grains	Single phase	--	Rolled to strip
Iridium	320	375	--	Equiaxed grains surrounded by second phase, probably IrO_2	IrO_2 dispersion	--	Rolled to strip
Ruthenium	339	350	--	Coarse columnar grains	Single phase	--	Not fabricable
Osmium	542	560	--	Coarse columnar grains	Single phase	--	Not fabricable
Platinum	58	94	--	--	Grain-boundary contamination	--	Rolled to strip
Palladium	60	84	--	--	Grain-boundary contamination	--	Rolled to strip
Rh-20 Pt	132	165	1.3	Single phase; coarse columnar grains	Grain-boundary contamination	--	Rolled to strip
-40 Pt	137	164	0.9	Ditto	Ditto	--	Ditto
-60 Pt	117	145	1.3	"	"	--	"
-80 Pt	103	123	2.1	Single phase; coarse columnar grains; some integranular cracking	"	--	"
Rh-20 Pd	178	178	5.0	Single-phase structures; coring in top and center of ingots but not at bottom; showing cooling rate effects	Grain-boundary contamination	--	Rolled to strip
-40 Pd	208	235	4.1		Ditto	--	Forged, cracked on rolling
-60 Pd	180	229	2.9		"	--	Ditto
-80 Pd	108	138	1.7		"	--	Rolled to strip
Rh-20 Ir	174	157	2.7	Single-phase structures with little or no coring; increased amounts of ϵ - β phase observed with increasing iridium. This is probably same phase noted in unalloyed iridium	Grain-boundary contamination	--	--
-40 Ir	225	177	1.2		Ditto	--	--
-60 Ir	234	171	3.3		"	--	--
-80 Ir	225	194	2.4		Single phase	--	--
Rh-20 Ru	193	203	1.5	Single phase	Grain-boundary contamination	Single phase, isotropic	--
-40 Ru	327	230	1.8	Considerable coring; possibly two phase	Ditto	Single phase, anisotropic	--
-60 Ru	286	330	6.6	Ditto	"	Two phase	--
-80 Ru	313	299	3.5	"	Single phase	Two phase	--
Rh-20 Os	206	203	1.8	Single phase, cored, shrinkage cracks	Grain-boundary contamination	Single phase, isotropic	Forged successfully
-40 Os	325	325	1.9	Ditto	Ditto	Single phase, isotropic	Ditto
-60 Os	502	475	4.5	Two phase, shrinkage cracks	Two phase	Two phase	Not fabricable
-80 Os	612	580	13.2	Single phase, cored, shrinkage cracks	Single phase, cored	Single phase, anisotropic	Ditto
Ir-20 Pt	289	235	1.1	Single phase, cored; IrO_2 grain-boundary dispersion	Single phase	--	Forged, cracked on rolling
-40 Pt	341	387	1.2	Single phase, cored, shrinkage cracks	Single phase	--	Rolled to strip
-60 Pt	345	479	1.2	Ditto	Grain-boundary contamination	--	Ditto
-80 Pt	208	299	1.6	Single phase, cored	Ditto	--	"

TABLE 8. (Continued)

Alloy	Hardness, VHN, 5-Kg Load		Weight Loss After Four Melts, per cent	Phase Relations and Microstructure			Fabricability
	As Cast	Annealed		As-Cast	Annealed 48 Hours at 1400 C		
					White Light	Polarized Light	
Ir-20 Pd	237	228	1.2	Structure outlined by IrO_2 dispersion	Single phase	--	Not fabricable
-40 Pd	406	590	6.9	Cored, shrinkage cracking	Cored	--	Ditto
-60 Pd	262	247	3.0	Structure outlined by IrO_2 dispersion, shrinkage cracks	Grain-boundary contamination	--	"
-80 Pd	148	448	1.8	Cored, apparently single phase	Ditto	--	"
Ir-20 Ru	283	263	4.2	Columnar grains; substructures outlined by IrO_2 dispersion	Single phase	Single phase, isotropic	Not fabricable
-40 Ru	452	336	3.9	Cored, apparently two phase	Cored	Two phase	Ditto
-60 Ru	244	308	7.0	Ditto	Cored	Single phase, anisotropic	"
-80 Ru	287	337	23.1	Single phase, cored	Cored	Ditto	"
Ir-20 Os	296	291	11.8	Cored, dentrites outlined by IrO_2 dispersion	Single phase	Single phase, isotropic	Not fabricable
-40 Os	396	412	13.1	Two phase	Single phase	Ditto	Ditto
-60 Os	534	548	5.6	Two phase	Two phase	Two phase	"
-80 Os	482	501	19.5	Single phase, cored	Cored	Single phase, anisotropic	"
Ru-20 Pt	329	330	11.2	Cored, possibly two phase	Cored	Single phase, anisotropic	Not fabricable
-40 Pt	516	446	4.0	Two phase	Cored	Two phase	Ditto
-60 Pt	310	293	3.0	Cored	Single phase	Single phase, isotropic	Rolled to strip
-80 Pt	246	253	2.2	Single phase	Single phase	Ditto	Ditto
Ru-20 Pd	287	412	20.6	Single phase, internal cracking	Single phase	Single phase, anisotropic	Not fabricable
-40 Pd	437	425	40.4	Two phase, cored	Single phase	Two phase	Ditto
-60 Pd	306	284	5.9	Two phase	Two phase	Ditto	Rolled to strip
-80 Pd	254	243	2.9	Two phase, dentritic	Two phase	"	Ditto
Ru-20 Os	328	430	6.0	Single phase, cored	Cored	Single phase, anisotropic	Limited forgeability, decreasing with increasing osmium content. All cracked slightly during forging
-40 Os	467	405	7.7	Ditto	Cored	Ditto	
-60 Os	440	447	5.7	"	Cored	"	
-80 Os	610	594	5.8	"	Cored	"	
Os-20 Pt	613	578	14.7	Single phase, integranular cracking	Single phase	Single phase, anisotropic	Not fabricable
-40 Pt	646	555	8.3	Two phase, dentritic, integranular cracking	Cored	Two phase	Ditto
-60 Pt	495	504	4.5	Two phase	Two phase	Ditto	"
-80 Pt	440	570	3.9	Severe cording, possibly two phase	Two phase	Single phase, isotropic	"
Os-20 Pd	506	--	--	Single phase, integranular cracking	No further work was done with these alloys		
-40 Pd	125	--	--	Ditto			
-60 Pd	567	--	14.5	"			
-80 Pd	472	--	6	Two phase; unmelted osmium visible			

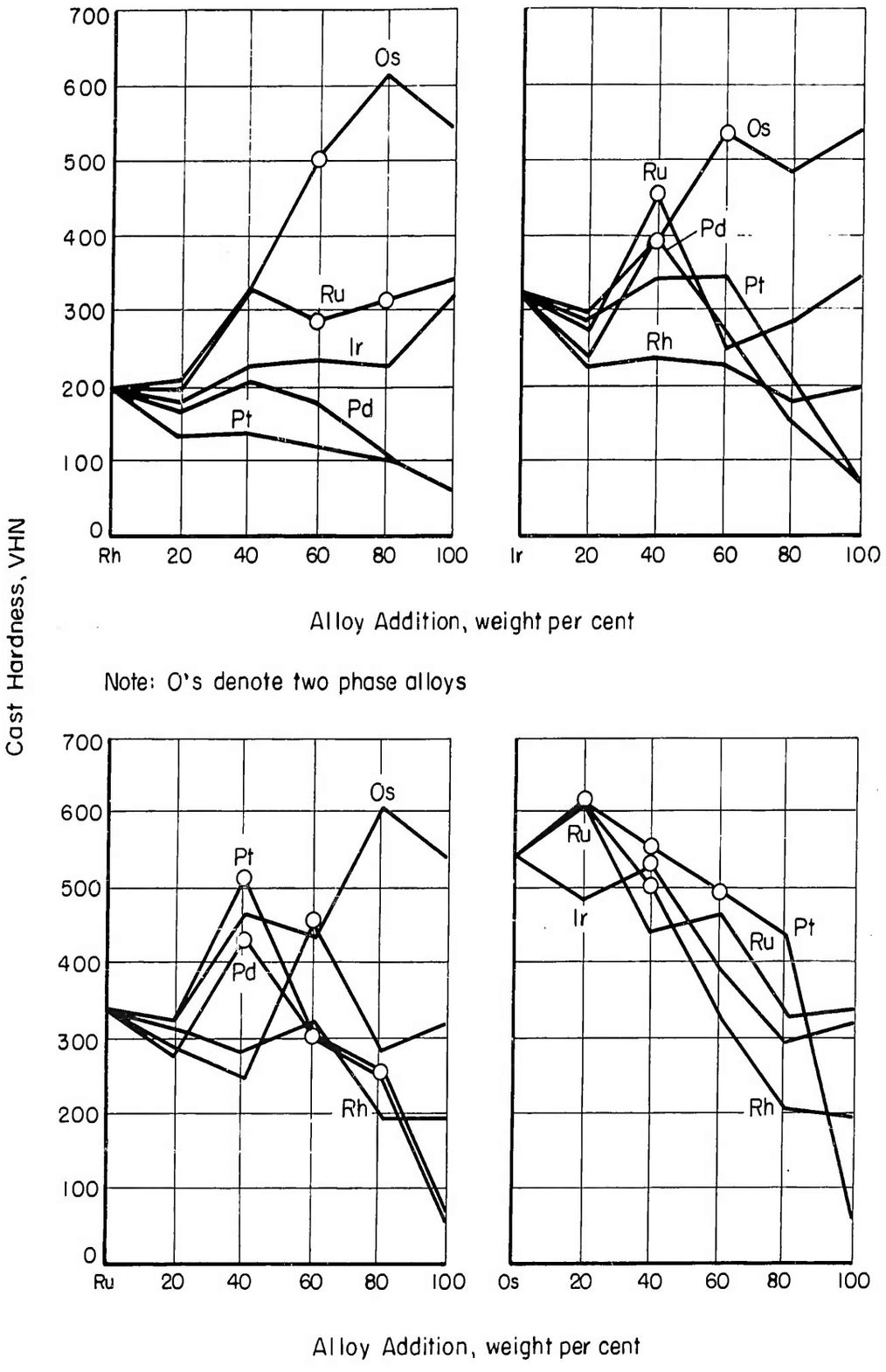

FIGURE 62. AS-CAST HARDNESS OF SEVERAL REFRACTORY NOBLE-METAL-ALLOY SYSTEMS (5)

and high oxygen content, 0.07 weight per cent, of the melting stock. Pure iridium contained a second phase, tentatively identified as IrO_2. There are no apparent reasons for the initial hardness reduction in rhodium- and ruthenium-base alloys.

The fabricability survey showed that none of the alloys based on a hexagonal close-packed structure is fabricable within the composition limits and working temperature studied. However, some ruthenium-osmium alloys showed limited forgeability. Two-phase alloys also, generally, were not fabricable. Most alloys containing 60 or 80 per cent of platinum or palladium were easily worked, whereas combinations of the refractory members of the group showed little, if any, fabricability.

The combinations of face-centered cubic metals with one another, produced continuous series of solid solutions. A two-phase region was observed in FCC-HCP combinations. It was often difficult to determine single-phase from two-phase structures because of the coring in these latter alloys. Cored, or unhomogeneous structures, were very stable and most often did not change during annealing 48 hours at 1400 C. Tentative solubility limits, based on this study, for FCC-HCP combinations are listed below:

Metal	Alloy Addition	Solubility in Metal, weight per cent	Solubility of Metal in Alloy Addition, weight per cent
Rhodium	Ruthenium	20	Not clear, probably 20
	Osmium	40	20
Iridium	Ruthenium	20	40
	Osmium	40	20
Ruthenium	Platinum	20	40
	Palladium	20	<20
Osmium	Platinum	20	Not clear
	Palladium	60	Not clear

The results of the qualitative study of the oxidation behavior of platinum-group metal interalloys are presented in Table 9. Of the face-centered cubic alloys, only three, Ir-40Pt, Ir-60Pd, and Rh-20Ir, showed a weight change in excess of 2 per cent at either exposure temperature. The Ir-40Pt alloy had a porous surface and apparently hollow interior after exposure at 1250 C. The Ir-60Pd specimen fell apart after exposure at 800 C. The Rh-20Ir alloy showed a large increase in weight indicative of pickup of foreign material. There is no apparent reason for these anomalous results.

Among the ruthenium- and osmium-containing alloys, the weight loss generally increases as the concentration of the less oxidation-resistant metal increases. This is especially noticeable after the higher temperature exposure. Virtually all the ruthenium alloys exposed at 800 C showed minor weight changes. Of the osmium alloys, those containing 20 and 40 weight per cent osmium often showed acceptable oxidation resistance at 800 C.

TABLE 9. CHANGE IN WEIGHT OF PLATINUM-GROUP METAL ALLOYS UPON EXPOSURE IN FLOWING AIR AT ELEVATED TEMPERATURES

Alloy	Change in Weight, per cent[a] 800 C	1250 C	Alloy	Change in Weight, per cent[a] 800 C	1250 C
Rhodium	+0.22	0	Ir-20 Ru	0	-1.90
Rh-20 Pt	0	+0.04	Ir-40 Ru	0	-7.52
Rh-40 Pt	-0.01	+0.06	Ir-60 Ru	-0.01	-33.79
Rh-60 Pt	0	+0.04	Ir-80 Ru	-0.03	-44.49
Rh-80 Pt	0	0	Ruthenium	-0.02	-5.43
Platinum	0	0	Ir-20 Os[b]	0	-1.63
Rh-20 Pd	-0.04	+0.16	Ir-40 Os	0	-2.25
Rh-40 Pd	+0.03	+0.25	Ir-60 Os	-0.95	-56.4
Rh-60 Pd	+0.07	+0.33	Ir-80 Os	-78.30	-47.30
Rh-80 Pd	+0.09	+0.11	Osmium	100	--
Palladium	0	-0.10	Ruthenium	-0.02	-5.43
Rh-20 Ir	+24.0	+0.01	Ru-20 Pt	-0.03	-26.24
Rh-40 Ir	0	-0.01	Ru-40 Pt	-0.01	+7.05
Rh-60 Ir	-0.01	-0.04	Ru-60 Pt	0	-14.91
Rh-80 Ir	+0.01	-0.16	Ru-80 Pt	-0.008	-1.63
Iridium	0	-1.55	Platinum	0	0
Rh-20 Ru	0	-0.06	Ru-20 Pd	-0.02	-25.69
Rh-40 Ru	+0.02	-8.57	Ru-40 Pd	+0.01	+9.25
Rh-60 Ru	+0.01	-21.19	Ru-60 Pd	+0.05	-33.03
Rh-80 Ru	0	-36.38	Ru-80 Pd	+0.02	-7.20
Ruthenium	-0.02	-5.43	Palladium	0	-0.10
Rh-20 Os[b]	-19.38	+0.07	Ru-20 Os[b]	-0.18	-5.05
Rh-40 Os	-0.08	-1.19	Ru-40 Os	+0.01	-6.69
Rh-60 Os	-0.78	-63.56	Ru-60 Os	-0.24	-9.42
Rh-80 Os	-100	--	Ru-80 Os	-72.06	-29.68
Osmium	-100	--	Osmium	100	--
Iridium	0	-1.55	Osmium[b]	100	--
Ir-20 Pt	+0.009	-0.53	Os-20 Pt	100	--
Ir-40 Pt	-0.02	-56.15	Os-40 Pt	100	--
Ir-60 Pt	-0.04	-0.15	Os-60 Pt	-17.36	-23.91
Ir-80 Pt	-0.099	-0.04	Os-80 Pt	-0.08	-8.98
Platinum	0	0	Platinum	0	0
Ir-20 Pd	0	-1.76			
Ir-40 Pd	+0.04	-0.98			
Ir-60 Pd	(c)	--			
Ir-80 Pd	0	+1.47			
Palladium	0	-0.1			

(a) All alloys showing a change in weight of 0.0002 gram or less (the sensitivity of the balance) are considered to have no change in weight.

(b) All osmium-containing alloys were exposed at 1200 C rather than 1250 C.

(c) Specimen fell apart in a flaky mass.

It is interesting that alloys containing 80 per cent ruthenium generally were less oxidation resistant than pure ruthenium at 1250 C.

It appears, from examination of specimens, that the weight losses were through volatilization, as would be expected. The volatilization was usually manifested as thermal etching, as illustrated in Figure 63. The alloys, Rh-20 Os and Rh-40 Os, show a typical development of microstructure after 24 hours at 1200 C. The alloy, Rh-80 Os, exposed at 800 C, is typical of many of the high osmium alloys. This specimen was intact upon removal from the furnace, but crumbled under the pressure of tweezers.

Although the results of the screening tests are only qualitative, they do point out the alloy compositions that would not be useful for elevated temperature service. In general, it appears that rhodium- and iridium-base alloys containing up to 40 weight per cent ruthenium or osmium would have reasonable oxidation resistance at 1200 C. Alloys containing more than 40 per cent osmium or ruthenium would not be serviceable at elevated temperatures in air.

Effect of Small Additions of Platinum-Group Metals on the Properties of Rhodium, Iridium, and Ruthenium

Rhodium-, iridium-, and ruthenium-base alloys containing 2.5 and 5.0 atomic per cent additions of the platinum-group metals were consolidated by powder metallurgy techniques at 15 to 20 tsi with a CCl_4 lubricant, using high purity powders. Rhodium and ruthenium alloys weighed 20 grams; iridium alloys weighed 40 grams. Rhodium- and iridium-base alloys were presintered 1 hour in vacuum at 1200 C and then

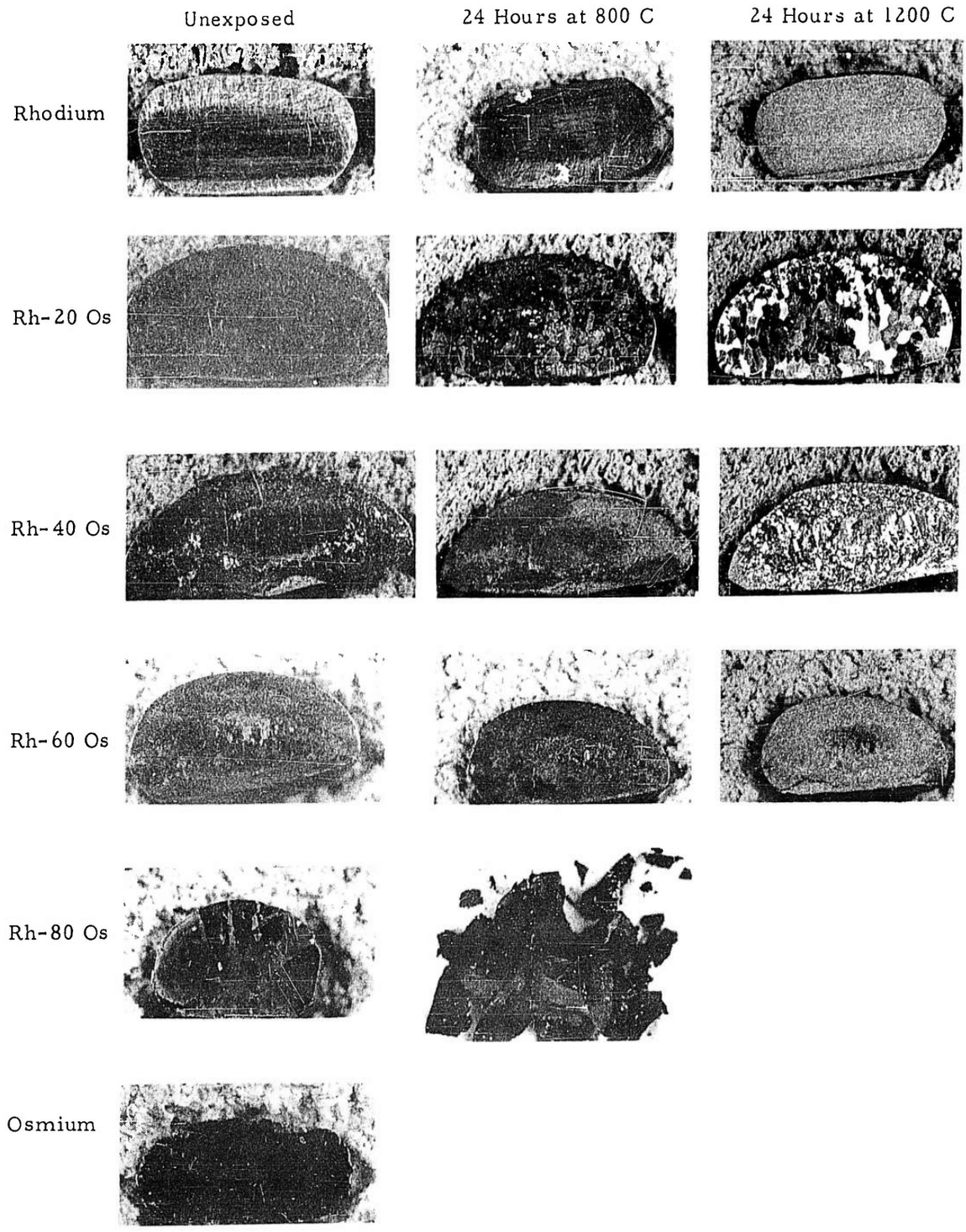

FIGURE 63. PHOTOGRAPHS OF RHODIUM-OSMIUM ALLOYS AFTER EXPOSURE TO OXIDIZING CONDITIONS

arc-cast as 3/8-inch-diameter, 1-inch-long cylinders. All arc-cast alloys were radiographed to check for cracking, pores, and inhomogeneities. Two to four melts of each alloy were required to produce acceptable ingots. Ruthenium-base alloys were presintered 3 hours at 1200 C and sintered 3 hours at 1800 C, both in hydrogen. The as-sintered densities of the alloys ranged from 88 to 92 per cent of the density of pure ruthenium.

Thin slices cut from the ends of selected rhodium and iridium alloys were flat rolled at 1750 C, to determine suitable fabrication schedules. Flat rolling tests were successful, indicating the alloys could be rod rolled directly in preparation for swaging. This was not the case; most alloys cracked severely during rod rolling. Hot forging, prior to rod rolling, or direct hot swaging, was therefore used for the fabrication of most alloys.

The fabrication procedures developed for pure rhodium and iridium, presented in a previous section of this report, were generally suitable for the fabrication of alloys. The established procedures for ruthenium fabrication were applied to the ruthenium alloys, but with little success. The fabrication schedules and results for each alloy are presented in Table 10.

The rhodium-base alloys were most fabricable; all but two were successfully fabricated to wire. Iridium-base alloys were less fabricable than the rhodium alloys. Ruthenium-base alloys could not be fabricated successfully.

TABLE 10. FABRICATION SCHEDULES FOR RHODIUM, IRIDIUM, AND RUTHENIUM-BASE ALLOYS

Alloy	Forging Temp (C) and Remarks	Rod Rolling Temp (C) and Remarks	Swaging Temp (C) and Remarks	Wire Drawing Remarks	Final Condition
Rh-2.5 Pt	1800	1800	1800 to 1250	Cold drawn, intermediate anneal at 650 C	0.064-inch-diameter wire
Rh-5.0 Pt	1800	1800	1800 to 950	Ditto	0.053-inch-diameter wire
Rh-2.5 Pd	1700	1700	1700 to 1250	"	0.071-inch-diameter wire
Rh-5.0 Pd	1800, cracked beyond recovery	--	--	--	Broken
Rh-2.5 Ir	1800	1500	1800 to 1100	Hot wire drawn	0.067-inch-diameter wire, as swaged
Rh-5.0 Ir	1800	1800	1700 to 950	Cold drawn, intermediate anneal at 650 C	0.058-inch-diameter wire
Rh-2.5 Ru	1800	1800	1700 to 1000	Ditto	0.055-inch-diameter wire
Rh-5.0 Ru	1800	1800	1700 to 950	"	0.064-inch-diameter wire
Rh-2.5 Os	1800	1500	1600 to 1300	Hot wire drawn	0.086-inch-diameter wire, as swaged
Rh-5.0 Os	No suitable ingot of this alloy was prepared		--	--	--
Ir-2.5 Pt	1750	1750	1650 increased to 1750; broke into fragments during each swaging pass		--
Ir-5.0 Pt[a]	1800, cracked beyond recovery	--	--	--	--
Ir-5.0 Pt[b]	1800	1800, cracked beyond recovery during first pass in rod rolls	--	--	--
Ir-2.5 Pd	1800	1800	1800 to 1100	--	0.068-inch-diameter wire, as swaged
Ir-5.0 Pd[a]	1800	1800, cracked beyond recovery	--	--	--
Ir-5.0 Pd[b]	1800	1800	1800 to 1250	--	0.068-inch-diameter wire, as swaged
Ir-2.5 Rh	1800	1800, cracked beyond recovery	--	--	--
Ir-5.0 Rh	1800	1800	1800 to 950	--	0.070-inch-diameter wire, as swaged
Ir-2.5 Ru[a]	1800	1800, cracked beyond recovery	--	--	--
Ir-2.5 Ru[b]	1800	1800	1800 to 1400	--	0.064-inch-diameter wire, as swaged
Ir-5.0 Ru	1800	1800	1750, cracking during each swaging pass, until completely fragmented	--	--
Ir-2.5 Os	1800	1800	1800, failed during swaging	--	--
Ir-5.0 Os[a]	1800	1800	1800 to 1600, failed during swaging	--	--
Ir-5.0 Os[b]	1800 (deep cracking)	1800	1700 to 1600, failed during swaging	--	--

TABLE 10. (Continued)

Alloy	Forging Temp (C) and Remarks	Rod Rolling Temp (C) and Remarks	Swaging Temp (C) and Remarks	Wire Drawing Remarks	Final Condition
Ru-2.5 Pd[a]	1800, cracked beyond recovery	--	--	--	--
Ru-2.5 Pd[b], arc melted	--	--	1800, failed during first swaging pass	--	--
Ru-5.0 Pd[a]	1800, cracked beyond recovery	--	--	--	--
Ru-5.0 Pd[b], arc melted	1800, cracked beyond recovery	--	--	--	--
Ru-2.5 Ir	1800	1800	1800 to 1650, failed during swaging	--	--
Ru-5.0 Ir	1800	1800	1800, failed during swaging	--	--
Ru-2.5 Rh[a]	1800	1800, cracked beyond recovery	--	--	--
Ru-2.5 Ru[b]	1800, cracked deeply	1800, cracked beyond recovery	--	--	--
Ru-5.0 Rh[a]	1800	1800, cracked beyond recovery	--	--	--
Ru-5.0 Rh[b]	1800	1800, slight cracking	1800, failed during swaging	--	--
Ru-2.5 Os[a,b]	1800, broke in two pieces	1800, cracked beyond recovery	--	--	--
Ru-5.0 Os[a,b]	1800	1800, cracked beyond recovery	--	--	--

(a) Original alloy.
(b) Duplicate alloy.

Most alloys studied showed slight cracking at various stages of reduction. Cracking was most severe during initial ingot breakdown, but could generally be removed by grinding. Intergranular cracking was found in all iridium- and ruthenium-base alloys that were examined. Cracking was associated with large grain size or a mixture of very large and very small grain sizes. The latter case was found most often in ruthenium-base alloys.

The as-cast hardness of most rhodium- and iridium-base alloys is illustrated in Figure 64. Few of the alloy additions are effective hardeners, as was found with alloys covered in the screening program. The addition of 2.5 atomic per cent platinum to rhodium does increase the hardness significantly; this was not reflected in the fabricability of this alloy.

The recrystallization characteristics of several of the rhodium-base alloys are illustrated in Figure 65. The alloy additions raise the temperature for 50 per cent softening by 100 to 300 C. The addition of 2.5 atomic per cent osmium is most effective in raising the recrystallization temperature.

The hardness and recrystallization studies are the only parts of the alloy evaluation that were completed during the contract period. The fabricated alloys will be held pending evaluation at a future date.

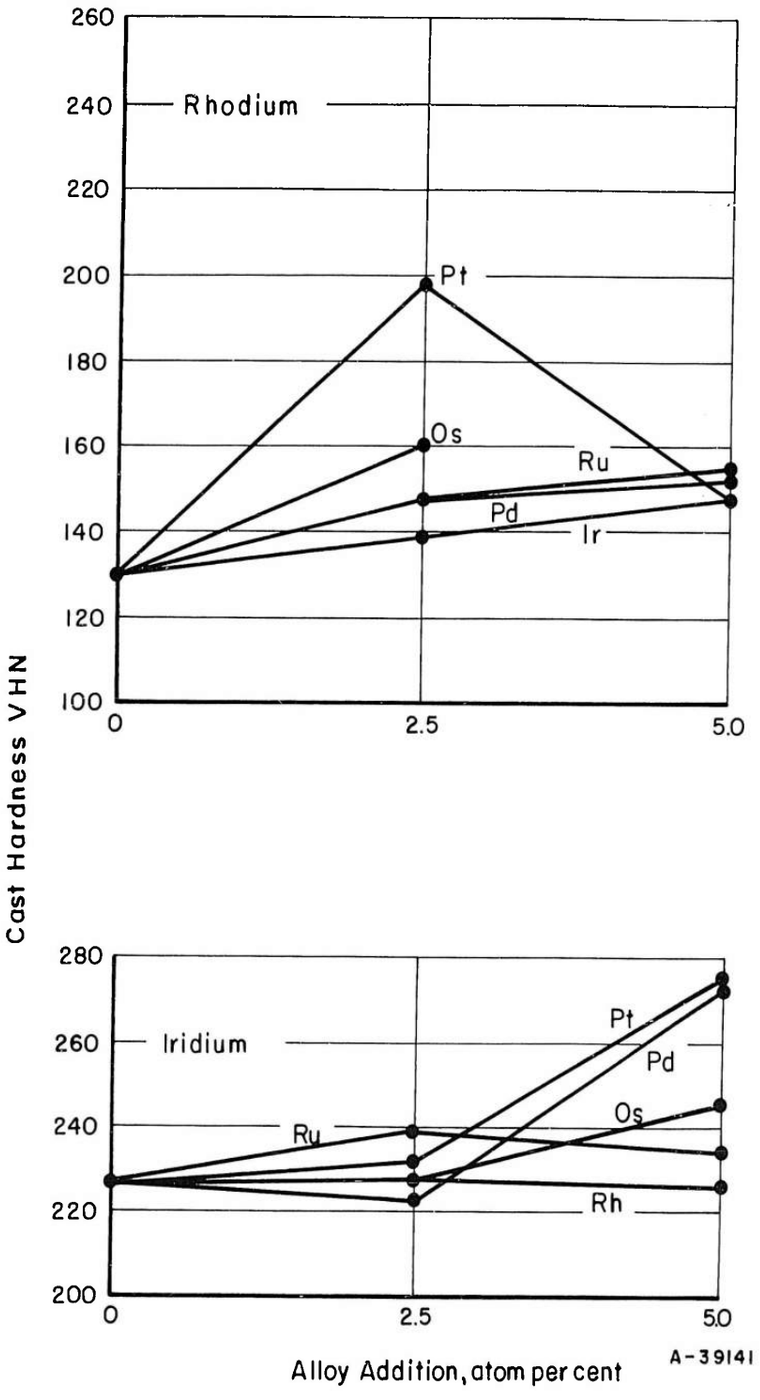

FIGURE 64. VARIATION OF CAST-HARDNESS WITH ALLOY CONTENT FOR RHODIUM AND IRIDIUM-BASE ALLOYS

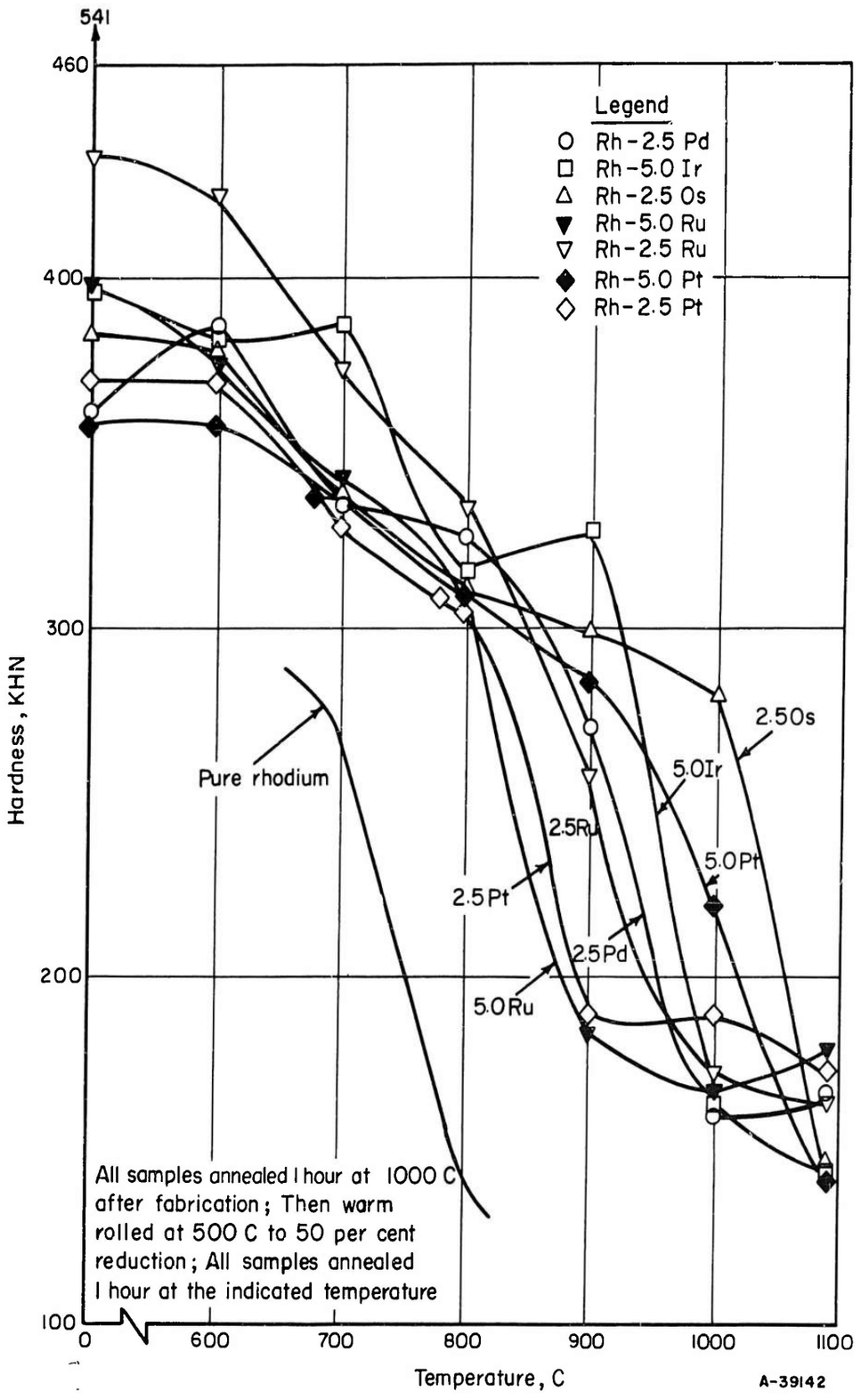

FIGURE 65. VARIATION OF HARDNESS WITH ANNEALING TEMPERATURE FOR WARM-WORKED RHODIUM-BASE ALLOYS

APPENDIX

OXIDATION CHARACTERISTICS OF THE UNALLOYED PLATINUM-GROUP METALS

The oxidation behavior of the platinum-group metals was relatively unexplored at the beginning of this research program. A complete investigation of this aspect was an undertaking too large to be within the scope of the over-all program. Therefore, studies were carried out to provide information on the effect of temperature on the rate of oxidation of these metals and to explore the nature of the process by which oxidation occurs.

The primary aim was to obtain base-line information on the platinum-group refractory metals. Several experiments were run on platinum because this metal had been investigated in other programs, and it was thought that the cumulative information would provide a better insight into the mechanism whereby oxidation occurs.

Materials

All specimens used in the oxidation studies were from the original shipment received for the program, as described at the beginning of this report.

Foil specimens of palladium, platinum, and rhodium were used to provide a greater surface area for oxidation and, thereby, provide large weight changes. Dimensions of the foils were 6-9 inches long by 0.7-0.7 inch wide by 0.003 inch thick. The foils were coiled around the center post of a quartz suspension basket with a spacing of 1/16-1/8 inch for the oxidation tests.

The specimens of iridium, ruthenium, and osmium were rectangular slabs cut from vacuum-arc-melted buttons, except for one specimen of osmium which was a powder metallurgy product prepared as follows:

Conditions	Density, per cent of theoretical
CCl_4 binder, 15 tsi	38
Presinter in H_2, 3 hours to 1200 C, 1 hour at 1200 C	44.5
Sinter in H_2, rapid heating to 1200 C, 3 hours from 1200 C to 1800 C, 6 hours at 1800 C	88

Preliminary oxidation tests had indicated that iridium, ruthenium, and osmium oxidized sufficiently rapidly that the smaller surface area specimens would give meaningful weight-change data.

All specimens were polished through 600-grit paper and degreased before oxidation.

Procedure

Oxidation of the specimens was done in a 1-5/8-inch inside diameter vertical tube furnace using an atmosphere of flowing air previously dried by passing through "Drierite". Except where noted, the flow rate of air was 1-3/4 scfh. The specimen position in the "Globar" heated furnace, in general, was automatically controlled to ±2 degrees C over the temperature range from 800 to 1400 C.

The coiled foil specimens of palladium, platinum, and rhodium sat on four small arms of a quartz basket and the slab specimens of iridium, ruthenium, and osmium were suspended in loosely fitting harnesses made of platinum wire.

Weight changes were measured automatically with a continuously recording analytical balance, and the total weight change during a test was checked from the initial and final weights of the specimens.

Table 11 summarizes the experimental results obtained for the oxidation of the platinum-group metals. With the following three exceptions, all of the specimens lost weight with a linear rate through the duration of the oxidation periods:

(1) Rhodium formed a protective oxide at 1000 C (Figure 66).

(2) The rate of oxidation of ruthenium was so rapid at 1400 C that the initial area of the specimen decreased significantly in a 6-hour test, making the rate of weight loss appear to decrease with time (Figure 67). The same effect could be expected for osmium, but more pronounced because of the much higher oxidation rate. The continuous weighing data for osmium were unreliable to show this because the rapidity with which weight was lost caused erratic behavior of the balance.

TABLE 11. SUMMARY OF EXPERIMENTAL RESULTS FOR OXIDATION OF THE PLATINUM-GROUP METALS

Experiment	Temp, C	Time, hr	Original Surface Area, cm^2	Weight Change, mg	Linear Rate of Weight Loss, $mg/cm^2/hr$
			Rhodium		
28-96	1000	20.9	76.1	+17.0	Protective oxide formed
28-92	1200	6	75.8	-0.7	1.5×10^{-3}(a)
25-8	1200	17	70.3	-1.1	9.2×10^{-4}
28-98	1300	6	76.4	-18.3	3.99×10^{-2}(a)
25-4	1300	17	70.0	-2.7	2.3×10^{-3}
28-94	1400	6	76.0	-3.2	7.0×10^{-3}(a)
25-10	1400	17	73.1	-9.2	7.4×10^{-3}
			Platinum		
28-95	1000	17	102.0	-0.1	--
25-7	1100	17	102.2	-0.9	5.2×10^{-4}
28-91	1200	6	101.4	-1.4	2.3×10^{-3}
28-99	1200	6	102.3	-2.7	4.4×10^{-3}(b)
25-16	1200	46.5	70.1	-5.6	1.72×10^{-3}
25-9	1300	17	103.6	-5.5	3.12×10^{-3}
25-17	1300	21.5	70.4	-6.5	4.29×10^{-3}
28-97	1400	6	102.0	-4.3	7.0×10^{-3}
25-11	1400	17	103.6	-18.0	1.02×10^{-2}
25-18	1400	22	67.8	-13.7	9.19×10^{-3}
			Iridium		
25-14	1000	6	4.41	-17.2	0.650
25-12	1200	6	4.26	-41.9	1.64
25-13	1400	6	4.50	-81.9	3.04
			Ruthenium		
28-59	415	6	2.98	-0.2	--(c)
28-60	685	6	2.98	-0.4	2×10^{-2}(c)
28-100	1000	17	2.87	-25.4	0.523
28-72	1020	6.03	1.81	-11.0	1.01(c)
28-68	1090	6	2.93	-39.7	2.26(c)
28-61	1090	6	2.58	-62.0	4.00(b, c)
25-5	1100	6	2.83	-56.8	3.34
25-1	1200	6	2.94	-218.7	12.4
25-7	1200	6	2.77	-273.3	16.4(b)
28-70	1280	6.04	2.99	-586.5	32.4(c)
28-49	1400	6	2.80	-1060	63.0(c)
25-2	1400	3	1.79	-544.0	101
			Osmium		
25-19	600	0.25	5.58	-1450.4	See text
28-49	1000	0.88	4.69	-5605.6	1350
28-1	1200	0.15	1.99	-242.7	810
28-49	1400	0.67	4.56	-3764.8	1240
			Palladium		
28-49	1000	6	103.4	+2.1	See text
28-1	1200	6	3.42	+1.3	See text

(a) Results considered to be in error due to inadequate removal of oxide scale which forms at lower temperatures.
(b) Flow of dry air was 8-3/4 scfh, 5 times the 1-3/4 scfh used for all tests except where indicated.
(c) Results considered to be less reliable than others because of inadequate temperature control on furnace.

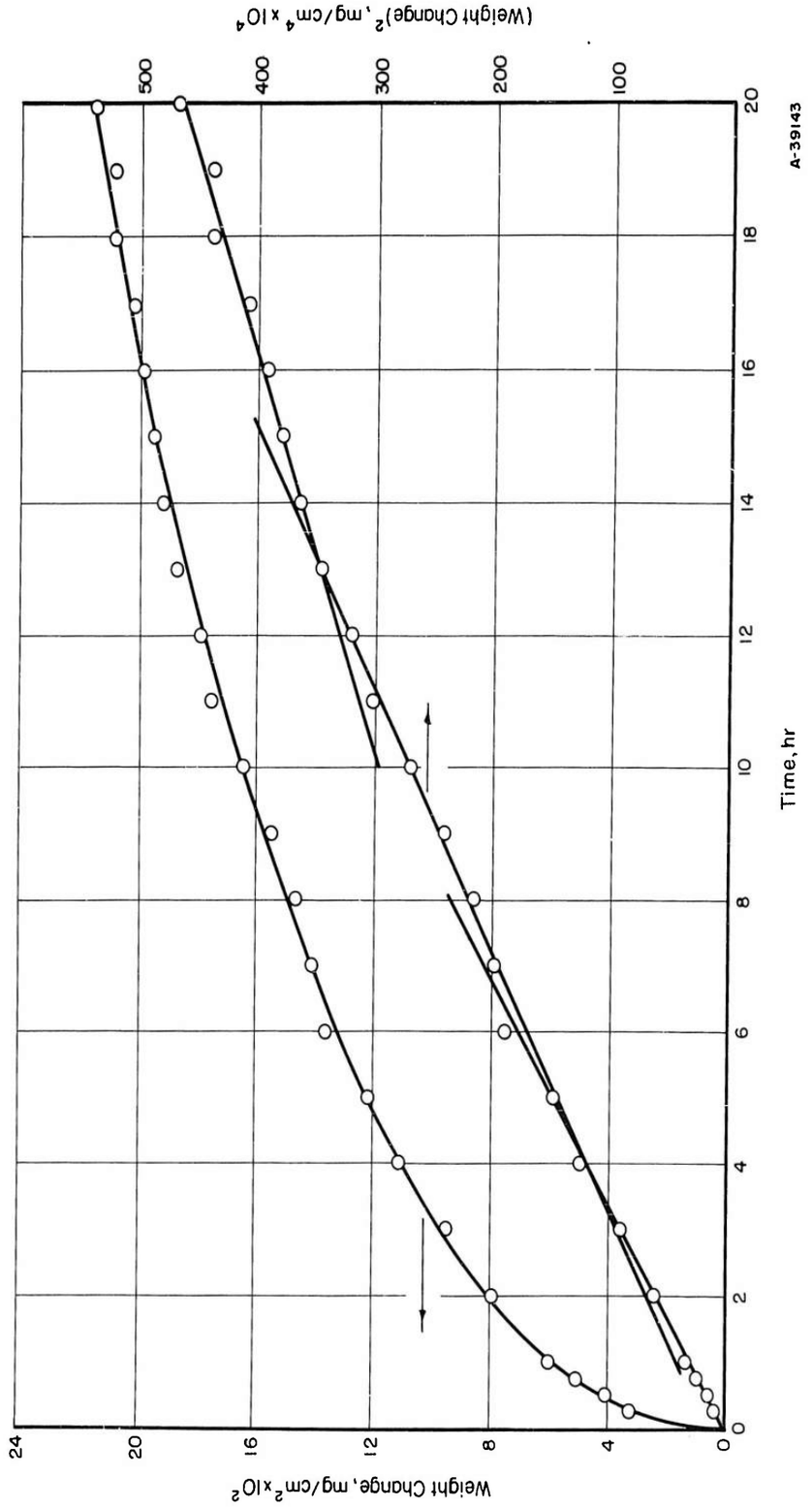

FIGURE 66. WEIGHT GAIN OF RHODIUM IN SLOWLY FLOWING DRY AIR AT 1000 C

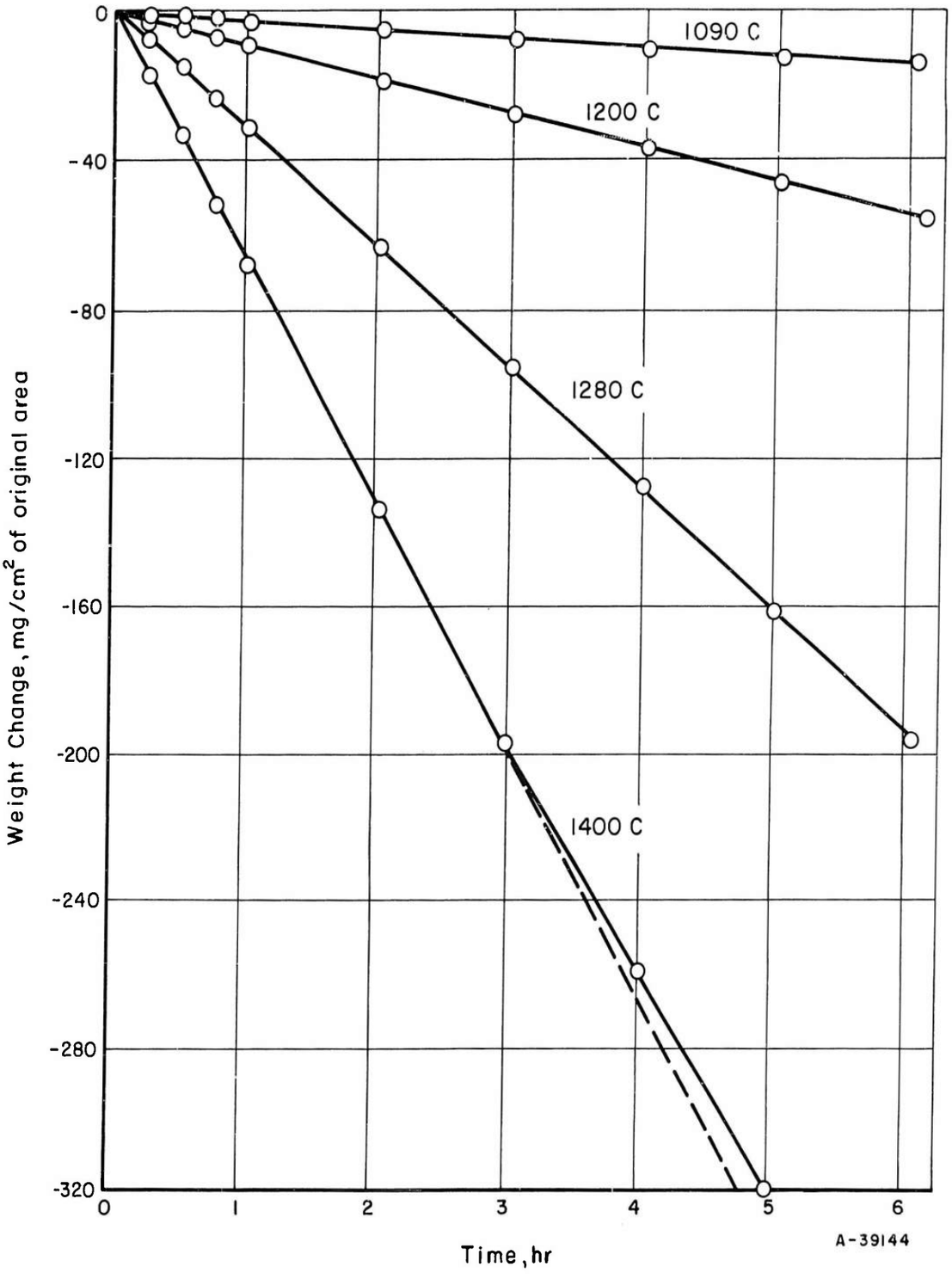

FIGURE 67. WEIGHT LOSS OF RUTHENIUM IN SLOWLY FLOWING DRY AIR AT ELEVATED TEMPERATURES

(3) Palladium gained weight at 1000 and 1200 C, which, according to other investigators, is due in large part to the solubility of oxygen in palladium (Figure 68).

Figure 69 shows an Arrhenius plot of the linear rates of weight loss observed for the platinum-group metals. The results in Table 11, footnoted as being of questionable accuracy, have not been included for simplicity in presentation. All of the data points in Figure 69 were obtained using an air flow of 1-3/4 scfh.

Figure 70 shows the effect of air velocity on the rate of oxidation of ruthenium and platinum. Within the ranges studied, increasing the air flow by a factor of 5 increased the rate of weight loss of platinum by a factor of 1.9-2.6 at 1200 C, and increased the rate of weight loss of ruthenium by a factor of 1.8 and 1.3 at 1090 and 1200 C, respectively.

Ruthenium

Purplish-black material, which was collected on the quartz suspension rods as a condensation product during the oxidation of ruthenium at 1200 C, was analyzed by X-ray diffraction. The interplanar spacings and relative intensities obtained from the diffraction pattern corresponded to those for RuO_2 as reported in the ASTM card file of powder diffraction data.

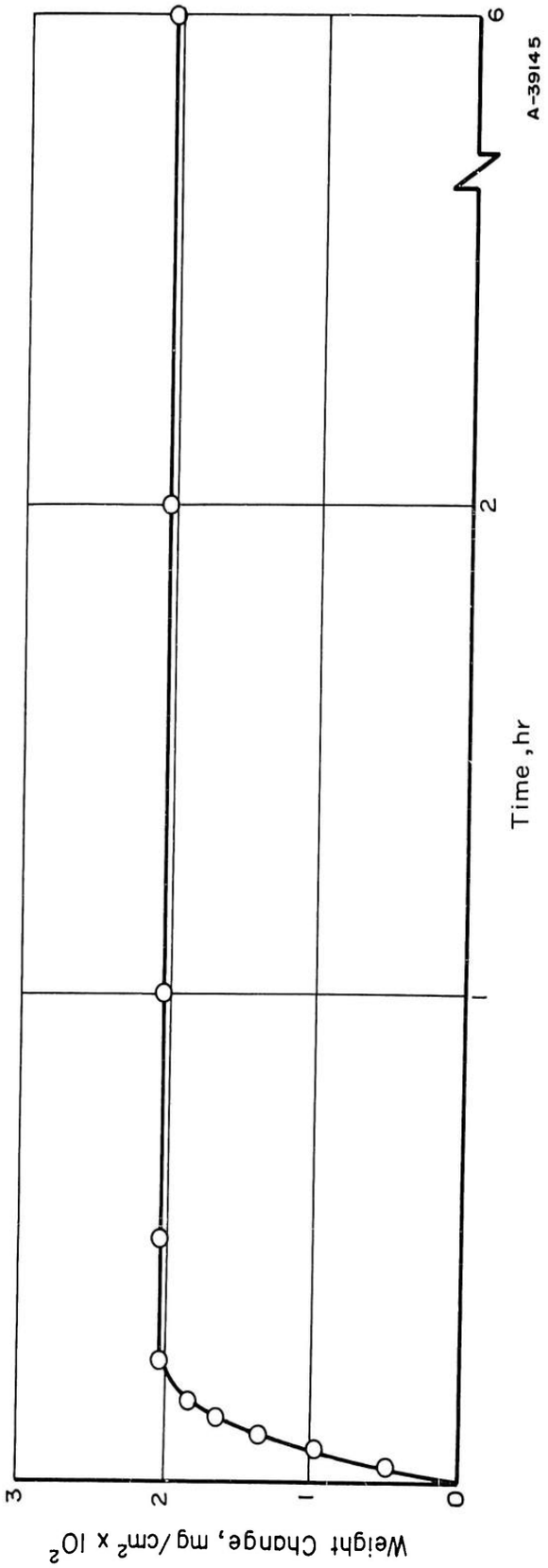

FIGURE 68. WEIGHT GAIN OF PALLADIUM IN SLOWLY FLOWING DRY AIR AT 1000 C

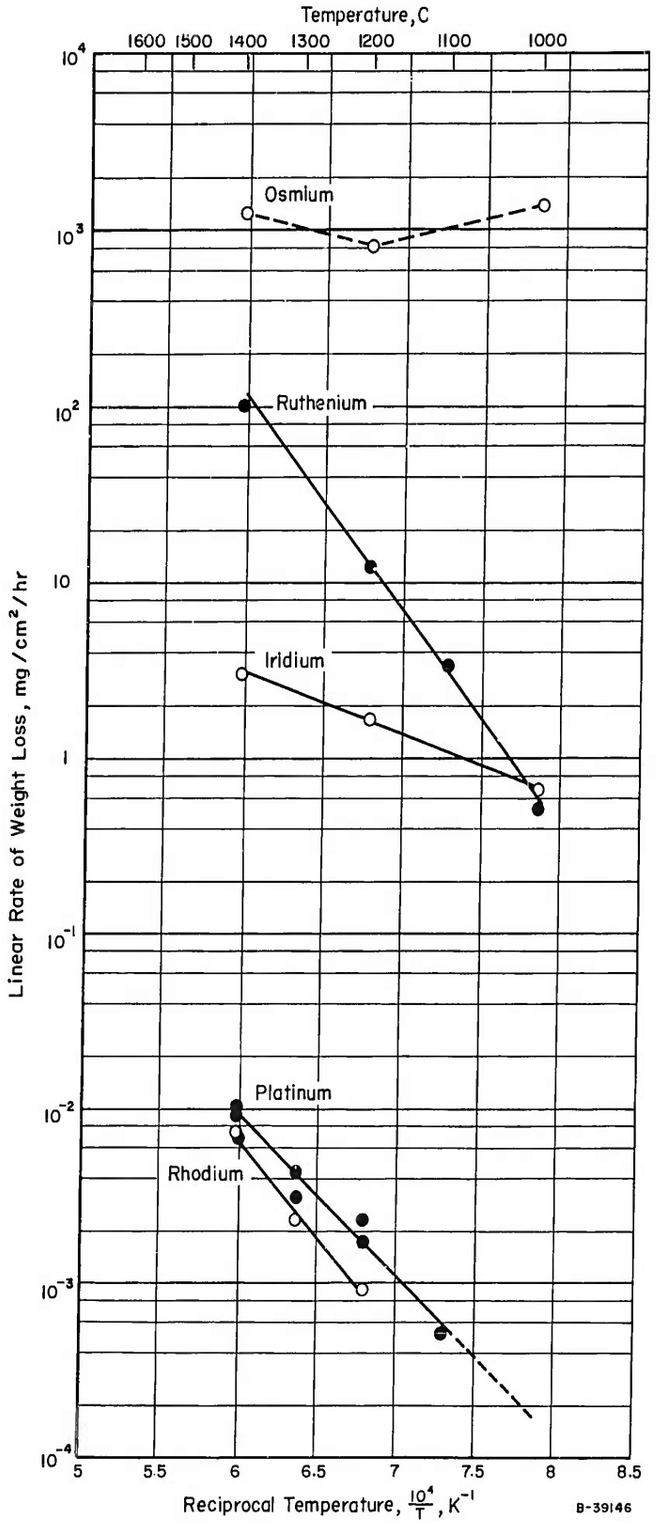

FIGURE 69. VARIATION WITH TEMPERATURE OF THE RATE OF WEIGHT LOSS IN AIR OF THE PLATINUM-GROUP METALS

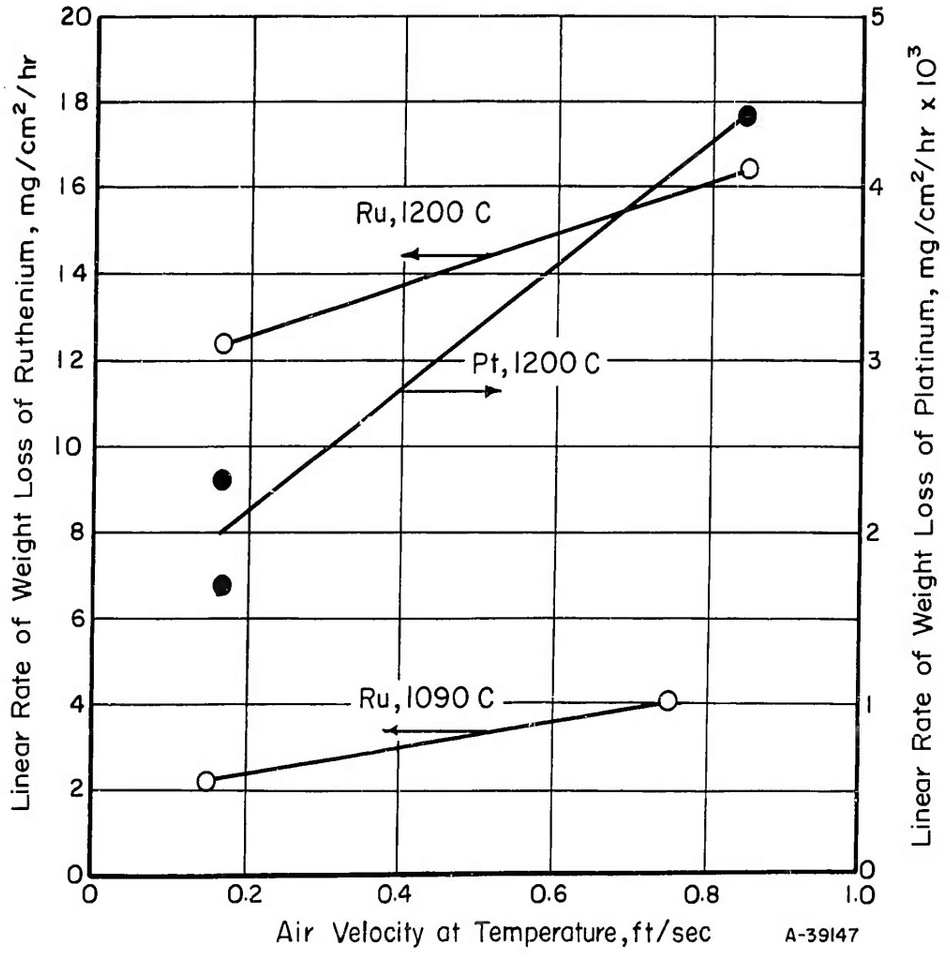

FIGURE 70. EFFECT OF AIR VELOCITY ON THE RATE OF OXIDATION OF RUTHENIUM AND PLATINIUM

Figure 71 shows the appearance of a specimen of ruthenium after being exposed 6 hours at 1200 C to slowly flowing air. Pitting of the surface and grain boundary attack is evident. These effects were greatly accentuated with osmium which also has the HCP structure.

Osmium

Severe heterogeneity of oxidation occurred for osmium specimens oxidized at 1000 to 1400 C, as shown by the surface appearance in Figures 72 through 75. The appearance of longitudinal and transverse sections of the specimens oxidized at 1000 and 1400 C is shown in Figures 76 and 77. All of these specimens were prepared by vacuum arc melting.

A test (25-19, Table 11) was run on a specimen which had been prepared by powder metallurgy as described under "Materials". The specimen, which had nominal dimensions of 1 x 0.2 x 0.2 inch and an initial surface area of 5.82 cm^2, was heated to 600 C in flowing argon for 35 minutes, and then oxidized in flowing air for 15 minutes. Final surface area was 5.58 cm^2, and the specimen lost 1.4504 grams out of the original 13.3600 grams. Two faces of the specimen were tarnished, but not grossly oxidized; the remaining four faces were badly oxidized and had a spongy appearance. The thickness between the two unoxidized faces was unchanged within ±0.001 inch. It is thought that the two unoxidized faces were consolidated more than the other four faces during pressing and sintering.

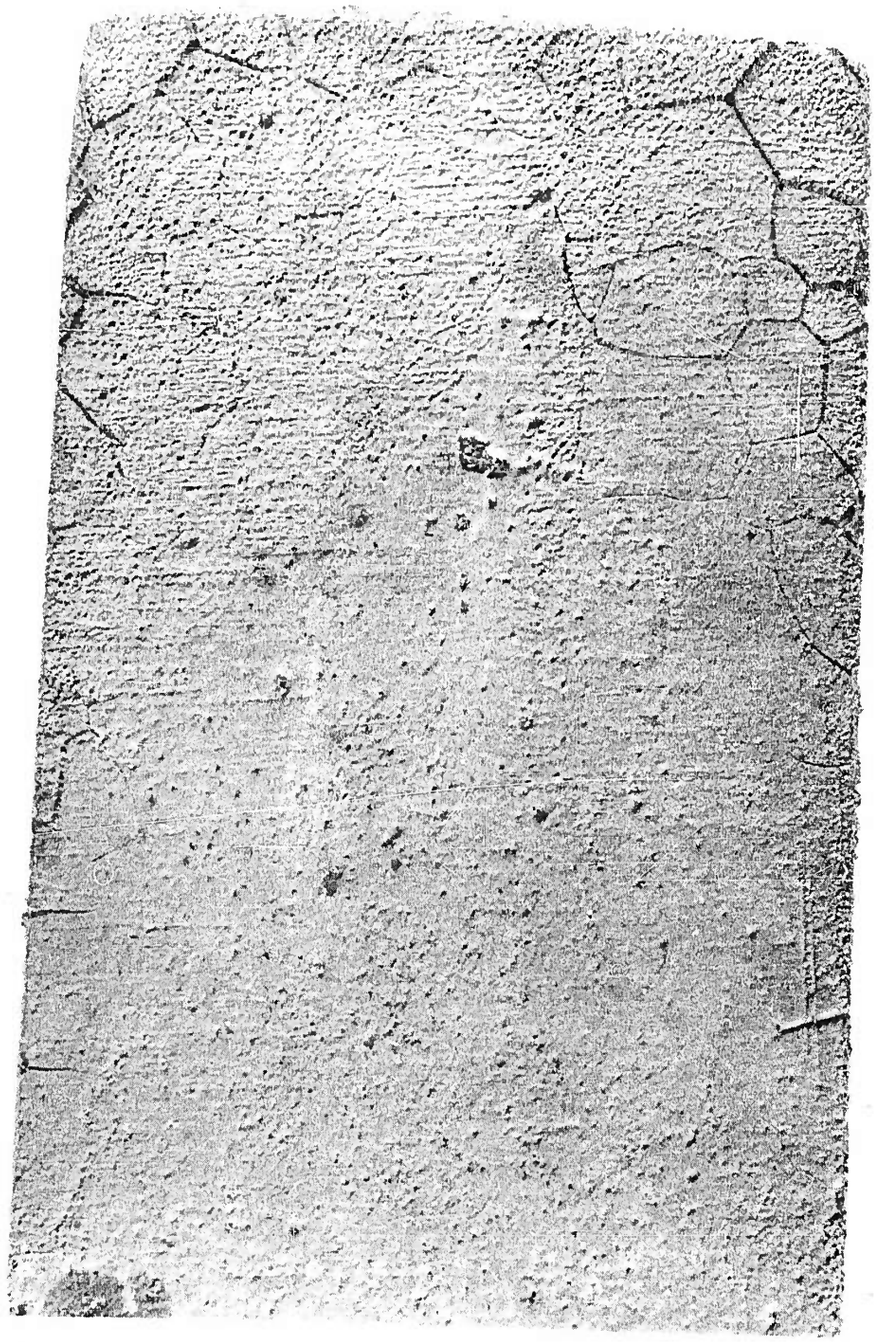

20X

N55744

FIGURE 71. APPEARANCE OF RUTHENIUM AFTER OXIDATION AT 1200 C FOR 6 HOURS

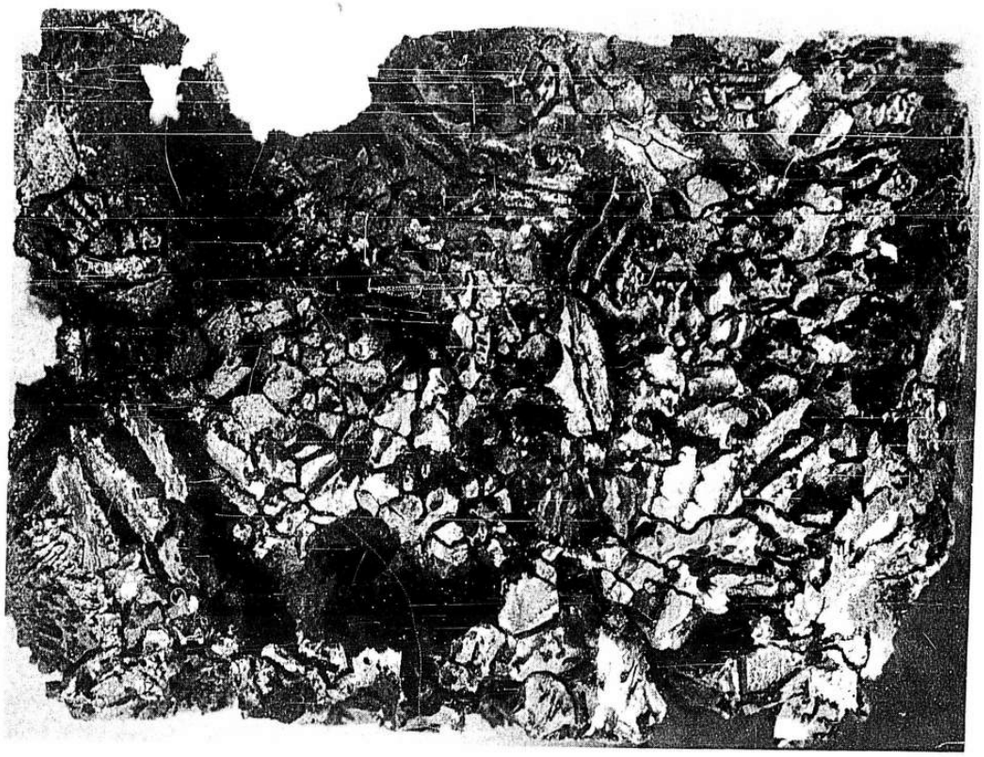

10X N57240

FIGURE 72. APPEARANCE OF OSMIUM AFTER OXIDATION AT 1000 C FOR 53 MINUTES

See Figure 75 for higher magnification.

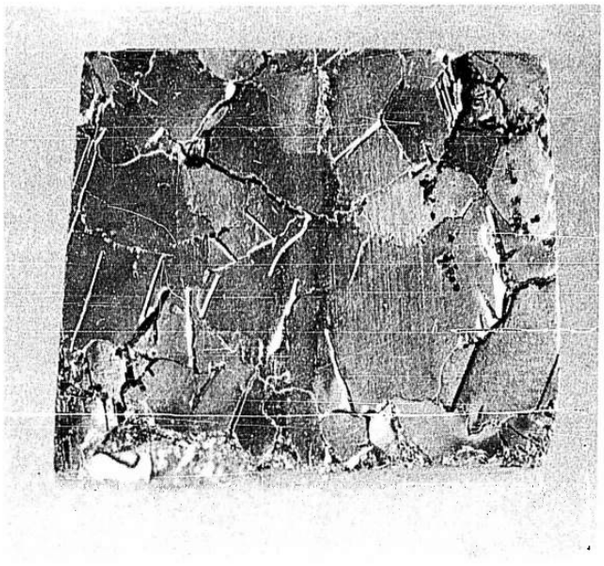

10X N57242

FIGURE 73. APPEARANCE OF OSMIUM AFTER OXIDATION AT 1200 C FOR 9 MINUTES

10X N57559

FIGURE 74. APPEARANCE OF OSMIUM AFTER OXIDATION AT 1400 C FOR 40 MINUTES

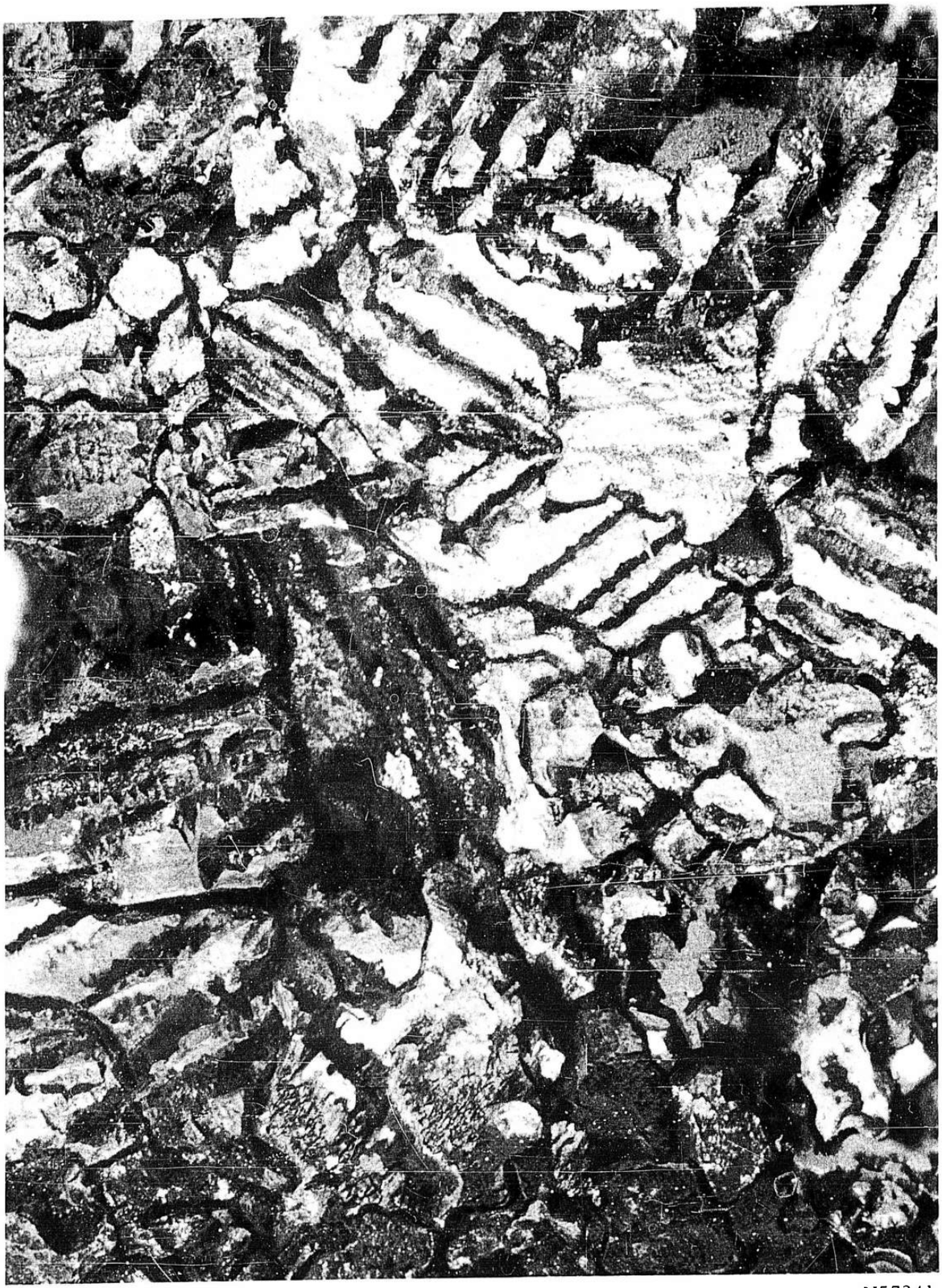

25X

N57241

FIGURE 75. SURFACE APPEARANCE OF OSMIUM AFTER OXIDATION AT 1000 C FOR 53 MINUTES

15X N57917

FIGURE 76. LONGITUDINAL (TOP) AND TRANSVERSE SECTIONS OF OSMIUM SPECIMEN OXIDIZED AT 1000 C FOR 53 MINUTES

15X N51918

FIGURE 77. LONGITUDINAL (TOP) AND TRANSVERSE SECTIONS OF OSMIUM SPECIMEN OXIDIZED AT 1400 C FOR 40 MINUTES

Derived Results

Although considerable additional research is necessary before it can be concluded that the kinetics of the oxidation of the platinum-group metals is fully understood, it is appropriate at this time to present a compilation of the "best" values of the rates of weight loss in air, based on the research done in this program. Table 12 gives these rates and the activation energies calculated from their temperature dependence as shown in Figure 69 by use of the usual Arrhenius relationship.

$$k = AC^{-\frac{Q}{RT}}$$

from which can be derived

$$Q = \frac{2.303R}{\frac{1}{T_1} - \frac{1}{T_2}} \log_{10} \frac{k_2}{k_1}$$

where

Q = activation energy

R = gas constant

T = absolute temperature

k = rate constant.

Discussion

At the beginning of this investigation, the thermodynamics, kinetics, and mechanism of the loss in weight of the platinum-group metals in air was relatively unexplored, particularly with respect to iridium, ruthenium, and osmium.[12] Recently, there has been evidence

TABLE 12. RATES OF WEIGHT LOSS IN SLOWLY FLOWING DRY AIR AND DERIVED ACTIVATION ENERGIES OF THE PLATINUM-GROUP METALS

Metal	Rate of Weight Loss, $mg/cm^2/hr$, at Indicated Temperature			Activation Energy, kcal/mole
	1000 C	1200 C	1400 C	
Rhodium	(a)	8.5×10^{-4}	6.8×10^{-3}	51
Platinum	(b)	1.7×10^{-3}	9.6×10^{-3}	42
Iridium	0.67	1.6	3.1	16
Ruthenium	0.58	12	120	56
Osmium(c)	(1350)	(810)	(1240)	--

(a) At 1000 C, a protective oxide coating formed on rhodium.
(b) Weight loss too small for measurement to give meaningful data.
(c) Osmium was not extensively studied, and data must be considered as very tentative (see Figure 69).

of considerable research activity in this area directed predominantly at identifying the volatile oxide species involved in the reactions and in defining the thermodynamic equilibria.

Oxidation Products

Alcock and Hooper,[18] Schäfer and Tebben,[19] and Schäfer and Heitland[20] recently reported results from investigations of the thermodynamics of the gaseous oxides of the platinum-group metals. These studies were done using the "transportation" or "carrier gas" technique. Reported volatile species resulting from the oxidation of the platinum-group metals were as follows:

	Volatile Oxide	
Metal	Reference 18	Reference 19 or 20
Os	-	-
Ir	Ir_2O_3 or IrO_3	IrO_3
Ru	RuO[a]	-
Rh	RhO_2	Rh_xO_2
Pt	PtO_2	PtO_2
Pd	-	-

(a) Molecule identified as Ru_xO and RuO thought to be probable.

The volatile oxide resulting from the oxidation of osmium normally has been assumed to be OsO_4. Brewer[21] reported that OsO_2 disproportionates at 650 C to 1 atm of OsO_4 gas. However, Grimley, Burns, and Inghram[22] identified OsO_3 and OsO_4 as being formed from

of considerable research activity in this area directed predominantly at identifying the volatile oxide species involved in the reactions and in defining the thermodynamic equilibria.

Oxidation Products

Alcock and Hooper,[18] Schäfer and Tebben,[19] and Schäfer and Heitland[20] recently reported results from investigations of the thermodynamics of the gaseous oxides of the platinum-group metals. These studies were done using the "transportation" or "carrier gas" technique. Reported volatile species resulting from the oxidation of the platinum-group metals were as follows:

	Volatile Oxide	
Metal	Reference 18	Reference 19 or 20
Os	-	-
Ir	Ir_2O_3 or IrO_3	IrO_3
Ru	RuO[a]	-
Rh	RhO_2	Rh_xO_2
Pt	PtO_2	PtO_2
Pd	-	-

(a) Molecule identified as Ru_xO and RuO thought to be probable.

The volatile oxide resulting from the oxidation of osmium normally has been assumed to be OsO_4. Brewer[21] reported that OsO_2 disproportionates at 650 C to 1 atm of OsO_4 gas. However, Grimley, Burns, and Inghram[22] identified OsO_3 and OsO_4 as being formed from

osmium in the temperature range of 825-1475 C (1100-1750 K) in oxygen at 1.2×10^{-5} or 3.5×10^{-5} atm. The equilibrium constant for the reaction $OsO_{4(g)} \rightleftharpoons OsO_{3(g)} + 1/2\ O_{2(g)}$ was calculated over the temperature range and a value for the heat of reaction at 1125 C (1400 K) was calculated as $\triangle H^\circ = 11.8$ kcal/mole. At temperatures greater than 1425 (1700 K), there was evidence of the existence of OsO_2; the intensity of the OsO_2 species was $\leq \frac{1}{1000}$ of the OsO_3 intensity.

Alcock and Hooper[18] reported that the volatile oxides identified as being produced by oxidation of the platinum-group metals at 1000 to 1600 C were not found to be stable at lower temperatures. Thus, identification of RuO_2 as the condensation product from the oxidation of ruthenium at 1280 C, as described under "Experimental Results", is not in conflict with the identification by Alcock and Hooper of RuO as the volatile oxide produced. It appears that the RuO formed at high temperatures oxidizes to RuO_2 at the lower temperatures.

Oxidation Rates

Because all of the platinum-group metals, with the possible exception of palladium, lose weight at high temperatures in an air atmosphere by formation of volatile oxides, it can be expected that equilibrium relationships might affect the kinetic data generated by different investigators using different sets of conditions.

$$x\,M_{(s)} + \frac{y}{2}\,O_{2(g)} \rightleftharpoons M_xO_y\ (g)$$

assuming ideal gas behavior:

$$K_p = \frac{p(M_xO_y)}{p(O_2)^{y/2}}$$

$$p(M_xO_y) = K_p\, p(O_2)^{y/2}$$

Alcock and Hooper[18] showed that the weight of metal loss under equilibrium conditions varied with the partial pressure of oxygen as follows:

Metal	Temperature, C	Weight of Metal Loss Proportional to:
Ir	1200	$p(O_2)^{3/2}$
Ru	1280	$p(O_2)^{1/2}$
Rh	1400	$p(O_2)$
Pt	1400	$p(O_2)$

The equilibrium partial pressure of volatile metal oxide is governed by the partial pressure of oxygen. Therefore, in an isothermal static system, the amount of metal loss should be governed by the partial pressure of oxygen and the total amount of oxygen available for reaction. Inasmuch as most equilibria are affected by temperature, this would also be expected to be a variable. These are thermodynamic considerations which are useful for determining the direction in which a system can travel, but they do not give information on how rapidly a system is reacting or can react. However, they have a real bearing on the

kinetics because a system at equilibrium will show no net reaction, and the rate at which reaction can occur may depend on how far the system is maintained away from its equilibrium point. This aspect has been emphasized by Fryburg and Murphy[13] for the case of platinum and has been indicated by others.

Thus, on the above basis, the kinetics of the reaction of the platinum-group metals with oxygen in a flowing system would be expected to depend on: (1) temperature, (2) partial pressure of oxygen, and (3) the flow rate of the gaseous stream insofar as this would determine the distance from the equilibrium point. The flow rate and chemical composition (aside from reactant and product) of the gas stream also can affect the nature of the aerodynamic boundary layer through which the volatile reactant and product must pass, as discussed by Wagner,[14] Modisette and Schryer,[15] and Waber.[16] In addition, the total gas pressure can be a factor in determining the nature of the boundary layer and also in determining how many of the oxide molecules escaping from the surface are reflected back by collisions with atoms or molecules in the gas phase. Therefore, chemical composition of the gas stream and total pressure are two additional variables which can affect the rates at which the platinum-group metals oxidize. These variables have been investigated with respect to the oxidation of molybdenum,[15,17] which, as is well known, forms volatile MoO_3 during oxidation.

Alcock and Hooper[18] studied the amount of metal lost by oxidation per liter of nitrogen-oxygen carrier gas at saturation as a function of the partial pressure of oxygen in the gas. Metals studied

were Pt, Rh, Ir, and Ru; data on this aspect were reported for only the first three. The results for 0.2 and 1.0 atm. oxygen are useful for this discussion:

Metal	Temperature, C	P_{O_2}, atm.	Weight of Metal/Liter of Oxide Saturated Gas, mg
Pt	1400	0.2	0.020
		1.0	0.10 *
Rh	1400	0.2	0.014
		1.0	0.07 *
Ir	1200	0.2	0.89 **
		1.0	8.9

*Extrapolated from graph which terminated at 0.85 atm.
**Extrapolated from graph which terminated at 0.25 atm.

Using this information and the experimental results presented in Table 11, it is possible to calculate the degree to which the flowing air was saturated with oxides in the experimental work. The degree of saturation during the experiments, based on these calculations, was as follows:

Metal	Temperature, C	Saturation of Flowing Air with Volatile Oxide, per cent
Pt	1400	72
		112
		63
Rh	1400	139
Ir	1200	16

Therefore, the air was saturated or close to being saturated in the platinum and rhodium tests at 1400 C, and was relatively unsaturated in the iridium test at 1200 C. Thus, it appears to be a distinct possibility that the rate data presented for platinum and rhodium are lower than what would be experienced in a more rapidly moving atmosphere, and the increase in the oxidation rate of platinum at 1200 C by a factor of 1.9-2.6 with a fivefold increase in air flow could well be due predominantly to maintaining a lower degree of saturation in the gas stream.

Osmium and Iridium. No data have been reported on the rate of oxidation of osmium and iridium and, therefore, no comparison can be made with the data generated in this program.

Ruthenium. Rhys[25] reported results for the oxidation of 1.0 x 0.20-inch-diameter ruthenium rods in still air at 900-1500 C. Results, which were reported in per cent weight loss and per cent weight loss per hour, are obviously not representative of the inherent oxidation rate of ruthenium above about 1200-1300 C because of substantial changes in the area of the specimens caused by oxidation, the effect of which is to give a decreasing rate of oxidation, as shown by this investigation in Figure 67. Also, the use of still air makes the results open to question, as pointed out earlier.

The data published by Rhys were recalculated to five rates in terms of $mg/cm^2/hr$ for comparison with the results from this investigation. Rhys' data, the results of the recalculation, and rates obtained in this investigation are as follows:

Temp. C	Reported by Rhys: Time, hr	Weight Loss: Per Cent	Weight Loss: Per Cent/Hr	Oxidation Rate, mg/cm^2/hr: Rhys*	Oxidation Rate, mg/cm^2/hr: This Investigation
900	90	0.41	4.5×10^{-3}	6.5×10^{-2}	8.8×10^{-2}**
1000	90	2.06	2.7×10^{-2}	0.33	0.58
1100	90	7.11	7.9×10^{-2}	1.1	3.0
1200	90	20.33	2.26×10^{-1}	3.2	12
1300	90	67.75	7.53×10^{-1}	1.1	41
1400	90	100.0	>1.0	--	120
1500	61	98.23	1.64	--	--

*Calculated from data reported by Rhys.
**Extrapolated from results at 1000-1400 C.

Rhodium. Raub and Plate[23] studied the behavior of rhodium in a flow of oxygen (0.4 liter/min. = 0.85 ft^3/hr) at 1100, 1200, and 1300 C.* At 1100 C, the rhodium gained about 0.07 mg/cm^2 in 6 hours, and the weight remained unchanged with time up to 20 hours, the duration of the test; this weight increase has been attributed predominantly to oxygen solubility. The behavior can be contrasted with that observed at 1000 C in this investigation (Figure 66). The sample continued to gain weight, but with a constantly decreasing rate throughout the 20-hour period. The rate was slightly less than parabolic. It is

*Platinum, palladium, silver, gold, and several alloys also were studied. Contrary to what would be expected, based on the earlier discussion, Raub and Plate reported no characteristic differences in reaction between using atmospheric air or oxygen. However, reaction rate was quite low in nitrogen containing 0.4 per cent oxygen.

believed that at 1000 C two processes occurred: (1) solution of oxygen in the rhodium foil and (2) development of a thin film of oxide on the surface. Brewer[21] lists the following decomposition temperatures (the temperature at which the dissociation pressure of the solid oxide equals one atmosphere) for rhodium oxides:

Oxide	Decomposition Temperature, C
Rh_2O	1127
RhO	1120
Rh_2O_3	880

Based on these data, the oxide formed should have been Rh_2O or RhO.

At 1200 C, Raub and Plate observed a very slight initial weight gain that was soon overcome by the weight loss resulting from oxidation to produce the volatile oxide. At 1300 C, the initial weight increase observed at 1200 C and caused by oxygen solubility was obscured by the increased rate of oxidation. However, a rhodium specimen after being heated in vacuum, following 9 hours in oxygen at 1300 C, had a weight loss of 2×10^{-4} mg/cm^2 amounting to 1.56 mg/100 g of rhodium, thus indicating a significant oxygen solubility at 1300 C.

A comparison of the oxidation rates of rhodium with those calculated from the data of Raub and Plate is as follows:

Investigation	Temp, C	Gas	$p(O_2)$, atm.	Flow Rate, scfh Gas	Flow Rate, scfh O_2	Oxidation Rate $mg/cm^2/hr$
Raub and Plate	1200	Oxygen	1	0.85	0.85	2.3×10^{-2}
This investigation	1200	Air	0.2	1.75	0.35	8.5×10^{-4}
Raub and Plate	1300	Oxygen	1	0.85	0.85	6.0×10^{-2}
This investigation	1300	Air	0.2	1.75	0.35	2.5×10^{-3}

Therefore, at 1200 C, Raub and Plate, by using 5 x the partial pressure of oxygen and about 2.5 x the oxygen volume-flow rate used in this investigation, obtained an oxidation rate 270 x greater. At 1300 C, the rate of Raub and Plate was 24 x greater than that measured in this investigation.

As discussed earlier, based on the data of Alcock and Hooper,[18] it is believed that the air in this investigation was saturated with respect RhO_2 and that the measured rate of oxidation was lower than what should have been allowed by the fundamental kinetics of the reaction. Multiplying the results from this investigation by 2.5 to give the same oxygen volume-flow rate as was used by Raub and Plate, still leaves the rates differing by factors of 108 and 10 at 1200 and 1300 C, respectively.

Palladium. This investigation did not study the behavior of palladium as extensively as the other metals because it was the least refractory of the group, Raub and Plate[23] had studied it rather extensively, and because the detail required for its study was outside the scope of this investigation.

Raub and Plate showed that palladium has substantial capacity for taking oxygen into solution, and that this capacity increases significantly with temperature. At 900 and 1000 C, the palladium reached its capacity for oxygen at about 2 and 4 hours, respectively, and showed no further weight change. At 1100-1300 C, the palladium showed an initial weight increase, the rate of which increased with temperature, and then a weight loss, the rate of which also increased with temperature.

Results of Raub and Plate which can be compared with results from this investigation are as follows:

Investigation	Temp, C	Gas	$p(O_2)$, atm.	Time, hr	Specimen Area cm^2	Weight Gain, mg/100 g
Raub and Plate	1000	Oxygen	1	6	5-10	12
This investigation	1000	Air	0.2	6	103	38
Raub and Plate	1200	Oxygen	1	6	5-10	71
This investigation	1200	Air	0.2	6	3.4	37

Alcock and Hooper[18] reported that palladium has appreciable vapor pressure at temperatures above 1200 C. These investigators reported only a slight enhancement of the volatility in oxygen over the normal vapor pressure of palladium, and this amounted to an increase of about 20 per cent at 1500 C. At 1200 C, where the normal vapor pressure of palladium was negligible, the volatility in oxygen was also found to be too small to permit accurate measurements.

Platinum. The data of Raub and Plate[23] show linear rates of weight loss for platinum at 1000 and 1100 C in oxygen. However, at 1200 and 1300 C, the rates departed from linearity. It is considered possible, as was discussed earlier for this investigation, that the 0.4 liter/min. (0.85 ft^3/hr) flow rate was insufficient to keep the reaction from approaching equilibrium.

Fryburg and Murphy[13] found that the oxidation rate of platinum at 1200 C increased linearly with the pressure of oxygen up to about 0.250 mm, at which pressure the mean free path of the gas molecules was roughly equal to the width of the platinum ribbon used for investigation. Above this pressure, the rate started to fall off from linearity with pressure, and fall off more and more as the pressure was increased. This fall off was ascribed to a "back reflection" of the volatilizing oxide by the molecules of the surrounding gas.

Results from the different studies for the rate of oxidation of platinum are as follows:

Investigation	Temp, C	Gas	P, atm.	$p(O_2)$, atm.	Flow Rate, scfh		Oxidation Rate, $mg/cm^2/hr$
					Gas	O_2	
Raub and Plate	1000	Oxygen	1	1	0.85	0.85	2.5×10^{-3}
This investigation	1000	Air	1	0.2	1.75	0.35	1.7×10^{-4}
Raub and Plate	1100	Oxygen	1	1	0.85	0.85	5.0×10^{-3}
This investigation	1100	Air	1	0.2	1.75	0.35	6.0×10^{-4}

Investigation	Temp, C	Gas	P, atm.	$p(O_2)$, atm.	Flow Rate, scfh Gas	Flow Rate, scfh O_2	Oxidation Rate, $mg/cm^2/hr$
Fryburg and Murphy	1200	Oxygen	2.0×10^{-4}	2.0×10^{-4}	--	--	4.2×10^{-2}
Raub and Plate	1200	Oxygen	1	1	0.85	0.85	3.6×10^{-2}
This investigation	1200	Air	1	0.2	1.75	0.35	1.7×10^{-3}
Raub and Plate	1300	Oxygen	1	1	0.85	0.85	5.4×10^{-2}
This investigation	1300	Air	1	0.2	1.75	0.35	4.6×10^{-3}

The differences between the partial pressures of oxygen, total pressures, and flow rates used in the different investigations again are believed to be responsible for the lack of agreement in the results.

The behavior of platinum in atomic oxygen at about 1000 C under low pressure has been under investigation.[26-28] From the standpoint of understanding the detailed mechanism whereby the platinum metals oxidize, and in view of the development of vehicles capable of flight at high Mach speeds and at extreme altitudes, the work reported by Fryburg[26] is considered particularly significant. Oxidation of platinum was studied at 1000 C and 0.50-mm pressure of oxygen using activated oxygen (i.e., oxygen gas containing oxygen atoms produced by electrical discharge). Under these conditions, it was found, using moist oxygen (2 per cent water vapor) that oxygen atoms were about 400 times more effective than oxygen molecules in causing oxidation of platinum. Preliminary results using dry oxygen indicated that atomic oxygen may be as much as 600 times more reactive to platinum than molecular oxygen.

Fryburg and Petrus[27] have also reported that the enhanced oxidation of platinum in activated oxygen occurs with little or no activation energy.

Mechanism of Oxidation

It has been known for some time that the platinum-group metals lose weight more rapidly at high temperatures in an oxidizing atmosphere than they do in vacuum or in an inert atmosphere. Although some of the earlier literature on the subject speculated as to whether the metals vaporized and then volatile oxides were formed or whether an oxide formed on the surface and then vaporized, it is apparent now that the latter is the case.

It is of interest in this regard to show how the "apparent vapor pressure" of the metals in an oxidizing atmosphere compares with the "normal vapor pressure" of the metals. Tabulated below are constants in the equation $\log P_{mm} = A - \frac{B}{T}$ for these two vapor pressures, where T is the Kelvin temperature. The equations listed for the "apparent

	Constants for Normal Vapor Pressure			Constants for Apparent Vapor Pressure		
Metal	A	B	Reference	A	B	Reference
Os	10.59	37,000	29	-	-	-
Ir	10.48	33,880	30	0.22, 0.52*	906	18
Ru	10.50	33,800	29	7.71	11,100	18
Rh	10.28	28,300	30	3.960	9,866	18
Pt	10.36	29,100	31	4.92	8,585	18
Pd	9.075	19,425	31	-	-	-
	8.30	16,860	32	-	-	-
	11.50	23,450	18	-	-	-

*0.22 assuming Ir_2O_3, and 0.52 assuming IrO_3 formation.

vapor pressure" were reported by Alcock and Hooper[18] as representing the vapor pressure of the metal oxides, though obviously, from the nature of their investigation, the equations represent the equilibrium oxide vapor pressure over the metal in an oxidizing atmosphere. The authors did not state what partial pressure of oxygen the equation referred to, although it is clear that the oxide vapor pressure over the metal is very dependent on the partial pressure of oxygen.

From these data can be calculated the factor by which the volatility of the metals is increased in an oxidizing atmosphere (although the partial pressure of oxygen is unspecified)

$$\log P_a - \log P_n = A_a - A_n - \frac{B_a}{T} + \frac{B_n}{T}$$

$$\log \frac{P_a}{P_n} = (A_a - A_n) - \frac{(B_a - B_n)}{T}$$

P_a = apparent vapor pressure; P_n = normal vapor pressure.

Results calculated from P_a/P_n at 1400 C are as follows:

Metal	P_a/P_n
Ir	$3\text{-}6 \times 10^9$
Ru	6×10^{10}
Rh	5×10^4
Pt	6×10^6

As indicated previously, even at 1500 C, P_a/P_n for palladium has been reported[18] as only about 1.2, and there exists considerable uncertainty at the present time in P_n for palladium.[31] An equation for P_a for osmium is not available. However, because osmium has the lowest P_n and the highest oxidation rate of the platinum-group metals, it would be reasonable to expect that P_a/P_n for osmium would be the highest of all of the above values.

Thus, except for palladium, the normal vapor pressure of the platinum-group metals cannot account for volatilization losses in an oxidizing atmosphere.

The detailed mechanism whereby the platinum metals oxidize has been the subject of much speculation.[34] Brewer,[21] after examining the thermodynamic properties of the oxides of the platinum-group metals, concluded that above about 1125 C no solid oxide phases can exist even in an atmosphere of oxygen because they dissociate into the metals and oxygen. Yet, it is clear that the reactions which occur in oxygen are solid-gas rather than gas-gas reactions, as discussed above. Actually, energy states at an interface can differ considerably from those in the bulk material. Consequently, compounds that are normally unstable in bulk state may be formed as thin, perhaps monomolecular, films on suitable surfaces.[33] Thus, although the thermodynamic data for the platinum-group oxides predict no bulk accumulation on the metals in air at high temperatures, and indeed none occurs, the data do not rule out the possibility of thin film formation to provide a reaction path.

Consideration of thin film formation immediately introduces the aspect of adsorption, which we believe plays a major role in the oxidation process. Several lines of evidence will be cited in support of this hypothesis.

The affinity of platinum for oxygen is appreciable. According to Kubaschewski and Hopkins,[33] a strongly adherent adsorbed layer, which is very difficult to remove, is formed during exposure to air. Treatment of normal platinum powder with dry hydrogen even above 1200 C removes the adsorbed oxygen only very slowly, and alternating treatment by hydrogen and evacuation has to be repeated a number of times in order to remove most of the oxygen. Quite clearly, for a gas to be held so tenaciously, the chemical forces associated with chemisorption are operative rather than the van der Waals or dispersion forces involved in physical adsorption. As will be discussed later, it is believed that the adsorbed oxygen is dissociated into atoms on the surface, at least in the process of forming the volatile oxide.

Knowing that strong adsorption of oxygen can occur at high temperatures, it can be suspected that a form of the adsorption equation might be applicable to the oxidation process. A suggested rate expression from oxidation is:

$$\frac{dw}{dt} = \frac{ap}{bp + 1}$$

where $\frac{dw}{dt}$ is the weight loss/unit area/unit time, a and b are constants,

and p is the partial pressure of oxygen in the bulk gas. At high temperatures or low pressures, when the surface is sparsely covered with adsorbed gas, the rate expression would become

$$\frac{dw}{dt} = kp.$$

When the surface is completely covered, a situation promoted by lower temperatures and higher pressures, the equation would become

$$\frac{dw}{dt} = \text{constant}.$$

These equations are in qualitative agreement with experimental observations reported by Fryburg and Murphy[13] on the oxidation of platinum at 1200 C, as discussed previously in this report. A full report on this work has not been published, thus attempts at quantitative fitting of the theory to their data cannot be made at this time.

Fryburg[26] reported that oxygen atoms were 400-600 times more effective than oxygen molecules in causing oxidation of platinum at 1000 C and 0.50 mm pressure of oxygen. This enhanced oxidation has been indicated to occur with little or no activation energy.[27] However, in air, relatively high activation energies were found in the present investigation (Table 12).

The gas-solid reaction between the platinum-group metals and molecular oxygen to give gaseous oxides can be considered to occur in six stages:

(1) Diffusion of oxygen to the surface.

(2) Adsorption of the oxygen on the surface.

(3) Dissociation of the adsorbed oxygen molecules.

(4) Reaction of the platinum-group metal with the oxygen atoms.

(5) Desorption of the oxide from the surface.

(6) Diffusion of the liberated oxide into the bulk gas phase.

Barring a large difference between the rate of adsorption of atomic and molecular oxygen on platinum, it appears that the rate-determining step in the oxidation of this metal using molecular oxygen is the dissociation to give oxygen atoms, Stage (3).

Future Work

A considerable amount of additional research must be done before not only the mechanism of oxidation is fully understood but also the true oxidation rates are known and can be used reliably by designers.

The exploratory studies carried out within the scope of the over-all program on the platinum-group metals has done much to lay the groundwork for a more comprehensive investigation. In particular, the oxidation rates should be determined as functions of oxygen partial pressure, total pressure, temperature, velocity of gas flow, and composition of the gas (aside from oxygen).

Further analysis of the applicability of adsorption theory should be done to understand the detailed mechanism whereby the platinum-group metals oxidize.

* * * * * * * * * * *

Original data on which the experimental portion of this section of the report is based are recorded in BMI Laboratory Record Books 15328 and 16225, pp 1-100 and 1-21, respectively.

W. E. Enderle contributed significantly in carrying out the research program.

REFERENCES

(1) Rhys, D. W., J. Less Common Metals, 1, 4, 1959, 269.

(2) Vines, R. F., The Platinum Metals and Their Alloys, The International Nickel Company, Inc., 1941.

(3) Baird, J. O., referred to in Platinum Metals Review, 4, 1, 1960, 31.

(4) Weber, R. L., Temperature Measurement and Control, Blakeston Company, 1941.

(5) Jaffee, R. I., Maykuth, D. J., and Douglass, R. W., "Rhenium and the Refractory Platinum-Group Metals, Paper presented at the AIME-IMD Refractory Metals Symposium, Detroit, 1960.

(6) Carreker, R. P., Jr., Guard, R. W., and Lenhart, R. F., "Investigation of Deformation and Fracture of Metals", WADC T.R. 55-303, May 1955.

(7) Cottrell, A. H., Relation of Properties to Microstructure, ASM, 1953.

(8) Bale, E. S., Platinum Metals Review, April 1958, 61.

(9) Seeger, A., Dislocations and Mechanical Properties of Crystals, John Wiley and Sons, 1956.

(10) Hall, E. O., Twinning, Butterworths Scientific Publications, 1954.

(11) Averbach, B. L., Felbeck, D. K., Hahn, G. T., and Thomas, D. A., Fracture, Technology Press and John Wiley and Sons, 1959.

(12) Douglass, R. W., Holden, F. C., and Jaffee, R. I., "Technical Phase Report on High Temperature Properties and Alloying Behavior of the Refractory Platinum-Group Metals", A Survey of the Literature, Contract NOnr-2547(00), NR 039-067 (Aug. 14, 1959).

(13) Fryburg, G. C. and Murphy, H. M., "On the Use of Furnaces in the Measurement of the Rate of Oxidation of Platinum and Other Metals Forming Volatile Oxides", Trans. Met. Soc. AIME (Oct. 1958), 660-661.

(14) Wagner, Carl, "Passivity During the Oxidation of Silicon at High Temperatures", J. Applied Physics 29 (9) (Sept. 1958) 1295-1297.

(15) Modisette, J. L. and Schryer, D. R., "An Investigation of the Role of Gaseous Diffusion in the Oxidation of a Metal Forming a Volatile Oxide", NASA TN D-222 (March 1960).

(16) Waber, J. T., "Kinetics of Oxidation in a Gas Stream", Chapter 4 in Metals for Supersonic Aircraft and Missiles, American Society for Metals, Cleveland (1958).

(17) Wilks, C. R., "Effects of Temperature, Pressure, and Mass Flow on Oxidation of Molybdenum", Paper presented at SAMPE Eastern Division Meeting, Kresge Hall, MIT (May 3, 1960).

(18) Alcock, C. B. and Hooper, G. W., "Thermodynamics of the Gaseous Oxides of the Platinum-Group Metals", Proc. Royal Soc. 254A (March 8, 1960) 551-561.

(19) Schäfer, V. H. and Telben, A., "Gleichgewichtsmessungen in System Platin-Sauerstoff, Gasförmiges Platindioxyd", Zeitschrift für anorganische und allgemeine Chemie, Bord 304 (1960) 317-321.

(20) Schäfer, V. H. and Heitland, H.-J., "Gleichgewichtsmessungen im System Iridium-Sauerstoff, Gasförmiges Iridiumtrioxyd", Zeitschrift für anorganische und allgemeine Chemie, Bord 304 (1960) 249-265.

(21) Brewer, Leo, "The Thermodynamic Properties of the Oxides and Their Vaporization Processes", Chem. Rev. 52 (1953) 1-75.

(22) Grimley, R. T., Burns, R. P., and Inghram, M. G., "Mass-Spectrometric Study of the Osmium-Oxygen System", J. Chem. Phys. 33 (1) (July 1960), 308-309.

(23) Raub, Ernst and Plate, Werner, "The Behavior With Respect to Oxygen of Noble Metals and Their Alloys in the Solid State at Elevated Temperatures", Zeitschrift für Metallkunde 48 (10) (1957) 529-539.

(24) Raub, Ernst, "Metals and Alloys of the Platinum Group", J. Less Common Metals, 1 (1959) 3-18.

(25) Rhys, D. W., "The Fabrication and Properties of Ruthenium", J. Less Common Metals 1 (1959) 269-291.

(26) Fryburg, G. C., "Enhanced Oxidation of Platinium in Activated Oxygen", J. Chem. Phys. 24 (2) (Feb. 1955) 175-180.

(27) Fryburg, G. C. and Petrus, H. M., "Variation with Temperature of the Recombination of Oxygen Atoms on a Platinum Surface", J. Chem. Phys. 32 (1960) 622-623.

(28) Mitani, Kazuo,and Harano, Yoshio, "Evolution of Atomic Oxygen from Platinum Surface Treated Previously with Discharged Oxygen Gas", Bull. Chem. Soc. of Japan 33 (2) (1960) 276.

(29) Dushman, Saul, Scientific Foundations of Vacuum Technique, John Wiley & Sons, New York (1949).

(30) Hasapis, A. A., Parish, M. B., and Rosen, C. L., "The Vaporization and Physical Properties of Certain Refractories", Quarterly Progress Report No. 3, Contract AF 33(616)-6840, ASTIA 244130 (Oct. 11, 1960).

(31) Dreger, L. H. and Margrave, J. L., "Vapor Pressures of Platinum Metals. I. Palladium and Platinum", J. Phys. Chem. 64 (1960) 1323-1324.

(32) Haefling, J. F. and Daane, A. H., "The Vapor Pressure of Palladium", Trans. Met. Soc., AIME (Feb. 1958) 115.

(33) Kubaschewski, O. and Hopkins, B. E., Oxidation of Metals and Alloys, Academic Press, Inc., New York (1953).

(34) Beamish, F. E., McBryde, W. A. E., and Barefoot, R. R., "The Platinum Metals", Chapter 17 in Rare Metals Handbook, Second Edition, C. A. Hampel, Editor, Reinhold Publishing Corp., New York (1961).